CENTRO DE INVESTIGACIONES EN ÓPTICA, A.C.

POLARIMETRY EMPLOYING CLASSICAL ENTANGLEMENT OF LIGHT

(Final version. Changes suggested by advisors are included)

MAESTRO EN CIENCIAS (ÓPTICA)

Adviser: Dr. Rafael Espinosa Luna

Co-adviser: Dr. Qiwen Zhan

Student: Eusebio Aguilar Fernández

November, 29th 2016
León, Guanajuato, México

Gratefulness

Firstly, I want to thank to my parents because they have been my support in all time of my life. Also, I want to thank my wife by all time that she has offered me her unconditional support and because she has given me away the greatest joy in my life. I also want to express my gratitude to my brothers and friends by all moments of joy that I have lived with them.

Actually, I only have gratitude words for my thesis adviser, the Dr. Rafael Espinosa Luna, who has been an exemplary person for me and from whom I have learned many lessons not only respect to the academic ambit, but also life lessons. Also, I want to express my gratefulness to my thesis co-adviser, he is the Professor Qiwen Zhan, because he has contributed with his extensive knowledge and experience in this work. As well, I want say thanks' to all group members (GIPyS), since they have given me great advices at all moment that I needed it. They are Lupita, Yaqui, Victor M. Rico, Izcoatl Saucedo, Eloy and Jason G. Jamaica.

Finally, I want to thank all CIO staff, since they allow us to all students a pleasurable stay in CIO. Especially, I want to thank to female Professor Reyna Duarte by sympathy and support, which she offered me. This work would not have been possible without the financial support provided by CONACyT, I am heavily grateful.

Ese sueño que empezó en algún momento está tomando su forma final; sin duda factores han influido, pero los dos más importantes han estado ahí para mí. Una dedicatoria muy en especial para mi pequeño motor que con un suave golpecito siempre me recuerda por qué debo seguir y no rendirme.

Eusebio Aguilar.

Abstract

In this thesis we present the theory, simulation and experimental results obtained for an experimental setup, which allows us to obtain the experimental Mueller matrix of a transparent birefringent sample. The experimental setup proposed was inspired from a theoretical description given by Professor Töppel and his work group [1]. An important advantage of this experimental setup with respect to other experimental setups described by different methods (the Ideal Polarimetric Arrangement method, IPA, for example) is that, this setup uses a single unconventional polarized beam (a radially polarized beam) to analyze the sample. By contrast, the IPA method uses at least four different polarized beams (conventional polarized, for example p-polarized, s-polarized, +45-polarized and right-handed polarized) to do that. In this sense, the main goal of this work is demonstrate that we can obtain useful information through determination of the Mueller matrix (associated to a transparent birefringent sample) by using classical entangled polarization modes (radially polarized beam). In order to do this, we are going to generate and analyze a radially polarized beam through a passive method by using a commercial device called S-waveplate. Then, we are going to use this beam in order to analyze a transparent sample (air, for example) and obtain its Mueller matrix associated, through the determination of the polarization modes.

Two main improvements to the theoretical proposal (Professor Töpple and his work group) for the determination of the Mueller matrix using classical entangled polarization modes (radially polarized beam) are presented. One of them is realized experimentally by substituting photodetectors, who provide a single number associated to a spatial average intensity over a solid angle, by a CMOS camera, which provides a spatial distribution. The other improvement consists in a modification of the original theoretical setup proposed, where now all the measurements are realized along two different arms only, not along the six arms originally considered. A new tool, recently proposed by our GIPYS Group, is applied to measure quantitatively the quality associated to the cross-section of any classical entangled or, more generally, to any unconventional polarization mode (the Symmetrical Average Symmetry metric). The characterization of the commercial passive converter employed, shows some mistakes present within the manufacturer´s manual. As a way to prove the setup system proposed, each main part is tested, in order to detect any probable mistake. The experimental Mueller matrix of the air is obtained by using a single incident unconventional (spatially non-homogeneous) polarized beam and two different methods. The radially polarized beam carries all polarizations at once in a classically entangled state [1]. That important characteristic, allows us to use a single radially polarized beam as an incident beam over the sample in order to analyze the output beam, once, it has interacted with the sample. According to Professor Töppel, one

possible representation of a radially polarized beam is as a superposition between a horizontal Hermite-Gaussian polarization mode (with horizontal polarization) and a vertical Hermite-Gaussian polarization mode (with vertical polarization). In other words, we are using two mutually orthogonal polarization beam modes entangled. The nature of the radially polarized beam indicates us, that it is necessary split mutually orthogonal polarization modes within it, in order to analyze the polarization that carries each of them. It was described by Professor Töppel an experimental setup, which allows us to do that, it is called transverse-mode beam splitter. Experimentally, we observed that it does not provide the expected results. In other words, we have observed experimentally that this optical device does not split the mutually orthogonal polarization modes. On the other hand, the simulation of the transverse-mode beam splitter shows us that it works very well when an incident radially polarized beam, which is generated as a superposition of two mutually orthogonal polarization modes, travels through it. We conclude that this is due to the generation method employed, who probably is based only in a basis set constituted by two mutually-orthogonal Hermite-Gauss polarized modes, without the presence of a couple of two mutually-orthogonal Laguerre-Gauss polarized modes.

Contents

Chapter 1

Introduction

In this thesis, a brief revision of the polarization concepts is presented from a classical point of view, using the optical physics limit. It is studied and described a classification of the polarization of light, the conventional and unconventional polarization. A particular contribution derived from this work, is the presentation of preliminary results associated to the characterization or analysis of some forms of unconventional or spatially non-homogeneous polarization modes with radial symmetry. In this Chapter, we present a general description of study done. In Chapter 2, we present the basic concepts of the conventional polarization of light by describing them with the Jones and the Stokes formalisms. We finish this chapter with the description of the Mueller matrices, which describe the polarization properties of the optical elements. In Chapter 3, it is described the background about the unconventional polarization and some optical systems, which allow us the determination of the polarization modes. The entanglement concept applied to a radially polarized beam mode of light is described in Chapter 4. In Chapters 5 and 6, we describe the experimental setup and the results obtained, respectively. Finally, in Chapter 7, we present the conclusions originated from this work.

The polarization state associated to a beam of light where the amplitude and phase are spatially homogeneous is named conventional polarization. In other words, the polarization state of this beam is independent of the position within the beam's cross section. On the other hand, an unconventional polarized beam is identified as a beam where the polarization state depends of each point within the beam cross section. It is said that the polarization state is spatially non-homogeneous within the beam's cross section but, this beam have a well-defined local polarization state [1]. Depending on the symmetry associated to the cross-section, a given beam can be denoted as azimuthal, radial, spiral or any other form of polarized modes. These general modes usually can be obtained as a linear superposition of more basic polarization modes. For example, a radially polarized Laguerre-Gaussian beam mode can be generated as a superposition of the horizontal and vertical Hermite-Gaussian polarization modes (which are denoted

along this work as HG_{10} and HG_{01} or ψ_{10} and ψ_{01}, respectively), which have horizontal and vertical polarization states, respectively. In this sense, we have an unconventional polarized beam, which carries locally all polarization states at once in a called classically entangled state [1]. This important characteristic of a radially polarized beam allows us to use it in polarimetric applications.

Entanglement is an important concept related with unconventional polarization. Frequently the entanglement phenomenon is related to the quantum mechanical nature (inter-beams entanglement, which is the entanglement between two separated beams). Nevertheless, this phenomenon also appears in classical beams (intra-beams) and it refers to the entanglement between different degrees of freedom (DoFs) of a single beam [1]. Within the radially polarized beam we have that the entanglement is present between the spatial and polarization DoFs. In this sense, the electric field of a radially polarized beam cannot be expressed as the product of a spatial distribution and a polarization [1].

Some polarimetric methods; for example the Ideal Polarimetric Arrangement method (IPA), requires that any polarization state generated be also analyzed after the interaction with the sample under study. That means that, we need to generate at least for classical polarized beams. Each classical polarized beam is used as incident beam on the sample. Once, each beam has interacted with the sample we need to analyze it, in order to know how was modified its polarization. Then, when we use a radially polarized beam as an incident beam on the sample, all polarization states will interact locally with it at once [1]. That represents an important advantage of the unconventional polarization over the conventional polarization. This is an interesting characteristic of a radially polarized beam because by manipulating a specific spatial distribution within the beam, we can get information about a specific polarization state, even more, we can know how was modified a specific polarization state once the beam has interacted with the sample (birefringent transparent sample, for example [1]).

The usual way to modify a given polarization state in the conventional polarization scheme, is by means of devices named retarders or wave plates. A half-wave plate allows the azimuthal rotation of linear polarization states; and, a quarter-wave plate allows the conversion of linear to circular polarization state.

There exist analogous devices within the unconventional polarization scheme, named mode converters. There are two important configurations of mode

converters named $\pi/2 - mode\ converter$ and $\pi - mode\ converter$. The first is used to convert a Laguerre-Gaussian beam polarization mode (which can carry the circular right- or left-handed polarization state) into a Hermite-Gaussian beam polarization mode (horizontal or vertical polarization mode), and conversely. The second converts a diagonal Hermite-Gaussian beam polarization mode (which can carry the +45- or -45-polarization state) into a Hermite-Gaussian beam polarization mode (horizontal or vertical polarization mode). This idea arises from the conversion of the polarization state of a beam by using optical elements such as retarders and polarizers, for example. In this sense, it is possible the conversion of the beam polarization modes with different spatial distributions and, which carry a specific polarization state, into the Hermite-Gaussian beam modes (horizontal and vertical). One important characteristic of such conversion is that the resultant beam mode (horizontal or vertical Hermite-Gaussian beam polarization mode) conserves the polarization state of the original beam mode (Laguerre- Gaussian or diagonal Hermite-Gaussian beam polarization mode). The importance of the horizontal and vertical Hermite-Gaussian polarization modes is that, the superposition of them generates a Laguerre-Gaussian beam mode. In this sense, it is important an optical system, which allows us to split them; this optical device is called transverse-mode beam splitter. This optical system consists of a modified Mach-Zehnder interferometer [1]. At one output of the modified Mach-Zehnder interferometer, we get the horizontal Hermite-Gauss beam mode, and at the other output, we get the vertical Hermite-Gaussian beam mode. In this sense, we can split the spatial distributions, which carry a specific polarization state each of them. So, we can analyze each output beam polarization mode of the modified Mach-Zehnder interferometer. The main idea is determine how was affected the polarization states of an incident radially polarized beam once it interacts with a birefringent transparent sample or any other non-depolarizing system.

Note that we have referred to beam polarization modes or simply polarization modes. This concept describes a specific spatial distribution of the beam's cross section, where the beam has a well defined polarization state.

Chapter 2

Conventional polarization

2.1 Introduction

In this chapter we are going to speak about the basic concepts of the polarization of light. Also, we are going to describe the conventional polarization characteristics and we will describe the conventional polarization states, as well as the conversion and analysis of these polarization states by using specific optical devices. The description and analysis of the conventional polarization states are made by using both the Stokes and the Jones formalisms.

We know that the light represents only a small range on the electromagnetic spectrum, which is located between 380 nm and 780 nm (this information can vary according to the reference used, because some authors consider it is defined between 400 nm and 800 nm). The study of the light has led us to understand it as an electromagnetic wave, that is, an electric field, $\boldsymbol{E}$, which oscillates within a fixed plane (named polarization plane, see figure 1 a), accompanied by a magnetic field, $\boldsymbol{B}$, which oscillates within a fixed plane and, which is perpendicular to the electric field plane and. These fields are traveling in a determinate direction, which is perpendicular to the oscillation planes.

When we speak about light and its interaction with matter, we need to do reference to the Maxwell equations and the constitutive relations (if we are speaking about linear responses), which are written in the International System of Units [2]:

$$\nabla \cdot \boldsymbol{E} = \frac{\rho}{\epsilon_0} \qquad Gauss\ law\ for\ electric\ field, \tag{2.1.1}$$

$$\nabla \cdot \boldsymbol{B} = 0 \qquad Gauss\ law\ for\ magnetic\ field, \tag{2.1.2}$$

$$\nabla \times \boldsymbol{E} = -\frac{\partial \boldsymbol{B}}{\partial t} \qquad Faraday\ law, \tag{2.1.3}$$

$$\nabla \times \boldsymbol{B} = \mu_0 \boldsymbol{J} + \mu_0 \epsilon_0 \frac{\partial \boldsymbol{E}}{\partial t} \qquad Ampere - Maxwell\ law, \tag{2.1.4}$$

Constitutive relations

$$\boldsymbol{D} = \epsilon_0 \boldsymbol{E} + \boldsymbol{P} = \epsilon_0 \boldsymbol{E} + \epsilon_0 \chi \boldsymbol{E} = \epsilon \boldsymbol{E}, \qquad (2.1.5)$$

$$\boldsymbol{B} = \mu_0 (\boldsymbol{H} + \boldsymbol{M}) = \mu_0 (\boldsymbol{H} + \chi_m \boldsymbol{H}) = \mu \boldsymbol{H}, \qquad (2.1.6)$$

$$\boldsymbol{J} = \sigma \boldsymbol{E}. \qquad (2.1.7)$$

where ϵ and μ are the electric permittivity and the magnetic permeability of the medium, respectively, and the subscript 0 is used in order to make reference to the free space. The parameters, χ and χ_m, are the electric and magnetic susceptibilities of the medium, respectively. Finally, σ is the electric conductivity. The vector $\boldsymbol{P} = \chi \epsilon_0 \boldsymbol{E}$ is called the dielectric polarization of medium and it is defined as the average electric dipole moment per unit volume. The magnetization denoted as $\boldsymbol{M} = \chi_m \boldsymbol{H}$ is defined as the average magnetic moment per unit volume.

If we consider an isotropic, homogeneous and non-dispersive medium, in order to simplify the problem, we can obtain the curl for the Faraday's equation and then we can introduce this result in the Ampere-Maxwell's equation, this mathematical development lead us to the general result (by replacing the vector electric field by a general vector field, $\boldsymbol{\Psi}(\boldsymbol{r}, t)$), which is known as the wave equation [2]:

$$\nabla^2 \boldsymbol{\Psi}(\boldsymbol{r}, t) = \frac{1}{v^2} \frac{\partial^2 \boldsymbol{\Psi}(\boldsymbol{r}, t)}{\partial t^2}, \qquad (2.1.8)$$

Where the parameter v denotes the phase velocity of the electromagnetic field in a medium; when this medium is the vacuum then $v = c$ (where c is the velocity of light in the vacuum). Generally, the analysis of the propagation of a given electromagnetic field is developed by using only the electric field; but, we can realize a similar analysis to the magnetic field. In this sense, the general field denoted as $\boldsymbol{\Psi}(\boldsymbol{r}, t)$ can be used to represent both electric and magnetic fields.

From Eq. (2.1.8) we have the wave equations for both electric and magnetic fields in vacuum, which are given by the following equations [2]:

$$\nabla^2 \boldsymbol{E} = \frac{1}{c^2} \frac{\partial^2 \boldsymbol{E}}{\partial t^2}, \qquad (2.1.9)$$

$$\nabla^2 \boldsymbol{H} = \frac{1}{c^2} \frac{\partial^2 \boldsymbol{H}}{\partial t^2}, \qquad (2.1.10)$$

Where, the spatial and temporal dependence have been suppressed in order to have an easy-to-handle equation.

Now, it is known that each component of the electric or magnetic field must satisfy the three-dimensional wave equation, which is given by the following expression [2]:

$$\nabla^2 f = \frac{1}{c^2}\frac{\partial^2 f}{\partial t^2}, \qquad (2.1.11)$$

Where f represent a scalar field. So, we can rewrite Eq. (2.1.11) in terms of electric field as:

$$\nabla^2 E = \frac{1}{c^2}\frac{\partial^2 E}{\partial t^2}, \qquad (2.1.12)$$

One solution of Eq. (2.1.12) is given by the general representation of a simple harmonic plane wave, which is given by the following equation [2]:

$$E = E_0 e^{i(\omega t - \boldsymbol{k}\cdot\boldsymbol{r} + \delta)}, \qquad (2.1.13)$$

Where $\boldsymbol{k}\cdot\boldsymbol{r} - \omega t$, is known as the propagator term, E_0 is the amplitude (real quantity) and δ, is the phase of the electric field. We must remember that only the real part of Eq. (2.1.13) represents a physically measurable quantity, but the complex representation is very useful in order to do several mathematical developments. Also, we have that the complex conjugate of Eq. (2.1.13) is a solution of Eq. (2.1.12).

In this Chapter we are going to describe a fundamental property of light which is directly related with its electric field, the *polarization*. In nature, the light is non-polarized or partially polarized, for instance the sunlight and its reflected light, respectively. That means that both, the electric field amplitude and the phase vary randomly, spatially and temporarily. On the other hand, a polarized light beam is one that has preference either as to transverse direction or as to the handedness associated therewith and, consequently, maintains its constant phase. Specifically, in this Chapter we are going to study conventional polarization of light. We can remember that conventional polarization is associated to spatially homogenous polarization; this means that, if we experimentally determine the polarization state on an arbitrary spatial point within the beam cross section, then this same result must be observed on any other spatial point of the same beam cross section. In this chapter, we will do a treatment and a description of the spatially homogeneous polarization, because it is the fundamental concept used to identify the conventional polarization.

In order to speak clearly about polarization of light we must define a framework. Let us consider a right-handed orthogonal coordinate Cartesian system. We have that polarization is directly related with amplitude, direction and phase values of the electric field vector components, then we will consider that a beam is traveling along the z axis with positive direction, therefore the electric field vector will be contained within the $x - y$ plane (see figure 2.1 a). In this sense, we will consider that we will be located in front of the beam, namely, the wave is traveling toward us. In this way when we refer to right-handed polarization, it is that the electric field vector is rotating clockwise. On the other hand, we will have a left-handed polarization (see figure 2.1 b).

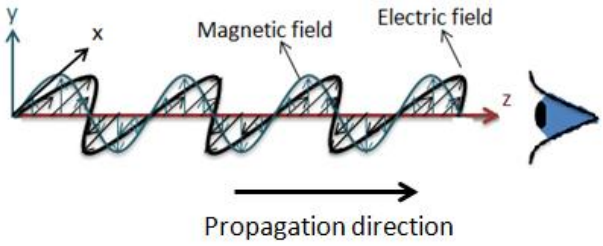

a)

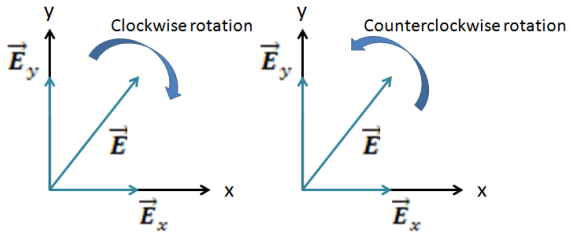

b)

Figure 2.1 a) Graphical representation of an electromagnetic wave and an observer, the wave is traveling toward him. In this figure the polarization plane is the plane that contains the electric field vector and b) transversal view of electric field vector which rotate either clockwise or counterclockwise.

The electric field vector can describe a geometric figure when it moves on the $x - y$ plane, after a period or a wavelength; generally, an ellipse describes this movement. The electric field components for a monochromatic electromagnetic wave (amplitude and phase are constant on time) that travels along the $z - axis$ can be described for the next equations [5]:

$$E_x(z,t) = E_x e^{i(\omega t - kz)}, \qquad (2.1.14)$$

$$E_y(z,t) = E_y e^{i(\omega t - kz)}, \qquad (2.1.15)$$

Where E_x and E_y, are the complex amplitudes for above components, and they are given as [5]:

$$E_x = E_{0x} e^{i\delta_x}, \qquad (2.1.16)$$

$$E_y = E_{0y} e^{i\delta_y}, \qquad (2.1.17)$$

In the above equations E_{0x} and E_{0x}, are real amplitudes and δ_x and δ_y, are the initial spatial phases. Now, if we substitute Eq. (2.1.16) and Eq. (2.1.17) into Eq. (2.1.14) and Eq. (2.1.15), respectively, and we take only the real part and finally we use the next trigonometric identity $cos(\gamma + \varepsilon) = cos(\gamma)\ cos(\varepsilon) - sin(\gamma)\ sin(\varepsilon)$ we get [5]:

$$\frac{E_x}{E_{0x}} = cos(\tau)\ cos(\delta_x) - sin(\tau)\ sin(\delta_x), \qquad (2.1.18)$$

$$\frac{E_y}{E_{0y}} = cos(\tau)\ cos(\delta_y) - sin(\tau)\ sin(\delta_y), \qquad (2.1.19)$$

Where $\tau = \omega t - kz$ is called the *propagator.*

Let's multiply Eq. (2.1.18) by $sin(\delta_y)$ and Eq. (2.1.19) by $-sin(\delta_x)$ and adding both results; and in a similar way, we multiply now Eq. (2.1.18) by $cos(\delta_y)$ and Eq. (2.1.19) by $-cos(\delta_x)$ and by adding those results, we get [5]:

$$\frac{E_x}{E_{0x}} sin(\delta_y) - \frac{E_y}{E_{0y}} sin(\delta_x) = cos(\tau)\, sin(\delta_y - \delta_x), \qquad (2.1.20)$$

$$\frac{E_x}{E_{0x}} cos(\delta_y) - \frac{E_y}{E_{0y}} cos(\delta_x) = sin(\tau)\, sin(\delta_y - \delta_x), \qquad (2.1.21)$$

Finally, squaring Eq. (2.1.20) and Eq. (2.1.21), and adding both results, we get [5]:

$$\frac{E_x^2}{E_{0x}^2} + \frac{E_y^2}{E_{0y}^2} - 2\frac{E_x E_y}{E_{0x} E_{0y}} \cos\delta = sin^2\,\delta, \qquad (2.1.22)$$

Generally, Eq. (2.1.22) represents an ellipse, geometrically; that is called *polarization ellipse*. Here $\delta = \delta_y - \delta_x$, is the phase difference between the initial phases. This allows us to have a representation of classical polarization states on an ellipse inscribed within a rectangle. The sides of this rectangle are parallel to the coordinate axes and have a length of $2E_{0x}$ and $2E_{0y}$, see Fig. 2.2.

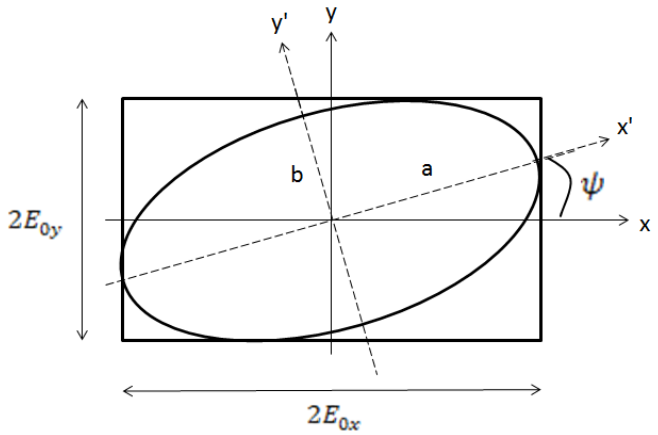

Figure 2.2 Geometrical representation, which describes an electric field vector when it moves on the x-y plane. The ellipse is described at a fixed point, after a period of time.

In this figure we have E_{0x} and E_{0y} are the maximum amplitudes for the $x-$ and $y-$ electric field components, respectively; a and b are the major and minor semiaxes for the ellipse, respectively. Also we can see that Eq. (2.1.22) has a crossed term with the product $E_x E_y$, this term is related with the rotation ellipse by an angle ψ respect to the x axis ($0 \leq \psi \leq \pi$), sometimes it is called *azimuth angle*. This rotation is given as a coordinates system change: $x-y$ to $x'-y'$. Mathematically, we can find that angle 2ψ is given as a function of amplitudes and phase difference δ [5]:

$$tan\, 2\psi = \frac{2E_{0x}\, E_{0y} \cos\delta}{E_{0x}^2 - E_{0y}^2}, 0 \leq \psi \leq \pi, \qquad (2.1.23)$$

Other interesting parameter is the *ellipticity*, $e = \frac{b}{a}$; where we can define the *ellipticity angle* as [5]:

$$tan\, \chi = \frac{\pm b}{a}, \quad -\frac{\pi}{4} \leq \chi \leq \frac{\pi}{4}, \qquad (2.1.24)$$

With a and b defined above. Also, there is another expression that relates the ellipticity angle, 2χ, with the amplitude and phase of the electric field components [5]:

$$sin\, 2\chi = \frac{2E_{0x}\, E_{0y}\, sin\, \delta}{E_{0x}^2 + E_{0y}^2}, \quad -\frac{\pi}{4} \leq \chi \leq \frac{\pi}{4}, \qquad (2.1.25)$$

In this sense, the most general state of polarization of light is *elliptical polarization*. This state is characterized because it presents a lot of possible geometrical shapes, which depend of azimuth and ellipticity values, as well as handedness. The circular

polarization state is a special case and it is obtained when we have the ellipticity value is 1 ($b = a$), also, this polarization state may vary depending its handedness. On the other hand, we have that the linear polarization state is obtained when we have an ellipticity value equal to 0 ($b = 0$). In the following figure we can see the geometrical representation of the polarization states described previously (see figure 2.3).

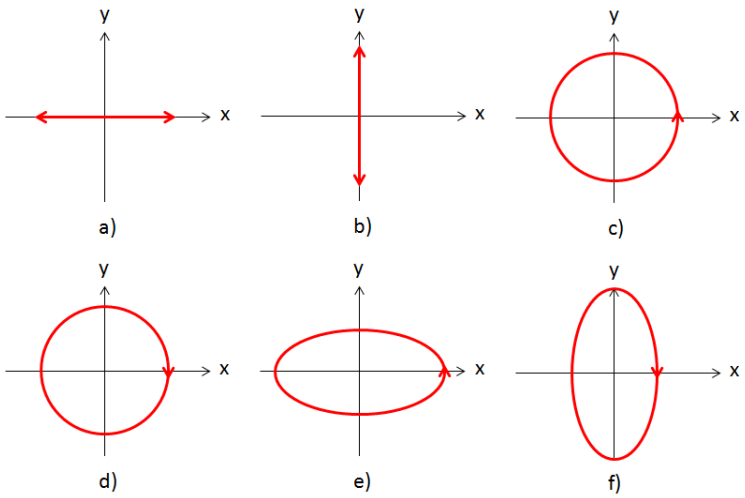

Figure 2.3 Different geometrical representations for a) horizontal polarization state, b) vertical polarization state, c) left-handed circular polarization state, d) right-handed circular polarization state, e) left-handed elliptical polarization state and f) right-handed elliptical polarization state. These geometrical figures are registered at a fixed point, after a period of time, according to an observer looking to the source.

The pairs of polarization states of figure 2.3 (a-b, c-d and e-f) exhibit a peculiar property and this is that each of them represents a pair of mutually orthogonal polarization states. We have that two linear polarized beams are orthogonal if the difference between azimuths is $\frac{\pi}{2}$. Two circular polarized beams are orthogonal if they are opposites about handedness and have the same amplitude. Finally, we have two elliptically polarized beams are orthogonal if the angle between their major semi-axes are equal to $\frac{\pi}{2}$ radians and, also they are opposites about handedness.

The above analysis for polarization states was realized taken into account the ellipticity and azimuth angles, but it can be realized on the other way if we analyze equations (2.1.14), (2.1.15) and (2.1.22) directly:

1. Horizontal and vertical polarization states.

We have a horizontal polarization state when the vertical component of the electric field vector is null, this means that, $E_{0y} = 0$, therefore $E_y = 0$. In this case we only have the horizontal component:

$$E_x(z,t) = E_x e^{i(\omega t - kz)}, \qquad (2.1.26)$$

We have a vertical polarization state, when the horizontal component for electric field vector is zero, $E_{0x} = 0$, therefore $E_x = 0$. So that we only have the vertical component:

$$E_y(z,t) = E_y e^{i(\omega t - kz)}, \qquad (2.1.27)$$

2. Linear $+45$ degrees and -45 degrees polarization states.

In this case, we consider two values for phase the difference $\delta = 0$ and $\delta = \pi$, from this we have that $sin\,\delta = 0$ and $cos\,\delta = 1, -1$; respectively. Therefore Eq. (2.1.22) can be written as:

$$\frac{E_x^2}{E_{0x}^2} + \frac{E_y^2}{E_{0y}^2} \pm 2\frac{E_x E_y}{E_{0x}E_{0y}} = 0, \qquad (2.1.28)$$

We can write this expression as:

$$\left(\frac{E_x}{E_{0x}} \pm \frac{E_y}{E_{0y}}\right)^2 = 0 \qquad \rightarrow \qquad E_y = \pm\left(\frac{E_{0y}}{E_{0x}}\right)E_x, \qquad (2.1.29)$$

The last expression represents the line equation, $y = mx$, with its slope $m = \pm\left(\frac{E_{0y}}{E_{0x}}\right)$. Hence, when we have $m = 1$, we refer to $\delta = 0$ and that led us to have a linear $+45$ polarization state:

$$E_y = E_x, \qquad (2.1.30)$$

The other situation is given when $m = -1$, which implies $\delta = \pi$ and therefore we have a linear -45 polarization state:

$$E_y = -E_x, \qquad (2.1.31)$$

3. Right- and left- handed circular polarization states.

Now we will consider the case for which $E_{0y} = E_{0x} = E_0$, taken into account two values for δ: $\frac{\pi}{2}$ and $\frac{3}{2}\pi$. With this values we have that $cos\,\delta = 0$ and $sin\,\delta = 1, -1$; respectively. Then, equation 2.1.22 can be written as:

$$\frac{E_x^2}{E_0^2} + \frac{E_y^2}{E_0^2} = 1, \qquad (2.1.32)$$

Given that the sum of two positive numbers never will give result negative. This is an equation for a circle of radius 1. Then we can say that this is the representation for circular left- and right- handed polarization states, respectively. Note that in this case, we can not specify the respective correspondence between handedness and values $\delta = \frac{\pi}{2}$ and $\delta = \frac{3}{2}\pi$.

4. Elliptical right and left polarization states.

In this case we will consider $\delta = \frac{\pi}{2}$ and $\delta = \frac{3}{2}\pi = -\frac{\pi}{2}$. This led us to have $cos\,\delta = 0$ and $sin\,\delta = 1, -1$, respectively. The amplitudes, E_{0x}^2 and E_{0y}^2, take different values between them ($E_{0x}^2 \neq E_{0y}^2$). Therefore the Eq. (2.1.22) is reduced to:

$$\frac{E_x^2}{E_{0x}^2} + \frac{E_y^2}{E_{0y}^2} = 1, \qquad (2.1.33)$$

This is the equation for a horizontal or vertical ellipse (depending on the values associated to the terms E_{0x}^2 and E_{0y}^2). In this case, we cannot differentiate between both cases: $\delta = \frac{\pi}{2}$ and $\delta = \frac{3}{2}\pi$.

Generally, the polarization state of a beam of light is changed once the beam interacts with matter; this behavior is due to the presence of anisotropies within the matter. As a matter of fact, even if the polarized beam is reflected by a flat homogeneous and isotropic surface, the reflected beam changes its polarization state due to the symmetry breaking at the interface defined between the incident and the reflected surface. The matter induces a change in the polarization state of an incident beam by changing its amplitude, direction of propagation or the relative phase between the electric field components, as well as, by transferring energy from polarized states to the un-polarized state [5].

An optical device, which changes the polarization state of an incident beam of light by changing the amplitude of the electric field components, is called *diattenuator*

or *polarizer*. A polarizer is defined as an optical device, which produces an appreciably polarized beam of light once a non-polarized beam of light travel through it. The polarizers can be classified according to the principle of operation as dichroic, birefringent, and by reflection. According to the polarization state we can have linear, circular or elliptical polarizers. For example, a linear polarizer is one that, given non-polarized light as superposition of two linear polarization states, enables the transmission of only one of them (see figure 2.4).

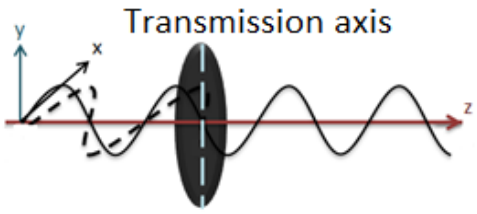

Figure 2.4 Scheme for a linear polarizer, in this case its transmission axis is parallel to the y axis.

The orientation of the state polarization that travels through a linear polarizer is parallel to a specific direction on it, this direction is called *transmission axis* of the linear polarizer (perpendicular to it is the extinction axis). An important parameter for this optical device is the *extinction coefficient*. This concept is related with the attenuation capability to extinguish a component along the extinction axis; it is expressed as a ratio between the transmittance of an incident linear polarization parallel to the transmission axis and an incident linear polarization perpendicular to the transmission axis. Then, a higher ratio means a higher quality; for example, calcite-based linear polarizers have an extinction ratio of 100,000: 1; while a typical commercial dichroic film have a ratio of 100:1. A polarizer also can be employed as an analyzer; it is a device which analyzes the linear polarization state for an incident beam. This can be easily tested by putting a non-polarized source followed by a linear polarizer, and finally we put an analyzer. If we employ a detector intensity device, accordingly as we rotate the analyzer, the intensity varies in accordance with *Malus Law* [5]:

$$I(\theta') = I(0)cos^2\,(\theta'), \qquad (2.1.34)$$

Where θ' is the angle, between polarizer and analyzer transmission axes; and $I(0)$ is the maximum intensity, which is obtained when both transmission axes are parallel one respect to the other.

A *retarder* (which also is known as *dephaser* or *wave plate*) is another optical element, which retards the phase of one electric field component, respect to the

other, generating an output polarization state which differs from the incident polarization state. A retarder, frequently, is a plate constructed of birefringent materials. This plate is cutted so that it has two orthogonal axes, one of them with a smaller refractive index than the other, it is called fast axis (the light travels faster along this than the other). The other axis is called *slow axis*. The amount of delay of one component respect to the other is named *retardance*, and it is an important parameter for these optical elements. Depending on the retardance, α, we can have different types of retarders, the most known are quarter-wave plates ($\alpha = \frac{\pi}{2}$) and half-wave plates ($\alpha = \pi$).

We can get different polarization states employing optical elements adequately, for instance, we can employ retarders in order to produce different polarization states, from non-polarized or polarized light sources. These configurations are called *polarization states generators* (PSG). We are going to describe them in the following points in this chapter. In figure 4, we can see different polarization states for some azimuth values.

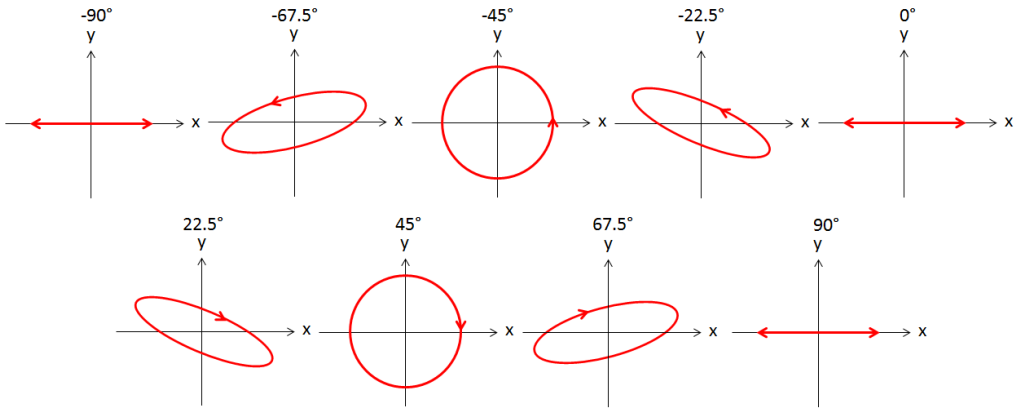

Figure 2.5 Different polarization states for some azimuth values ($-90°$ to $90°$, upper title of each figure) after an incident beam with horizontal polarization travels through a quarter-wave plate.

When the polarization change is given by a change in the direction of the orthogonal electric field components, actually, we make reference to a coordinate transformation. Later, we are going to see that this polarization change can be related with a physical rotation of the principal axis of any optical element, such as a polarizer or a retarder. Finally, we have that the optical element, which change the polarization of an incident beam of light by transferring energy from polarized states to the un-polarized state is called *depolarizer*. This optical device reduces the amount of polarization uniformly, of an incident beam of light. This reduction depends of the incident beam polarization [5].

2.2 Jones formalism

The Jones formalism refers to a mathematical tool developed by physicist R. Clark Jones [5]; it describes polarization characteristics employing amplitudes and phases through a complex notation. This tool allows us to represent the polarization state of a beam by using a 2x1 column matrix, which is called *the Jones vector*; also, it allow us to represent the linear optical properties of an optical element by using a 2x2 matrix, which is called *the Jones matrix*. The Jones formalism has some disadvantages respect to the Stokes formalism (described below), one of them is that the Jones formalism uses a complex notation in order to describe optical phenomena. The Jones formalism is used when we describe totally polarized phenomena, as well as, amplitude superposition problems.

From equations (2.1.16) and (2.1.17), we can write the Jones vector for an elliptically polarized beam as [5]:

$$\boldsymbol{E} = \begin{pmatrix} E_x \\ E_y \end{pmatrix} = \begin{pmatrix} E_{0x} e^{i\delta_x} \\ E_{0y} e^{i\delta_y} \end{pmatrix}, \qquad (2.2.1)$$

Where E_x and E_y are the complex amplitudes of the components of the electric field, see figure 2.6; E_{0x} and E_{0y} are the real amplitudes for each electric field component and, they are real quantities; δ_x and δ_y are the initial phase of the electric field components.

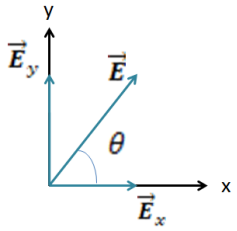

Figure 2.6 Components of an electric field rotated by an arbitrary angle θ.

If we consider that $\delta = \delta_y - \delta_x$, so that, $\delta_y = \delta_x + \delta$, then we can rewrite Eq. (2.2.1) as [5]:

$$\boldsymbol{E} = \begin{pmatrix} E_{0x} e^{i\delta_x} \\ E_{0y} e^{i(\delta_x + \delta)} \end{pmatrix} = \begin{pmatrix} E_{0x} \\ E_{0y} e^{i\delta} \end{pmatrix} e^{i\delta_x}, \qquad (2.2.2)$$

Since Eq. (2.2.1) we can get the intensity as [5]:

$$I = \boldsymbol{E}^{\dagger} \cdot \boldsymbol{E}, \qquad (2.2.3)$$

Where $\boldsymbol{E}^{\dagger}$ is the adjunct of the Jones vector, which is given as: $(E_x^* \quad E_y^*)$. So, the intensity is calculated as [5]:

$$I = (E_x^* \quad E_y^*)\begin{pmatrix} E_x \\ E_y \end{pmatrix} = E_{0x}^2 + E_{0y}^2 = E_0^2, \qquad (2.2.4)$$

Also, the Jones vector can be written in normalized form when it is fulfilled, through the following equation: $E_0^2 = \boldsymbol{E}^{\dagger} \cdot \boldsymbol{E} = 1$.

If we consider that $\delta_x = 0$ (without losing generality), we have that equation 2.2.2 can be written as [5]:

$$\boldsymbol{E} = \begin{pmatrix} E_{0x} \\ E_{0y}e^{i\delta} \end{pmatrix}, \qquad (2.2.5)$$

This equation represents an elliptical polarization state of light (the most general polarization state). Given this general form, we can describe some specific totally polarized states of light:

1. Jones vector for horizontal and vertical polarization states ($p-$ and $s-$ polarization states).

From Eq. (2.2.5), when we consider that the y component is equal to zero, we have the Jones vector to horizontal polarization state:

$$\boldsymbol{E}_h = \begin{pmatrix} E_{0x} \\ 0 \end{pmatrix}, \text{ applying the normalized condition we have } \boldsymbol{E}_h = \begin{pmatrix} 1 \\ 0 \end{pmatrix}, \qquad (2.2.6)$$

Similarly, we can write the Jones vector to vertical polarization state of light as:

$$\boldsymbol{E}_v = \begin{pmatrix} 0 \\ E_{0y} \end{pmatrix}, \text{ applying the normalized condition we have } \boldsymbol{E}_v = \begin{pmatrix} 0 \\ 1 \end{pmatrix}, \qquad (2.2.7)$$

We must remember that $\delta = 0$ for linear polarization states.

2. Jones vector for linear $+45$ and -45 polarization states.

Given that $\delta = 0$ and taking into account that in this case $E_{0x} = E_{0y} = E_0$, we can write the Jones vector to $+45$-polarization state:

$$\boldsymbol{E}_+ = \begin{pmatrix} E_0 \\ E_0 \end{pmatrix}, \text{ applying the normalized condition we have } \boldsymbol{E}_+ = \frac{1}{\sqrt{2}}\begin{pmatrix} 1 \\ 1 \end{pmatrix}, \qquad (2.2.8)$$

In the other case we have that $E_{0x} = -E_{0y}$. So, we can write the Jones vector to-45-polarization state:

$\boldsymbol{E}_{-} = \begin{pmatrix} E_{0x} \\ -E_{0x} \end{pmatrix}$, applying the normalized condition we have $\boldsymbol{E}_{-} = \frac{1}{\sqrt{2}}\begin{pmatrix} 1 \\ -1 \end{pmatrix}$, (2.2.9)

3. Jones vector for circular right- and left- handed polarization states.

For both circular polarization states it must be fulfilled that $E_{0x} = E_{0y} = E_0$.

Now when we consider a circular right-handed polarization state we have that $\delta = \frac{\pi}{2}$, therefore we can write its Jones vector as:

$\boldsymbol{E}_r = \begin{pmatrix} E_0 \\ E_0 e^{i\frac{\pi}{2}} \end{pmatrix}$, applying the normalized condition we have $\boldsymbol{E}_r = \frac{1}{\sqrt{2}}\begin{pmatrix} 1 \\ i \end{pmatrix}$, (2.2.10)

For circular left-handed polarization state we have that $\delta = -\frac{\pi}{2}$, and then the Jones vector is written as:

$\boldsymbol{E}_l = \begin{pmatrix} E_0 \\ E_0 e^{-i\frac{\pi}{2}} \end{pmatrix}$, applying the normalized condition we have $\boldsymbol{E}_l = \frac{1}{\sqrt{2}}\begin{pmatrix} 1 \\ -i \end{pmatrix}$, (2.2.11)

Now, we can speak about Jones matrices of polarizing elements. In general, it is assumed a linear relation between the incident and the emerging beams, once the incident beam has traveled through the polarizing element. Mathematically, this relation can be written as [5]:

$$\begin{pmatrix} E'_x \\ E'_y \end{pmatrix} = \begin{pmatrix} j_{xx} & j_{xy} \\ j_{yx} & j_{yy} \end{pmatrix}\begin{pmatrix} E_x \\ E_y \end{pmatrix}, \quad (2.2.12)$$

Where the symbol (') refers to output beam and, the elements j_{op} (with $o, p = x, y$) are transforming factors. The 2x2 matrix:

$$\boldsymbol{J} = \begin{pmatrix} j_{xx} & j_{xy} \\ j_{yx} & j_{yy} \end{pmatrix}, \quad (2.2.13)$$

It is known as Jones matrix of optical polarizing elements [5].

For example, we can characterize the effect on an incident beam by a linear polarizer as [5]:

$$\begin{pmatrix} E'_x \\ E'_y \end{pmatrix} = \begin{pmatrix} p_x & 0 \\ 0 & p_y \end{pmatrix}\begin{pmatrix} E_x \\ E_y \end{pmatrix}, \quad (2.2.14)$$

In this case $j_{xx} = p_x, j_{yy} = p_x$ and $j_{xy} = j_{yx} = 0$. Here p_x and p_y refer to transmission or attenuation coefficients. This is, $p_{x,y} = 0$ means complete

attenuation and $p_{x,y} = 1$ means complete transmission. So that $0 \leq p_{x,y} \leq 1$, therefore the Jones matrix for the linear polarizer is given as [5]:

$$\boldsymbol{J}_P = \begin{pmatrix} p_x & 0 \\ 0 & p_y \end{pmatrix}, \qquad (2.2.15)$$

In this sense, we can determine the Jones matrices for both horizontal and vertical (it refers to its transmission axis position respect to the horizontal plane, in this case the holographic table) linear polarizers. When we consider only a total transmission along the $x - direction$ ($p_x = 1$ and $p_y = 0$), then we have the Jones matrix of a horizontal linear polarizer (ideal case), which is given as [5]:

$$\boldsymbol{J}_{PH} = \begin{pmatrix} 1 & 0 \\ 0 & 0 \end{pmatrix}, \qquad (2.2.16)$$

For a vertical linear polarizer the total transmission is along the y$-direction$ ($p_x = 0$ and $p_y = 1$), in this case we have the Jones matrix of a vertical linear polarizer (ideal case), which is given as [5]:

$$\boldsymbol{J}_{PV} = \begin{pmatrix} 0 & 0 \\ 0 & 1 \end{pmatrix}, \qquad (2.2.17)$$

The retarders are other important polarizing elements. A retarder induces a total phase shift α between the orthogonal electric field components, which is known as retardance. The Jones matrix for a retarder (which has a retardance of α) is given by the following equation [5]:

$$\boldsymbol{J}_R(\alpha) = \begin{pmatrix} e^{i\frac{\alpha}{2}} & 0 \\ 0 & e^{-i\frac{\alpha}{2}} \end{pmatrix}, \qquad (2.2.18)$$

So, the Jones matrix of the quarter wave plate (retarder, which has a retardance of $\alpha = \frac{\pi}{2}$) and the Jones matrix of a half wave plate ($\alpha = \pi$) are given by the following equations [5]:

$$\boldsymbol{J}_R\left(\frac{\pi}{2}\right) = e^{i\frac{\pi}{4}} \begin{pmatrix} 1 & 0 \\ 0 & -i \end{pmatrix}, \qquad (2.2.19)$$

$$\boldsymbol{J}_R(\pi) = i \begin{pmatrix} 1 & 0 \\ 0 & -1 \end{pmatrix}, \qquad (2.2.20)$$

In practice, it is important to know the Jones matrices of specific optical elements, which have their principal axis located at a fixed angle θ, respect to the horizontal plane. In this sense, the rotation matrix is very useful. This is defined as [5]:

$$\boldsymbol{J}_{Rot}(\theta) = \begin{pmatrix} cos\ \theta & sin\ \theta \\ -sin\ \theta & cos\ \theta \end{pmatrix}, \qquad (2.2.21)$$

When we need to obtain the Jones matrix of a specific polarizing element rotated by an angle θ respect to the horizontal plane, then we must to use the rotation transformation, which is given by the following equation [5]:

$$\boldsymbol{J}' = \boldsymbol{J}_{Rot}(-\theta)\boldsymbol{J}\boldsymbol{J}_{Rot}(\theta), \qquad (2.2.22)$$

Where, $\boldsymbol{J}$ is the Jones matrix of the polarizing element and $\boldsymbol{J}'$ is the Jones matrix rotated by an angle of θ respect to the horizontal plane.

We can obtain the Jones matrix of a linear polarizer and the Jones matrix of a retarder (with a retardance of α), which are located at an angle of θ (respect to the horizontal plane), by applying the rotation matrix in both cases [5]:

$$\boldsymbol{J}_P(\theta) = \begin{pmatrix} p_x cos^{\,2}\theta + p_y sin^{\,2}\theta & (p_x - p_y)\sin\theta\cos\theta \\ (p_x - p_y)\sin\theta\cos\theta & p_x sin^{\,2}\theta + p_y cos^{\,2}\theta \end{pmatrix}, \qquad (2.2.23)$$

$$\boldsymbol{J}_R(\alpha,\theta) = \begin{pmatrix} e^{i\frac{\alpha}{2}} cos^{\,2}\theta + e^{-i\frac{\alpha}{2}} sin^{\,2}\theta & \left(e^{i\frac{\alpha}{2}} - e^{-i\frac{\alpha}{2}}\right) sin\,\theta\,cos\,\theta \\ \left(e^{i\frac{\alpha}{2}} - e^{-i\frac{\alpha}{2}}\right) sin\,\theta\,cos\,\theta & e^{i\frac{\alpha}{2}} sin^{\,2}\theta + e^{-i\frac{\alpha}{2}} cos^{\,2}\theta \end{pmatrix}, \qquad (2.2.24)$$

From Eqs. (2.2.23 and 2.2.24), we can obtain particular Jones matrices, for instance, the Jones matrix for an ideal linear polarizer with its principal axis located at an angle of θ and the Jones matrix of the quarter and half wave plates with their axis tilted by an angle θ, respectively; etc.

2.3 Stokes formalism

If we remember, the polarization is a phenomenon, which is described essentially by the electric field. Also, we must remember that the intensity of light is a measurable quantity, which is given as the square of electric field module; in this sense, we have that the polarization state of a beam of light can be expressed in terms of intensities (time-averaged intensity, properly speaking). In 1852 the mathematician and physicist G. G. Stokes developed an experimental procedure, which allows us to determinate the polarization state of a beam from direct measurements of intensity on the light beam under study. The Stokes formalism allows the representation of non- and partial-polarized light, as well as, total polarized light; also in this representation, we can express monochromatic and non-monochromatic beams. The Stokes formalism is very useful in order to describe intensity superposition problems.

So any beam of light (treated as plane wave) can be described by four parameters, which are known as *the Stokes parameters*. These parameters are given in order to describe a monochromatic beam specifically (given that a monochromatic beam is constant in both amplitude and phase), in this manner we simplify the problem but do not lose its generality. Considering Eq. 2.1.22, but in this case we take into account the average over the time of observation [5]:

$$\frac{\langle E_x^2(t)\rangle}{E_{0x}^2}+\frac{\langle E_y^2(t)\rangle}{E_{0y}^2}-2\frac{\langle E_x(t)E_y(t)\rangle}{E_{0x}E_{0y}}\cos\delta=sin^2\,\delta, \qquad (2.3.1)$$

We can see that, generally, E_{0x} and E_{0x} are implicitly dependent on time. The next equation is employed in order to get the average over time [5]:

$$\langle E_i(t)E_j(t)\rangle=\lim_{\mathrm{T}\to\infty}\frac{1}{\mathrm{T}}\int_0^{\mathrm{T}}E_i(t)E_j(t)\;dt \qquad i,j=x,y, \qquad (2.3.2)$$

Here it is considered the average over a period of oscillation given the periodicity of $E_x(t)$ and $E_y(t)$. If we multiply Eq. (2.3.1) by $4E_{0x}^2E_{0y}^2$ we get [5]:

$$4E_{0y}^2\langle E_x^2(t)\rangle+4E_{0x}^2\langle E_y^2(t)\rangle-8E_{0x}E_{0y}\langle E_x(t)E_y(t)\rangle\,cos\,\delta=(2E_{0x}E_{0y}\sin\delta)^2, \qquad (2.3.3)$$

Once we calculate $\langle E_x^2(t)\rangle=\frac{1}{2}E_{0x}^2$, $\langle E_y^2(t)\rangle=\frac{1}{2}E_{0y}^2$ and $\langle E_x(t)E_y(t)\rangle=\frac{1}{2}E_{0x}E_{0y}\cos\delta$ by using Eq. (2.3.2), and before its substitution into Eq. (2.3.3), we complete the perfect square by adding and subtracting the quantity E_{0x}^4+E_{0y}^4 to the left-hand side of Eq. (2.3.3), we get [5]:

$$2E_{0y}^2E_{0x}^2+2E_{0x}^2E_{0y}^2-(2E_{0x}E_{0y}\,cos\,\delta)^2+E_{0x}^4+E_{0y}^4-E_{0x}^4-E_{0y}^4=(2E_{0x}E_{0y}\sin\delta)^2, \qquad (2.3.4)$$

In this way we can get:

$$\left(E_{0x}^2+E_{0y}^2\right)^2-\left(E_{0x}^2-E_{0y}^2\right)^2-\left(2E_{0x}E_{0y}\,cos\,\delta\right)^2=\left(2E_{0x}E_{0y}\,sin\,\delta\right)^2$$

$$s_0^2-s_1^2-s_2^2=s_3^2, \qquad (2.3.5)$$

From Eq. (2.3.5) we can get the Stokes parameters [5]:

$$s_0=E_xE_x^*+E_yE_y^*=E_{0x}^2+E_{0y}^2, \qquad (2.3.6)$$

$$s_1=E_xE_x^*-E_yE_y^*=E_{0x}^2-E_{0y}^2, \qquad (2.3.7)$$

$$s_2=E_xE_y^*+E_yE_x^*=2E_{0x}E_{0y}\,cos\,\delta, \qquad (2.3.8)$$

$$s_3 = i\left(E_x E_x^* - E_y E_y^*\right) = 2E_{0x}E_{0y}\,sin\,\delta, \qquad (2.3.9)$$

This representation is very helpful in order to represent totally, partially, and non-polarized states of light, in both cases: as a function of electric field components and their conjugate complex; and as a function of amplitude and phase.

The first parameter, s_0, represents total intensity of beam and the other three parameters are related with the polarization state of the beam. s_1 describes the predominance of horizontal polarization state, s_2 describes the tendency of linear $+45$ polarization state and s_3 describes the predominance of circular right-handed polarization state. All Stokes parameters represent observables; this means that they are real quantities.

An important relation that the Stokes parameters obey is the following. It describes totally polarized and partially polarized (or un-polarized) light. The inequality of the following equation is related with partially or un-polarized light. We have that Eqs. (2.3.6) through (2.3.9) also describe partially polarized light for short time intervals. On the other hand, the equality is related with totally polarized light [5].

$$s_0^2 \geq s_1^2 + s_2^2 + s_3^2, \qquad (2.3.10)$$

Now, it exist a specific form to arrange the Stokes parameters like a column vector (though some authors do not consider it as a vector, mathematically speaking, given that Stokes vector does not have any direction, only magnitude), this is known as Stokes vector [5]:

$$\boldsymbol{S} = \begin{pmatrix} s_0 \\ s_1 \\ s_2 \\ s_3 \end{pmatrix} = \begin{pmatrix} E_{0x}^2 + E_{0y}^2 \\ E_{0x}^2 - E_{0y}^2 \\ 2E_{0x}E_{0y}\,cos\,\delta \\ 2E_{0x}E_{0y}\,sin\,\delta \end{pmatrix}, \qquad (2.3.11)$$

Other way to represent a Stokes vector is employing its normalized form; this is obtained when we divide each vector element over the first element. Also, we have that two Stokes vectors are orthogonal if their second, third and fourth elements have opposite sign. Finally, it is important to mention an interesting principle: the principle of Stokes' optical equivalence. This principle says that, if two beams have the same Stokes vector then, it is said that these beams are indistinguishable as regards intensity, degree of polarization, and polarization state.

From the Eq. (2.3.11), we can consider special cases in order to write the Stokes vector for specific polarization states:

1. Stokes vectors for horizontal and vertical polarization states.

For a horizontal polarization state, we know that $E_{0y} = 0$, given this condition then we can write the Stokes vector as:

$$\boldsymbol{S}_h = \begin{pmatrix} E_{0x}^2 \\ E_{0x}^2 \\ 0 \\ 0 \end{pmatrix}, \text{if we normalize it, we have } \boldsymbol{S}_h = \begin{pmatrix} 1 \\ 1 \\ 0 \\ 0 \end{pmatrix}, \qquad (2.3.12)$$

For vertical polarization state, we have that $E_{0x} = 0$. Then the Stokes vector is given as:

$$\boldsymbol{S}_v = \begin{pmatrix} E_{0y}^2 \\ -E_{0y}^2 \\ 0 \\ 0 \end{pmatrix}, \text{if we normalize it, we have } \boldsymbol{S}_v = \begin{pmatrix} 1 \\ -1 \\ 0 \\ 0 \end{pmatrix}, \qquad (2.3.13)$$

2. Stokes vectors for linear $+45$ and -45 polarization states.

A linear $+45$ polarization state is being obtained when we have the next conditions: $E_{0x} = E_{0y} = E_0$, and $\delta = 0$. It led us to the next Stokes vector:

$$\boldsymbol{S}_+ = \begin{pmatrix} 2E_0^2 \\ 0 \\ 2E_0^2 \\ 0 \end{pmatrix}, \text{if we normalize it, we have } \boldsymbol{S}_+ = \begin{pmatrix} 1 \\ 0 \\ 1 \\ 0 \end{pmatrix}, \qquad (2.3.14)$$

Now, the conditions for linear -45 polarization state are: $-E_{0x} = E_{0y}$ and $\delta = 0$. Therefore we have the Stokes vector:

$$\boldsymbol{S}_- = \begin{pmatrix} 2E_{0x}^2 \\ 0 \\ -2E_{0x}^2 \\ 0 \end{pmatrix}, \text{if we normalize it, we have } \boldsymbol{S}_- = \begin{pmatrix} 1 \\ 0 \\ -1 \\ 0 \end{pmatrix}, \qquad (2.3.15)$$

3. Stokes vectors for circular right- and left- handedned polarization states.

We know that a circular right-handed polarization state has the next characteristics: $E_{0x} = E_{0y} = E_0$ and $\delta = \frac{\pi}{2}$. With those values we get its Stokes vector is given as:

$$\boldsymbol{S}_{right} = \begin{pmatrix} 2E_0^2 \\ 0 \\ 0 \\ 2E_0^2 \end{pmatrix}, \text{if we normalize it, we have } \boldsymbol{S}_{right} = \begin{pmatrix} 1 \\ 0 \\ 0 \\ 1 \end{pmatrix}, \qquad (2.3.16)$$

For a circular left-handed polarization state the conditions are: $E_{0x} = E_{0y} = E_0$ and $\delta = -\frac{\pi}{2}$. Therefore, we get its Stokes vector:

$$\boldsymbol{S}_{left} = \begin{pmatrix} 2E_0^2 \\ 0 \\ 0 \\ -2E_0^2 \end{pmatrix}, \text{if we normalize it, we have } \boldsymbol{S}_{left} = \begin{pmatrix} 1 \\ 0 \\ 0 \\ -1 \end{pmatrix}, \qquad (2.3.17)$$

4. Stokes vectors for elliptical right- and left-handed polarization states.

In a general case, when all elements of the Stokes vector have arbitrary values, we can differentiate between elliptical right- and left- handed polarization states [5]:

$$\boldsymbol{S}_{ellip} = \begin{pmatrix} E_{0x}^2 + E_{0y}^2 \\ E_{0x}^2 - E_{0y}^2 \\ 2E_{0x}E_{0y}\, cos\, \delta \\ 2E_{0x}E_{0y}\, sin\, \delta \end{pmatrix}, \text{if we normalize it, we have } \boldsymbol{S}_{ellip} = \begin{pmatrix} 1 \\ \mathrm{a} \\ \mathrm{b} \\ \mathrm{c} \end{pmatrix}, \qquad (2.3.18)$$

Where $a = \frac{E_{0x}^2 - E_{0y}^2}{E_{0x}^2 + E_{0y}^2}$, $b = \frac{2E_{0x}E_{0y}\, cos\, \delta}{E_{0x}^2 + E_{0y}^2}$ and $c = \frac{2E_{0x}E_{0y}\, sin\, \delta}{E_{0x}^2 + E_{0y}^2}$. Also, $a^2 + b^2 + c^2 = 1$.

It is said that we have an elliptical right-handed polarization state when $c > 0$ and a left-handed polarization state if $c < 0$.

5. Partially- and non-polarized light

We must remember that one of the main goals of G. G. Stokes' was to describe mathematically non-polarized light. He observed that, non-polarized light was not affected by rotation of transmission axis of a linear polarizer neither by interaction with a retarder. Therefore he observed that $s_1 = s_2 = s_3 = 0$; then he concluded that those parameters were related with the polarizing behavior of light. In this way the Stokes vector which denotes non-polarizer light, $\boldsymbol{S}_{un}$, is given as [5]:

$$\boldsymbol{S}_{un} = \begin{pmatrix} E_{0x}^2 + E_{0y}^2 \\ 0 \\ 0 \\ 0 \end{pmatrix}, \text{if we normalize it, we have } \boldsymbol{S}_{un} = \begin{pmatrix} 1 \\ 0 \\ 0 \\ 0 \end{pmatrix}, \qquad (2.3.19)$$

Now, from Eq. (2.3.10) we said that a totally polarized light can be described by equation $s_0^2 = s_1^2 + s_2^2 + s_3^2$, these polarization states are linear, circular and elliptical. On the other hand, we said that non-polarized light is represented by the Stokes vector, $\boldsymbol{S}_{un}$, this vector must fulfills that $s_0 > 0$ and $s_1 = s_2 = s_3 = 0$. The above cases correspond to opposite polarization states of light (totally and non-polarized light). There exist an intermediate case; called *partially polarized light*. Thus, Eq. (2.3.10) can describe all cases when we put the adequate symbol: $s_0^2 = s_1^2 + s_2^2 + s_3^2$represents totally polarized light; $s_0^2 > s_1^2 + s_2^2 + s_3^2$ with $s_1 = s_2 = s_3 = 0$, represents non-polarized light; and finally, $s_0^2 > s_1^2 + s_2^2 + s_3^2$ represents partially polarized light.

Finally, if the total intensity of beam is zero, then, it is said that we have absence of light, which is represented by a Stokes vector as [5]:

$$\boldsymbol{S}_{zero} = \begin{pmatrix} 0 \\ 0 \\ 0 \\ 0 \end{pmatrix}, \qquad (2.3.20)$$

We can see that it is possible describe any beam of light (non-, partially or totally polarized beam) employing the Stokes vectors. This representation has many advantages; one of them is that any Stokes vector can be determined from the measurements. Above, it was shown the representation of Stokes vectors for ideal cases; now, we must take into account a description of real sources which we call *test source* (these sources can be considered non-, partially- and totally-polarized, but in most real cases they fluctuate on time and they are not polarized ideally) and we will speak about experimental methods employed to measure the Stokes parameters. Basically, this method requires a linear polarizer (LP), a quarter wave plate (QWP) and a photo detector (PD); in figure 5 we can see that the polarization state analyzer (consists) consists of a QWP and a LP:

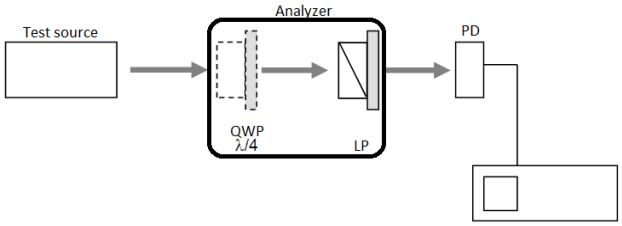

Figure 2.6 Experimental setup, which is used to measure the Stokes parameters associated to an arbitrary source of light. The polarization state analyzer (PSA) consists of a QWP and a LP.

The general procedure consist of measuring the intensity at different orientations of the fast and the transmission axes associated to the quarter wave-plate and the linear polarizer, respectively, according to the following relationships [4]:

$$s_0 = I_{0^\circ} + I_{90^\circ}, \qquad (2.3.21)$$

$$s_1 = I_{0^\circ} - I_{90^\circ}, \qquad (2.3.22)$$

$$s_2 = I_{+45^\circ} - I_{-45^\circ}, \qquad (2.3.23)$$

$$s_3 = I_{right} - I_{left}, \qquad (2.3.24)$$

Generally, the determination of the linear polarization states (horizontal, vertical, $+45$ and -45 polarization states) can be realized by using only a LP as an analyzer with its transmission axis oriented at $0°$, $90°$, $+45°$ and $-45°$, respectively. For instance, when we test for the existence of horizontal polarization contribution, it is sufficient to employ a LP with its transmission axis parallel to the holographic table (taken into account that our coordinate system is referred to a holographic table) as an analyzer. Now, to test for the existence of circular right- and left-handed polarization states, it is possible employ a PSG (described in Section 2.1) operated properly.

In this sense, we can define an important polarization concept as a function of Stokes parameters, the degree of polarization (DoP); it defines the percentage of polarized light into a beam [4].

$$0 \leq DoP = \frac{\sqrt{s_1^2+s_2^2+s_3^2}}{s_0} \leq 1, \qquad (2.3.25)$$

Other representation for *DoP*, is given as [5]:

$$DoP = \frac{I_{pol}}{I_{tot}}, \qquad (2.3.26)$$

Where, I_{tot} is the total intensity and I_{pol} is the polarized intensity of the beam. In this way, when *DoP* is equal to 0, we have a non-polarized beam; if *DoP* is equal to 1, we have a totally polarized beam, and if *DoP* is a value between 0 and 1, we have a partially polarized beam. With this in mind, we have that partially polarized light can be expressed as a superposition of a completely polarized Stokes vector,$\boldsymbol{S}_P$, and a non-polarized Stokes vector $\boldsymbol{S}_U$, as [6]:

$$S_{partially} = S_P + S_U = s_0 DoP \begin{pmatrix} 1 \\ \frac{s_1}{(s_0 DoP)} \\ \frac{s_2}{(s_0 DoP)} \\ \frac{s_3}{(s_0 DoP)} \end{pmatrix} + (1 - DoP) s_0 \begin{pmatrix} 1 \\ 0 \\ 0 \\ 0 \end{pmatrix}, \qquad (2.3.27)$$

In fact, the superposition of several incoherent beams (there is no relation between their amplitudes and phases) can be described by Stokes vectors as [6]:

$$S^a + S^b = \begin{pmatrix} s_0^a \\ s_1^a \\ s_2^a \\ s_3^a \end{pmatrix} + \begin{pmatrix} s_0^b \\ s_1^b \\ s_2^b \\ s_3^b \end{pmatrix} = \begin{pmatrix} s_0^a + s_0^b \\ s_1^a + s_1^b \\ s_2^a + s_2^b \\ s_3^a + s_3^b \end{pmatrix} = S_{super}, \qquad (2.3.28)$$

In this example we have two incoherent beams, $S^a$and S^b, that is, they travel from independent sources.

Other variables related with the polarization ellipse are the azimuth angle and the ellipticity angle; these can be expressed as a function of Stokes parameters as [5]:

$$tan\, 2\psi = \frac{s_2}{s_1},\ 0 \leq \psi \leq \pi, \qquad (2.3.29)$$

And

$$sin\, 2\chi = \frac{s_3}{s_0},\ -\frac{\pi}{4} \leq \chi \leq \frac{\pi}{4}, \qquad (2.3.30)$$

In this way, they can be obtained experimentally.

In order to analyze and represent the polarization change of a beam of light, which interacts with optical polarizing elements, some mathematical tools such as the algebraic methods can become very tedious and complex. Given this, the physicist and mathematician Henri Poincarè employed a method denominated *stereographic projection* in order to build a tridimensional representation of polarization states, starting from the polarization ellipse. The stereographic method was developed by astronomer Hipparchus. This method allows us to map out a three-dimensional sphere on a two-dimensional plane since it has a very important property: the longitudes and latitudes for a sphere continue to intersect each other without modifying the intersection angles. Poincarè employed this method in order to map out the polarization ellipse onto a sphere, this is called *Poincarè sphere* in honor to him. The Poincarè sphere is an alternative method that allows to represent any totally polarized state (speaking of conventional

polarization states) of light as a point on its surface; also, on the Poincarè sphere we can see the behavior of polarized light (graphically) when interacts with optical polarizing elements. Polarization change of light is given as a path or trajectory on the Poincarè sphere.

It is usual to represent a Poincarè sphere normalizing respect to the total intensity. There exists a direct relation between Stokes parameters and the Poincarè sphere, that is, any point on its surface can be determined using three parameters; these are the Stokes parameters. That led us to distinguish three regions: all points on the spherical surface correspond to a totally polarized state; any point inside the Poincarè sphere represents partially polarized states; and the origin represents the non-polarized light. A fourth region concerns to points outside the the Poincarè sphere, in this region there is no physical meaning (see figure 2.7).

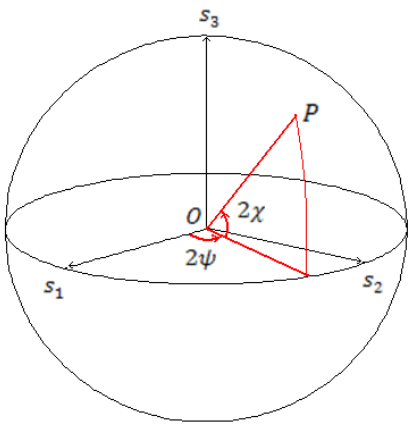

Figure 2.7 Graphical representation of the unitary Poincarè sphere.

In figure 2.7, we can see that any point on the surface of a unitary Poincarè sphere can also be described employing the azimuth and the ellipticity angles, defined above. For this, we have the Stokes parameters as a function of azimuth and ellipticity angles [5]:

$$s_1 = r\,cos(2\chi)\,cos(2\psi), \qquad (2.3.31)$$

$$s_2 = r\,cos(2\chi)\,sin(2\psi), \qquad (2.3.32)$$

$$s_3 = r\,sin(2\chi)\,cos(2\psi), \qquad (2.3.33)$$

Where, $r = 1$ corresponds to totally polarized states, they are points on the surface of unitary Poincarè sphere. In a similar way we can represent r and the azimuth and ellipticity angles as a function of Stokes parameters [5]:

$$\psi = \frac{1}{2} tan^{-1}\left(\frac{s_2}{s_1}\right), \qquad (2.3.34)$$

$$\chi = \frac{1}{2} sin^{-1}\left(\frac{s_3}{s_0}\right), \qquad (2.3.35)$$

$$r = (s_1^2 + s_2^2 + s_3^2)^{\frac{1}{2}}, \qquad (2.3.36)$$

If we remember, in Section 2.1, we said that linear polarizer states are particular polarization states which fulfill the condition that their ellipticity is equal to zero ($\chi = 0$), this means that linear polarizer states are located on the equator of the Poincarè sphere ($s_3 = 0$). In this sense, we have the horizontal polarization state corresponds to coordinates ($s_1 = 1, s_2 = 0, s_3 = 0$) or $\psi = 0$, and the vertical polarization state corresponds to coordinates ($s_1 = -1, s_2 = 0, s_3 = 0$) or $\psi = \frac{\pi}{2}$. Also, the linear $+45$ polarization state is represented by ($s_1 = 0, s_2 = 1, s_3 = 0$) or $\psi = \frac{\pi}{4}$, and the linear -45 polarization state by ($s_1 = 0, s_2 = -1, s_3 = 0$) or $\psi = \frac{3}{4}\pi$. On the other hand, we have circular polarization states when the azimuth is equal to zero ($\psi = 0$). Particularly, we have the circular right-handed polarization state is given by coordinates ($s_1 = 0, s_2 = 0, s_3 = 1$) or $\chi = \frac{\pi}{4}$, and the circular left-handed polarization state is given by coordinates ($s_1 = 0, s_2 = 0, s_3 = -1$) or $\chi = -\frac{\pi}{4}$; these states correspond to the north-pole and south-pole, respectively (described as looking to the source). Any other point on the north-hemisphere and the south-hemisphere correspond to elliptical right- and left-handed polarization states, respectively; without take into account the poles and the equator.

Once it has been described the polarization state of a beam of light by using the Stokes formalism, then, it is important to describe its interaction with the matter. We are going to consider a linear response of an incident beam of light respect to the output beam once the incident beam has interacted with matter. In this sense, it is possible to describe such interaction by the following equation system, which has been written in matrix form [5]:

$$\begin{pmatrix} s_0' \\ s_1' \\ s_2' \\ s_3' \end{pmatrix} = \begin{pmatrix} m_{00} & m_{01} & m_{02} & m_{03} \\ m_{10} & m_{11} & m_{12} & m_{13} \\ m_{20} & m_{21} & m_{22} & m_{23} \\ m_{30} & m_{31} & m_{32} & m_{33} \end{pmatrix} \begin{pmatrix} s_0 \\ s_1 \\ s_2 \\ s_3 \end{pmatrix}, \qquad (2.3.37)$$

Where the superscript ‘, denotes the Stokes vector elements of the output beam. The matrix product on the right side of this equation is between the *Mueller matrix*

and the Stokes vector of the incident beam of light. The Mueller matrix is denoted as $\boldsymbol{M}$ and, its elements affect each of the Stokes vector parameters of an incident beam; in this sense, it is said that the Mueller matrix represents the polarization-altering characteristics of a sample [6]. In other words, the Mueller matrix of a sample carries all the information about the properties of that sample such as diattenuation, depolarization, and retardance. We can determinate the Mueller matrix of an optical polarizing element, an optical system, a surface and so on. This means that, it is possible to get the Mueller matrix of any interaction of a beam of light with the matter, which produces a reflected, diffracted, refracted or scattered beam [7].

We know that the effect of a linear polarizer or diattenuator on an incident beam is the attenuation of the orthogonal electric field components [5]:

$$E'_x = p_x E_x, \qquad (2.3.38)$$

$$E'_y = p_y E_y, \qquad (2.3.39)$$

Where $0 \leq p_{x,y} \leq 1$ is the amplitude attenuation coefficient along each orthogonal axis ($x-$ and $y-$axis, respectively), so that, $p_{x,y} = 0$ means a total attenuation along the corresponding axis and, $p_{x,y} = 1$ means a total transmission. In this sense, if we calculate the matrix product dictated by Eq. (2.3.37), then we find the following result [5]:

$$\begin{pmatrix} s'_0 \\ s'_1 \\ s'_2 \\ s'_3 \end{pmatrix} = \frac{1}{2}\begin{pmatrix} p_x^2 + p_y^2 & p_x^2 - p_y^2 & 0 & 0 \\ p_x^2 - p_y^2 & p_x^2 + p_y^2 & 0 & 0 \\ 0 & 0 & 2p_x p_y & 0 \\ 0 & 0 & 0 & 2p_x p_y \end{pmatrix}\begin{pmatrix} s_0 \\ s_1 \\ s_2 \\ s_3 \end{pmatrix}, \qquad (2.3.40)$$

From Eq. (2.3.40), we have that the Matrix Mueller by a linear polarizer is given as [5]:

$$\boldsymbol{M}_P = \frac{1}{2}\begin{pmatrix} p_x^2 + p_y^2 & p_x^2 - p_y^2 & 0 & 0 \\ p_x^2 - p_y^2 & p_x^2 + p_y^2 & 0 & 0 \\ 0 & 0 & 2p_x p_y & 0 \\ 0 & 0 & 0 & 2p_x p_y \end{pmatrix}, \qquad (2.3.41)$$

From this Mueller matrix, it is easy to see that the Muller matrix of an ideal horizontal linear polarizer ($p_y = 0$, which means a total attenuation along the $y-$axis) and, an ideal vertical linear polarizer ($p_x = 0$, which means a total attenuation along the $x-$axis) are given as, respectively [5]:

$$\boldsymbol{M}_{HP} = \frac{1}{2}\begin{pmatrix} 1 & 1 & 0 & 0 \\ 1 & 1 & 0 & 0 \\ 0 & 0 & 0 & 0 \\ 0 & 0 & 0 & 0 \end{pmatrix}, \qquad (2.3.42)$$

$$\boldsymbol{M}_{VP} = \frac{1}{2}\begin{pmatrix} 1 & -1 & 0 & 0 \\ -1 & 1 & 0 & 0 \\ 0 & 0 & 0 & 0 \\ 0 & 0 & 0 & 0 \end{pmatrix}, \qquad (2.3.43)$$

In a similar way, we can find that the Mueller matrix of a retarder with a retardance of α is given by the following matrix [5]:

$$\boldsymbol{M}_{R}(\alpha) = \begin{pmatrix} 1 & 0 & 0 & 0 \\ 0 & 1 & 0 & 0 \\ 0 & 0 & cos\,\alpha & sin\,\alpha \\ 0 & 0 & -sin\,\alpha & cos\,\alpha \end{pmatrix}, \qquad (2.3.44)$$

An important characteristic of an ideal retarder is that the total intensity of the incident beam of light does not present losing, respect to the total intensity of the output beam. If we remember, there are two important retardance values, these are $\alpha = \pi$ and $\alpha = \frac{\pi}{2}$, which are associated with a half wave plate (HWP) and a quarter wave plate (QWP), respectively. These retarders have a specific Mueller matrix each of them [5]:

$$\boldsymbol{M}_{R}(\pi) = \begin{pmatrix} 1 & 0 & 0 & 0 \\ 0 & 1 & 0 & 0 \\ 0 & 0 & -1 & 0 \\ 0 & 0 & 0 & -1 \end{pmatrix}, \qquad (2.3.45)$$

$$\boldsymbol{M}_{R}\left(\frac{\pi}{2}\right) = \begin{pmatrix} 1 & 0 & 0 & 0 \\ 0 & 1 & 0 & 0 \\ 0 & 0 & 0 & 1 \\ 0 & 0 & -1 & 0 \end{pmatrix}, \qquad (2.3.46)$$

In the laboratory sometimes is necessary to rotate the principal axis of the used optical elements. This fact leads us to represent the Mueller matrix of any optical element, whose principal axis is tilted by an angle of θ, respect to the horizontal plane (holographic table). In this sense, the Mueller matrix for rotation is very important, inasmuch as it allows us to do that. The Mueller matrix for rotation is given by the following matrix [5]:

$$\boldsymbol{M}_{Rot}(2\theta) = \begin{pmatrix} 1 & 0 & 0 & 0 \\ 0 & cos\,2\theta & sin\,2\theta & 0 \\ 0 & -sin\,2\theta & cos\,2\theta & 0 \\ 0 & 0 & 0 & 1 \end{pmatrix}, \qquad (2.3.47)$$

By using the Eq. (2.3.47) we can obtain the Mueller matrix of a retarder and a linear polarizer whose principal axes are located at an angle of θ, respect to the horizontal plane. The rotated Mueller matrix for each polarizing component is obtained by applying the following equation [5]:

$$\boldsymbol{M}(2\theta) = \boldsymbol{M}_{Rot}(-2\theta)\boldsymbol{M}\boldsymbol{M}_{Rot}(2\theta), \qquad (2.3.48)$$

Where $\boldsymbol{M}$ and $\boldsymbol{M}(2\theta)$ are the Mueller matrix and the rotated Mueller matrix of the polarizing component, respectively. The Mueller matrix of a linear polarizer with its principal axis tilted by an angle of θ (respect to the horizontal plane) is given by the following matrix [6]:

$$\boldsymbol{M}_P(2\theta) = \frac{1}{2}\begin{pmatrix} p_x^2 + p_y^2 & (p_x^2 - p_y^2)\,cos\,2\theta & (p_x^2 - p_y^2)\,sin\,2\theta & 0 \\ (p_x^2 - p_y^2)\,cos\,2\theta & (p_x^2 + p_y^2)cos^2 2\theta + 2p_x p_y sin^2 2\theta & (p_x^2 + p_y^2 - 2p_x p_y)\,sin\,2\theta\,cos\,2\theta & 0 \\ (p_x^2 - p_y^2)\,sin\,2\theta & (p_x^2 + p_y^2 - 2p_x p_y)\,sin\,2\theta\,cos\,2\theta & (p_x^2 + p_y^2)sin^2 2\theta + 2p_x p_y cos^2 2\theta & 0 \\ 0 & 0 & 0 & 2p_x p_y \end{pmatrix}, \qquad (2.3.49)$$

By using Eq. 2.3.49, it is possible obtain the Eq. (2.3.42) and the Eq. (2.343), which correspond to the Mueller matrices of linear polarizer horizontal and vertical, respectively, with their principal axes parallel to the horizontal plane. Another important result is the Mueller matrix for the rotated retarder by an angle θ (respect to the horizontal plane) and whose retardance is α: [5]:

$$\boldsymbol{M}_R(\alpha, 2\theta) = \begin{pmatrix} 1 & 0 & 0 & 0 \\ 0 & cos^2 2\theta + sin^2 2\theta\,\cos\alpha & sin\,2\theta\,cos\,2\theta\,(1 - cos\,\alpha) & -sin\,2\theta\,sin\,\alpha \\ 0 & sin\,2\theta\,cos\,2\theta\,(1 - cos\,\alpha) & sin^2 2\theta + cos^2 2\theta\,\cos\alpha & cos\,2\theta\,sin\,\alpha \\ 0 & sin\,2\theta\,sin\,\alpha & -cos\,2\theta\,sin\,\alpha & cos\,\alpha \end{pmatrix}, \qquad (2.3.50)$$

Similarly, from Eq. (2.3.50) we can obtain the Eq. (2.3.45) and the Eq. (2.3.46). Generally, we can obtain the Mueller matrices of a HWP and a QWP, whose principal axes are tilted by an arbitrary angle θ, respect to the horizontal plane. These results are very useful in order to obtain the Mueller matrices of a polarization states generator (PSG) and a polarization states analyzer (PSA), which are two important optical systems in the generation and the analysis of polarization states.

2.4 Determination of the Mueller matrix

2.4.1 Polarization state generation (PSG)

The polarimetry is considered as the science of measuring polarization states of light such as direction of oscillation and handedness of the electric field vector, degree of polarization, and so on. Its experimental determination implies the use of an optical system called Polarimeter. If the measured polarization state comes from a given optical material, assuming a linear response of the material to an originally incident polarization state, it is possible to assign optical characteristics to the material under study such as diattenuation, retardation, and depolarizing properties, among many other characteristics. The general procedure consists of the following steps: fix a setup of polarizing elements, these allow us to generate a specific polarization state when a non-polarized initial incident beam travels through them; that setup is known as polarization state generator (PSG). Next, select a set of generated polarization states to illuminate the sample under study. Use a polarization state analyzer (PSA) to identify the modified polarization states emerging from the system under study and register its intensity values using a photo-detector if the spatial average is the main goal or a CMOS or CCD camera if the intention is the identification of the spatially distributed linear response. Once the beam has been characterized polarimetrically, the user has the possibility to employ different physical models and mathematical relationships to identify completely the optical properties associated to the system under study. In general, these properties will depend also on the angles of incidence and detection, of the incident wavelength, and the own physical characteristics of the sample under study. The main idea is the obtainment of a relationship between the polarization states of the incident and the exiting beams from a sample (transmitted, reflected, diffracted, or scattered). One of the problems present on an accurate polarimetry determination is related with the fact that polarization elements have not associated ideal responses; nevertheless, it is possible manipulate the error generated between the physical response and the theoretical considerations, employing a method called data reduction. Also, it is important a good calibration for both PSG and PSA, respectively.

A classical setup for a PSG is composed by a linear polarizer (LP) follow by a half-wave-plate (HWP), and finally a quarter-wave plate (QWP), see figure 2.8.

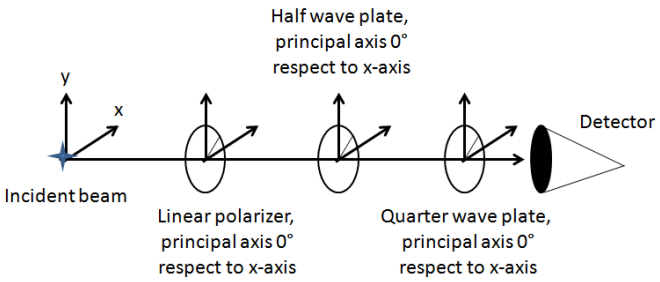

Figure 2.8 Experimental setup for a PSG.

Accordingly to the previous description, when the principal axes of all optical components are parallel to the $x-axis$, at the output we get a linear horizontal polarization state. It is due to only the electric field components of beam whose are parallel to transmission axis of LP can travel through it; therefore, the output beam has a well defined polarization state (horizontal) which has only one component, $x-component$, given that when this beam travel through HWP and QWP can suffer a phase shift but its polarization state is not modified. In a similar way we can get a linear vertical polarization state. On the other hand we can generate a $+45$ polarization state of beam employing a LP with its principal axis parallel to $x-axis$ followed by HWP with its principal axis to 22.5° respect to same axis; we can remember that a HWP rotates the input polarization towards it twice the angle between incident polarization and its fast axis, that is the output polarization has symmetry respect to fast axis, in this case it is no necessary to employ a QWP. Similarly, we get a -45 polarized beam. Finally, a circular right-handed polarization can be getting employing a LP with its transmission axis 0° and a QWP with its fast axis to 45 ° both respect to $x-axis$, in this case the HWP can be omitted. A circular left-handed polarization can be getting in a similar way. One can generate at least the six polarization states described before.

2.4.2 Polarization state analysis (PSA)

A PSA is an optical device or system (depending on the number of elements), which specifies the polarization state of an incident beam of light; that means, a PSA allows us determine if a beam has a specific polarization state or not; in fact, this is the reason to use a detector after the PSA. So for example, once an incident vertical polarized beam of light travels through the PSA, which analyze for horizontal polarization, then the detector measures a value equal to zero. In this sense it is said that the incident beam is vertically polarized and the principle used by this method is known as *null condition*, given that, the detector measures a null intensity. This procedure is very useful when the detector is our eye because it is

easier to see a null intensity over a screen that to see a maximum intensity. It is known that a PSG can be used as a PSA when it is used suitably. The classical setup for the PSA consists of a QWP followed by a HWP and finally a LP, see figure 2.9.

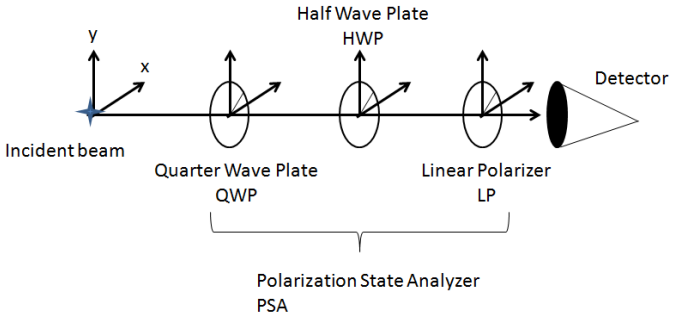

Figure 2.9 Experimental setup for a PSA.

Experimentally, we can use a linear polarizer (LP) as a PSA or a PSG, which allows us to analyze or generate linear polarization states ($p-$, $s-$, $+45$ and -45-polarization states), respectively. In a similar way, we have that a PSG which generates a circular right-handed polarized beam can be used as a PSA, which analyzes circular right-handed polarization state into the beam (null condition, we analyze the minimum intensity on the detector). On the other hand, this PSA can be used in order to analyze a left-handed polarization state (total transmission condition), in this case we use a commercial detector in order to analyze the maximum intensity registered on the detector. Some authors define both source and detector as components of PSG or PSA; nevertheless, we are taking into account that both PSG and PSA consist only by optical elements.

When we work with Mueller calculus, we can employ the Stokes vectors, $\boldsymbol{S}$, in order to represent the polarization state of a beam and Mueller matrices, $\boldsymbol{M}$, to represent the polarization characteristics of a sample. In order to characterize a beam of light, we must employ only a PSA (a light-measuring polarimeter or Stokesmeter); but, if we need to determine the Mueller matrix of a sample (sample-measuring polarimeter or Muellerometer) we need to employ both PSG and PSA.

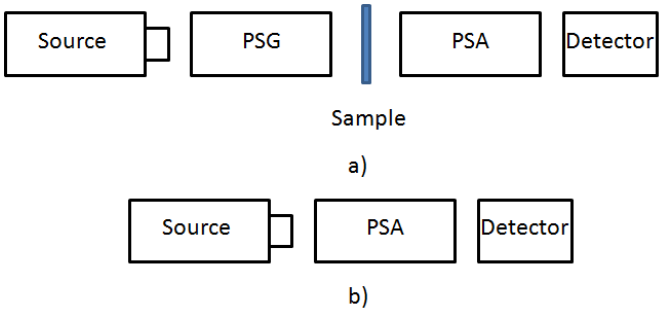

Figure 2.8 Graphical representation of a) a Muellerometer or sample-measuring polarimeter and b) a Stokesmeter or light-measuring polarimeter.

Generally, a Muellerometer works taking measurements sequentially from a PSA. In this sense, we generate a well known polarization state by using a PSG, so that, the beam generated is employed as an incident beam over a sample. When this beam travels through the sample then the output beam is modified by the sample and therefore we need to analyze it by using a PSA in order to quantify how it was modified. There are different methods to determine the state of polarization of a given beam of light. We are going to describe one of them, the named Ideal Polarimetric Arrangement, IPA, which considers the optical responses associated to the polarizing devices employed as ideal. The idea is generate the six ideal polarization states with a PSG (horizontal, vertical, $+45$, -45, right- and left-handed polarization states) and to use each of them the incident beam over the sample. Once we have generated a beam with the first of the six polarization states and it has traveled through the sample, we analyze the output beam with a PSA for the same six polarization states in order to determine how it was modified the polarization of the incident beam. This procedure must be repeated with the other five polarization sates.

It has been reported the following equations in order to obtain the sixteen Mueller matrix elements of a sample by using the IPA method by using only four polarizations generated and analyzing each of them [7, 8].

$$m_{00} = \frac{1}{2}\left(I_{pp} + I_{ps} + I_{sp} + I_{ss}\right), \qquad (2.4.2.1)$$

$$m_{01} = \frac{1}{2}\left(I_{pp} + I_{ps} - I_{sp} - I_{ss}\right), \qquad (2.4.2.2)$$

$$m_{02} = I_{+p} + I_{+s} - \frac{1}{2}\left(I_{pp} + I_{ps} + I_{sp} + I_{ss}\right), \qquad (2.4.2.3)$$

$$m_{03} = I_{rp} + I_{rs} - \frac{1}{2}\left(I_{pp} + I_{ps} + I_{sp} + I_{ss}\right), \qquad (2.4.2.4)$$

$$m_{10} = \frac{1}{2}\left(I_{pp} - I_{ps} + I_{sp} - I_{ss}\right), \qquad (2.4.2.5)$$

$$m_{11} = \frac{1}{2}\left(I_{pp} - I_{ps} - I_{sp} + I_{ss}\right), \qquad (2.4.2.6)$$

$$m_{12} = I_{+p} - I_{+s} - \frac{1}{2}\left(I_{pp} - I_{ps} + I_{sp} - I_{ss}\right), \qquad (2.4.2.7)$$

$$m_{13} = I_{rp} - I_{rs} - \frac{1}{2}\left(I_{pp} - I_{ps} + I_{sp} - I_{ss}\right), \qquad (2.4.2.8)$$

$$m_{20} = I_{p+} + I_{s+} - \frac{1}{2}\left(I_{pp} + I_{ps} + I_{sp} + I_{ss}\right), \qquad (2.4.2.9)$$

$$m_{21} = I_{p+} - I_{s+} - \frac{1}{2}\left(I_{pp} + I_{ps} - I_{sp} - I_{ss}\right), \qquad (2.4.2.10)$$

$$m_{22} = 2I_{++} - I_{+p} - I_{+s} - I_{p+} - I_{s+} + \frac{1}{2}\left(I_{pp} + I_{ps} + I_{sp} + I_{ss}\right), \qquad (2.4.2.11)$$

$$m_{23} = 2I_{r+} - I_{rp} - I_{rs} - I_{p+} - I_{s+} + \frac{1}{2}\left(I_{pp} + I_{ps} + I_{sp} + I_{ss}\right), \qquad (2.4.2.12)$$

$$m_{30} = I_{pr} + I_{sr} - \frac{1}{2}\left(I_{pp} + I_{ps} + I_{sp} + I_{ss}\right), \qquad (2.4.2.13)$$

$$m_{31} = I_{pr} - I_{sr} - \frac{1}{2}\left(I_{pp} + I_{ps} - I_{sp} - I_{ss}\right), \qquad (2.4.2.14)$$

$$m_{32} = 2I_{+r} - I_{+p} - I_{+s} - I_{pr} - I_{sr} + \frac{1}{2}\left(I_{pp} + I_{ps} + I_{sp} + I_{ss}\right), \qquad (2.4.2.15)$$

$$m_{33} = 2I_{rr} - I_{rp} - I_{rs} - I_{pr} - I_{sr} + \frac{1}{2}\left(I_{pp} + I_{ps} + I_{sp} + I_{ss}\right), \qquad (2.4.2.16)$$

In the previous set of equations the subscripts are related with the four polarization states: p (p-polarization state), s (s-polarization state), + (+45-polarization state), and r (circular right-handed polarization state). The capital letter I refers to the measured intensity. Given a measured intensity, the first subscript corresponds to the generated polarization state and the second subscript corresponds to the analyzed polarization state. In this sense, the measured intensity denoted as I_{pp} corresponds to the measurement of p-polarization state by using the PSA when it was used a p-polarized beam as an incident beam of light over the sample and, which was generated by using the PSG. We must remember that a general representation of the Mueller matrix is the following.

$$\boldsymbol{M}_{IPA} = \begin{pmatrix} m_{00} & m_{01} & m_{02} & m_{03} \\ m_{10} & m_{11} & m_{12} & m_{13} \\ m_{20} & m_{21} & m_{22} & m_{23} \\ m_{30} & m_{31} & m_{32} & m_{33} \end{pmatrix}, \qquad (2.4.2.17)$$

Where the IPA subscript refers to that this Mueller matrix was obtained by using this method. In the following chapters we will see that there is at least one method different to the IPA method, which is used to obtain the Mueller matrix for an optical device or in general for a surface.

Chapter 3

Unconventional polarization

3.1 Introduction

It is well known that amplitude, wavelength, frequency, and polarization are the fundamental properties of light. Polarization is related with the electric (or magnetic) field of light. This property has been studied since around a century. We know that some types of polarization states can be defined, based in their characteristics, among which we can mention linear, elliptical, and circular polarization. These types of polarization have in common that they are spatially homogeneous states in amplitude and phase and consequently they do not depend on the spatial location into the beam cross section. In the recently years, it has been identified and studied other kind of polarization with non-spatially homogeneous distribution of amplitude and phase. The interest in this kind of polarization has been increased in the last years, because it is expected to lead us to new effects and phenomena that can expand the functionality and therefore the capability of the optical systems.

In general, the beams that present this kind of polarization are called cylindrical vector beams and we can differentiate between two of them: radially and azimuthally polarized beams. We will focus our attention to the radial polarization mode because it is the beam that we will employ in the laboratory.

3.2 Radial and azimuthal polarization modes

In Chapter 2 we described conventional polarization. We saw that conventional polarization is characterized because have a spatially homogeneous polarization distribution. In this chapter, we are going to see that the cylindrical vector beams or CV beams arise as Maxwell's vector wave equation solutions in the paraxial approximation, see Eq. (3.2.1). The main characteristic of CV beams is that they obeys axial symmetry in both amplitude and phase [3]. CV beams are represented mathematically by a family of localized Bessel-Gauss beam solutions,

which describes the entire transverse electric field; therefore, this is an important tool when the beams have unconventional polarization [9].

$$\nabla \times \nabla \times \boldsymbol{E} - k^2 \boldsymbol{E} = 0, \qquad (3.2.1)$$

This equation is obtained from Eq. (2.1.9) by applying the following solution (monochromatic wave equation of frequency ω) $\vec{\mathrm{E}}(\vec{r},t) = \vec{E}(x,y,z)e^{-i\omega t}$ and, by applying the following relationship $\nabla \times \nabla \times \boldsymbol{E} = \nabla(\nabla \cdot \boldsymbol{E}) - \nabla^2 \boldsymbol{E}$. One solution of Eq. (3.2.1) is given by an electric field in the azimuthal direction; see Eq. (3.2.2) [3]:

$$\boldsymbol{E}(r,z) = U(r,z)e^{i(kz-\omega t)}\boldsymbol{e}_{\phi}, \qquad (3.2.2)$$

Where $\boldsymbol{e}_{\phi}$ represents to unitary vector in the azimuthal direction. We have that employing the paraxial and slowly varying envelope approximation we get the equation [3]:

$$\frac{1}{r}\frac{\partial}{\partial r}\left(r\frac{\partial U}{\partial r}\right) - \frac{U}{r^2} + 2ik\frac{\partial U}{\partial r} = 0, \qquad (3.2.3)$$

One solution of Eq. (3.2.3) is given by [3]:

$$U(r,z) = E_0 J_1\left(\frac{\beta r}{1+{}^{iz}/_{z_0}}\right) e^{\left(-\frac{i\beta^2 z/2k}{1+{}^{iz}/_{z_0}}\right)} u(r,z), \qquad (3.2.4)$$

Where $u(r,z)$ is the fundamental Gaussian solution, see Eq. (3.2.5).

$$u(r,z) = E_0 \frac{w_0}{w(z)}\, e^{[-i\varphi(z)]}\, e^{\left[i\frac{k}{2q(z)}r^2\right]}, \qquad (3.2.5)$$

where E_0 is a constant electric field amplitude; defined as before, β is a constant scale parameter, $z_0 = \frac{\pi w_0^2}{\lambda}$ is the Rayleigh range and k is wave number; and finally $J_1(x)$ is the first-order Bessel function of the first kind. So that, Eq. (3.2.2) can be written as [3]:

$$\boldsymbol{E}(r,z) = E_0 J_1\left(\frac{\beta r}{1+{}^{iz}/_{z_0}}\right) e^{\left(-\frac{i\beta^2 z/2k}{1+{}^{iz}/_{z_0}}\right)} u(r,z)e^{i(kz-\omega t)}\boldsymbol{e}_{\phi}, \qquad (3.2.6)$$

Eq. (3.2.6) corresponds to an azimuthally polarized Bessel-Gauss beam.

A radially polarized Bessel-Gauss beam can be represented as a magnetic field solution like Eq. (3.2.6), but in this case it is written in terms of the magnetic field, see Eq. (3.2.7). In this sense, there exists an electric field perpendicular to the

magnetic field described by Eq. (3.2.7). An electric field in the radial direction fulfills this condition [3].

$$\boldsymbol{H}(r,z) = -H_0 J_1\left(\frac{\beta r}{1+{}^{iz}/_{z_0}}\right) e^{\left(-\frac{i\beta^2 z/2k}{1+{}^{iz}/_{z_0}}\right)} u(r,z) e^{i(kz-\omega t)} \boldsymbol{h}_\phi, \qquad (3.2.7)$$

Where, H_0 is the constant magnetic field amplitude and, $\boldsymbol{h}_\phi$ is a unit vector in the azimuthal direction.

Also, it has been reported that the unconventional Laguerre-Gaussian (LG) beam modes can be expressed as a superposition of two mutually orthogonal Hermite-Gaussian (HG) beam polarization modes [3]. Specifically, the azimuthally polarized LG beam mode can be obtained as a superposition between a horizontal Hermite-Gaussian polarization mode (denoted as HG_{10} or ψ_{10}), which has vertical polarization and a vertical Hermite-Gaussian polarization mode (denoted as HG_{01} or ψ_{01}), which has horizontal polarization. On the other hand, a radially polarized beam is obtained as a superposition of a HG_{10} with horizontal polarization and a HG_{01} with vertical polarization. Finally, the generalized CV beams are given as a superposition of a radially and an azimuthally polarized beams [3]. In figure 3.1 it is shown a graphical representation of both azimuthally and radially polarized beams.

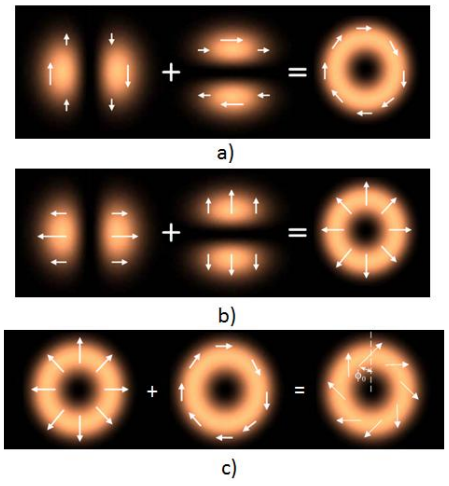

Figure 3.1 Graphical representation of a) azimuthally and b) radially polarized beams as a superposition of two HG polarization modes of light, and c) a generalized CV beam as a superposition of a) and b). Figure taken from [3].

There are different methods employed in CV beams generation and they are classified in two main categories: the passive generation methods (PGM), which do not affect to the gain medium into a laser source; and active generation methods

(AGM), which do it. The PGM have a subdivision: the PGM in free space, which generate CV beams in the free space; and PGM using optical fiber, which works employing a few mode fiber [3]. In this work, we generate a radially polarized beam by using a PGM in free space. In this case, a space variant polarization converter was used; this is an optical device fabricated by laser nano-structuring technique in a UVFS (UV Fused Silica, SiO2) substrate; it is named S-waveplate [10].

Basically, a polarization converter uses linearly or circularly (right- and left-handed) polarized light as the incident beam, and converts them to a radial or azimuthal polarized beam, depending of the incident polarization (orientation or handedness) [10]. Generally, these devices are fabricated on silica glass, which possess spatially variant birefringence produced by the subwavelengths gratings (nanostructures). Normally, the recording of these structures on the glass employs a femtosecond laser, which defines the resolution obtained with it [11]. The birefringence is induced by subwavelengths gratings due to the behavior of both electric fields, parallel (TE polarization) and perpendicular (TM polarization) with respect to the groove gratings. These components of polarization are governed by different boundary conditions, and these conditions are given as a result of two different effective refractive index for each polarization, respectively (TE and TM) [11]. In other words, there is a fast and a slow axis, perpendicular and parallel respect to the groove gratings (depending on the refractive index values), and they are varying spatially. According to the last statement, a polarization converter, which works with a linearly polarized incident beam, has a behavior which figures a half-wave plate, but in this case the fast axis is varying its direction continuously. Due to this variation, it rotates the linear polarization of the incident beam by a necessary angle to produce a radially or azimuthally polarized beam, respectively [11].

3.3 Determination of the polarization modes

3.3.1 Cylindrical lenses as mode converters

It is well known that in the paraxial approximation the beams of light carry a *spin angular momentum*, which is directly related with its polarization state, most specifically with an axial component of its electromagnetic field [12]. We can remember that any completely polarized state of light can be represented as a point on the surface of the Poincarè sphere (polarization vector space), see figure 3.2(a). The north and south poles of this sphere (circularly left- and right-handed polarized states of light, respectively, described as looking to the propagation

direction) represent spin eigenstates, which have a spin angular momentum of $+\hbar$ and $-\hbar$ per photon, respectively [12-14]. Then, any other polarization state can be represented as a superposition of circular left- and right-handed polarization states. For instance, a linear polarization state can be represented as a superposition of the circular left- and right-handed polarization states, which has a same intensity and where the relative phase of the superposition will represent the orientation for the resultant polarization.

On the other hand, we have that the two fundamental transverse modes are the Hermite-Gaussian (HG) and the Laguerre-Gaussian modes (LG), which represent eigensolutions of the paraxial wave equation for Cartesian and Cylindrical coordinates, respectively [15]. It has been reported that some beam modes of light carry an *orbital angular momentum,* which is independent of its polarization state [16]. The *orbital angular momentum* arises from the azimuthal component of light beams' linear momentum, given the inclination of its phase fronts [11, 16]. The most common beam modes that carry an *orbital angular momentum* are the Laguerre-Gaussian beam modes; nevertheless, there are other beam modes with this characteristic such as Bessel, Mathieu, and Ince-Gaussian beam modes [17]. These beam modes have helical wave fronts and, in general are named *helically phased beams*. They are characterized by an azimuthally phase dependence in the transverse plane, so that, its amplitude can be written in the general form as [11, 14, 16]:

$$u(x, y, z, \phi) = u_0(x, y, z)e^{-ikz}e^{il\phi}, \qquad (3.3.1.1)$$

Here, the angle ϕ is the azimuthal coordinate in the cross section of light beam. The Laguerre-Gaussian beam modes (LG mode beams) have an amplitude expression, which figures to Eq. (3.3.1.1); see Eq. (3.3.1.2).

$$u(r, \phi, z) = E_0 \left(\sqrt{2}\frac{r}{\omega}\right)^l L_p^l \left(2\frac{r^2}{\omega^2}\right) \frac{w_0}{w(z)}\, e^{\left[-i\varphi_{pl}(z)\right]}\, e^{\left[-i\frac{k}{2q(z)}r^2\right]} e^{[il\phi]}, \qquad (3.3.1.2)$$

Where L_p^l are the generalized Laguerre Polynomials, $\varphi_{pl}(z) = (2p + l + 1)\psi(z)$ where $\psi(z) = tan\left(\frac{z}{z_0}\right)$ is called Gouy phase shift which appears in a Gaussian mode, and the term $e^{[-il\phi]}$ is called a vortex term.

L. Allen in 1992 found that, in general, the Laguerre-Gaussian beam modes (which posses an azimuthally term $e^{il\phi}$ and, which are denoted as LG_p^l, where p and l are the azimuthal and radial indices, respectively and, with $N = 2p + |l|$ known as the order of the mode [13]) are orbital angular momentum eigenstates, which carry an

orbital angular momentum of $l\hbar$ per photon, where l is an integer value (positive or negative) [13]. The sign of l denotes the handedness of the phase structure rotation respect to the beam mode direction (for instance, $l = -1$ for counter clockwise direction and $l = 1$ in the opposite case), this like circular right- and left-handed polarization states have a well defined handedness [11, 17]. Specifically, we have the left- and the right-handed Laguerre-Gaussian beam modes (denoted as LG_0^{+1} andLG_0^{-1}, respectively), which have azimuthal phase terms of $e^{+i\emptyset}$ and $e^{-i\emptyset}$, respectively. These beam modes are stable structurally (with $N = 1$) and they represent orbital angular momentum eigenstates, which posses an orbital angular momentum of $+\hbar$ and $-\hbar$ per photon, respectively [3, 13]. In this way, it has been defined an analogous sphere to the Poincarè sphere as a superposition of the left- and the right-handed Laguerre-Gaussian beam modes, which is called the sphere of first order modes (spatial vector space) [13]. Therefore, in a similar way how the Poincarè sphere was conceptualized, we have that in this case each point on the surface of the sphere of first order modes corresponds to a beam mode with order 1, also any beam mode of order 1 corresponds to a point on the surface of the sphere of first order modes [13]. Also, in an analogous way we have that given two Laguerre-Gaussian modes (left- and right-handed, respectively) which have the same intensities, the superposition of them gives as result a Hermite-Gaussian mode, denoted as $HG_{1,0}$ or$\psi_{1,0}$, which fulfills the condition $N = m + n = 1$. The relative phase of the superposition determines the orientation of the mode [3], see figure 3.2(b).

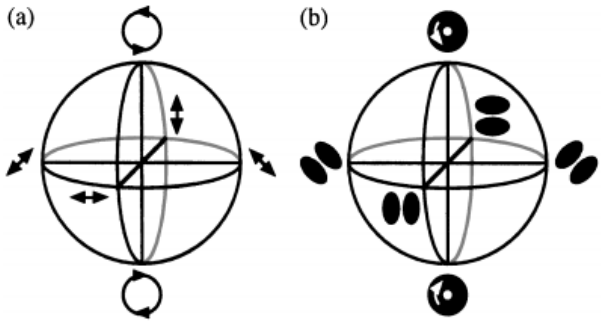

Figure 3.2 In this figure they are shown a) the Poincarè sphere and b) the sphere of first-order modes. Figure taken from [12].

Indeed, $l = 1$ and $l = -1$, are very important values of Laguerre-Gaussian beam modes as previously it was explained and, since it has been reported experimentally that they present similar mechanical characteristics with respect to the *spin angular momentum* for circular right- and left-handed polarization states, respectively [16].

These similarities between *spin* and *orbital* angular momentum allowed to researchers to think in the generation of Laguerre-Gaussian beam modes using Hermite-Gaussian beam modes as incident mode beams. This idea arises from the fact that a quarter-wave plate converts a linear polarized beam into a circular right- or left-hand polarized beam (depending on the angle between the incident polarization plane and the fast axis of quarter-wave plate). In fact, there are some methods in order to generate *helically phased beams*, more specifically, Laguerre-Gaussian mode beams of light. One of them uses a couple of identical cylindrical lenses, which are separated by a distance of $\sqrt{2}f$ (measured from the principal focal plane of the lenses), where, f is the focal length of each lens, see figure 3.3. Generally, these devices are called *mode converters* (see figure 3.2) and, there are two important configurations: $^{\pi}/_{2} - mode\ converter$ and $\pi - mode\ converter$, see figure 3.3. A $^{\pi}/_{2} - mode\ converter$ works according to the principle that, a first-order LG mode beam can be represented as a superposition of HG_{10} and HG_{01} beam modes, which have a $^{\pi}/_{2}$ relative phase difference between them. In principle, a high-order LG beam mode can be represented as a superposition of HG beam modes of the same order, which have a $^{\pi}/_{2}$ relative phase difference between successive components [11, 18]. Indeed, the name of this optical device is due to this fact [14, 16].

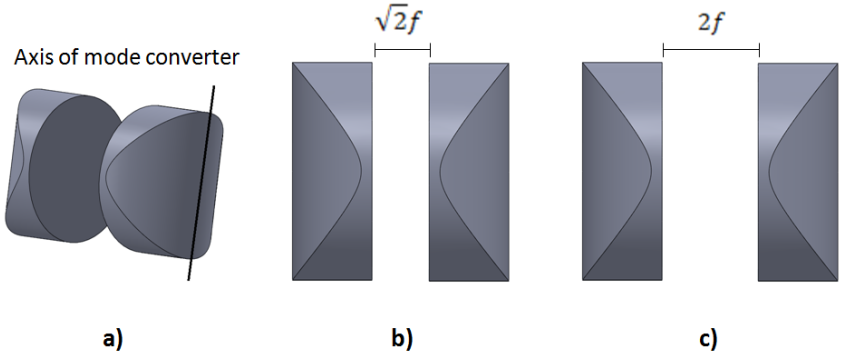

Figure 3.3 Graphical representation of a) the axis of the mode converter, which is a parallel line of the cylinder axis, and can be represented as a line on the cylindrical surface of the mode converter, the configuration of b) a $^{\pi}/_{2} - mode\ converter$ and c) a $\pi - mode\ converter$.

It has been reported theoretical and experimentally that, a $^{\pi}/_{2} - mode\ converter$ (with its axis parallel to the horizontal plane, in this case the holographic table) converts an incident diagonal HG beam mode with indices m and n (with its axis tilted to 45° respect to the horizontal plane) into a LG beam mode with indices $l = m - n$ and $p = min(m, n)$ [11, 14]. This statement is very important because in order to get the best conversion, we must ensure that

the angle between the incident HG beam mode axis and the mode converter axis is of 45°, see figure 3.4. Also, it has been recognized the reversed case, that is, a $^{\pi}/_{2} - mode\ converter$ converts a first-order LG beam mode into a HG beam mode (given the relative phase difference of $^{\pi}/_{2}$ between a HG_{10} and a HG_{01}); also, the above statement has been generalized to modes of arbitrary order [14].

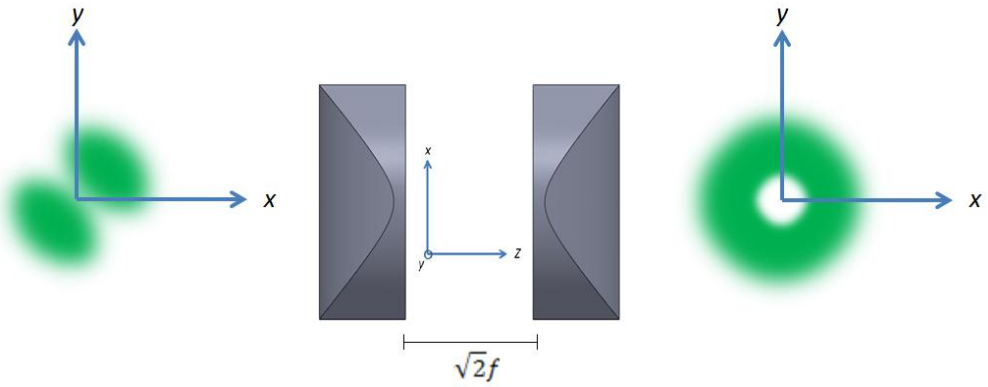

Figure 3.4 Configuration of a $^{\pi}/_{2} - mode\ converter$. It converts an incident diagonal HG beam mode in a LG beam mode.

One trouble found in practice with a $^{\pi}/_{2} - mode\ converter$ is that, the output beam mode diverges and, therefore it is necessary to use some lenses arrangement in order to collimate it. Simulated results have been reported for a specific value of the focal length of the used cylindrical lenses [18].

There is another important mode converter called $\pi - mode\ converter$, this optical device consists in a couple of identical cylindrical lenses separated by a distance of $2f$, where again, f is the focal length of each lens. A $\pi - mode\ converter$ with its axis tilted to 22.5° respect to the horizontal plane (holographic table or $x - axis$) converts a diagonal HG beam mode (with its axis tilted to 45° respect to the horizontal plane) into a HG_{10} beam mode (horizontal Hermite-Gauss beam mode) and conversely; in a similar way, it converts a diagonal HG (with its axis tilted to 135° respect to the horizontal plane) into a HG_{01} beam mode (vertical Hermite-Gauss beam mode), and vice versa, see figure 3.5. In this sense, a $\pi - mode\ converter$ works like a half-wave plate works with an incident linearly polarized light beam; that is, the incident HG beam mode rotates (toward the axis of mode converter) twice the angle between the beam mode axis and mode converter axis. Also, it has been reported that when a helically phased beam travels through the $\pi - mode\ converter$ then, the handedness of the output beam mode is opposite respect to the incident beam

mode [18]. This is another analogue behavior of the $\pi - mode\ converter$ respect to a half wave-plate, which change the handedness of a circularly polarized beam of light traveling through it.

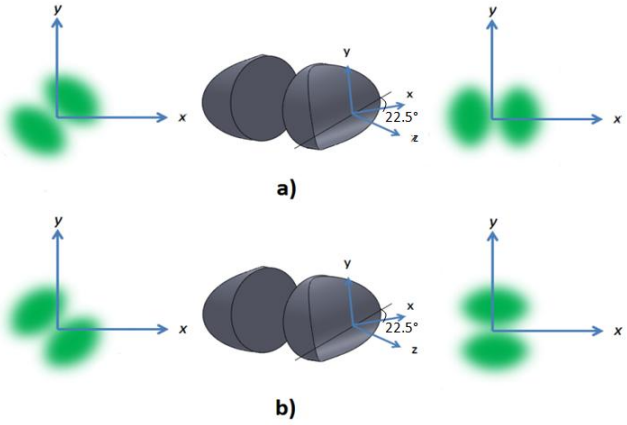

Figure 3.5 Configuration of a $\pi - mode\ converter$ with its axis tilted by an angle of 22.5° respect to the horizontal plane. It converts a) an incident diagonal HG beam mode (with its axis tilted by an angle of 45° respect to the horizontal plane) into a horizontal HG beam mode (HG_{10}) and, b) an incident diagonal HG beam mode (with its axis tilted by an angle of 135° respect to the horizontal plane) into a vertical HG beam mode (HG_{01})

An interesting observation is that, given the nature of each angular momentum (spin and orbital), it has been observed experimentally that a mode converter does not affect to the polarization state of the incident beam mode and, a retarder does not affect to the spatial distribution of the incident beam mode.

3.3.2 Modified Mach-Zehnder interferometer

Along of this section, it is presented the theoretical description of an experimental setup of the *modified Mach-Zehnder interferometer.* This optical device was designed from a classical configuration of a Mach-Zehnder interferometer, simply by adding an extra mirror in one of its arms and by putting a half-wave plate in the other. Then, it is important remember that a Mach-Zehnder interferometer is an optical device, which consists of two 50%-reflected (or a different percentage) mirrors and two 100%-reflected mirrors, basically. Of course, it must be illuminated by a collimated source and, in each of the two output arms it is important to put a detector (a screen, for example), see figure 3.6.

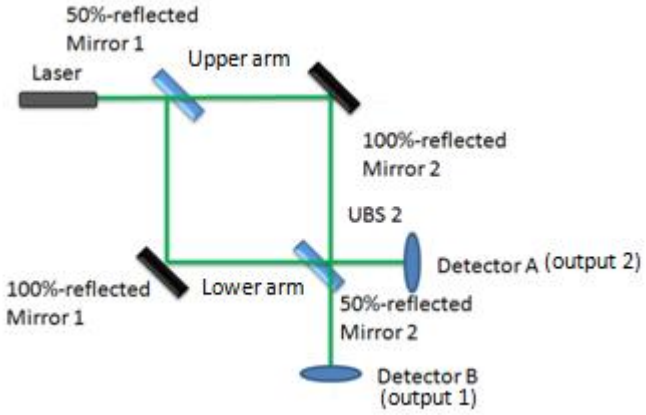

Figure 3.6. Classical configuration of a Mach-Zehnder interferometer.

By using a Mach-Zehnder interferometer, it is possible see the interference between two beams of light, which were generated by the same source. Therefore, it is said that the interference is generated by division of amplitude. From the theory, it was reported that, when a beam of light is reflected by a plane mirror, the reflected beam has a phase shift of π [19]. Also, it is known that the total distance traveled by the beam (in each arm) induces a phase shift. Finally, when a beam travels through a glass (beam splitter), it is induced a phase shift, which depends of the optical path length traveled into the glass [19]. In this sense, a complete analysis of the total phase shift on each arm, leads us at the following result for the phase difference between the two arms in the detector A or output 2 (Fig. 3.6) [19]:

$$\delta = 2\pi\left(\frac{l_1 - l_2}{\lambda}\right), \qquad (3.3.2.1)$$

And, the phase difference between the two arms in the detector B or output 1 as [19]:

$$\pi + \delta = \pi + 2\pi\left(\frac{l_1 - l_2}{\lambda}\right), \qquad (3.3.2.2)$$

Where δ is the phase shift, l_1 and l_2 are the path lengths of the lower and upper arms, respectively, and λ is the wavelength of the source used. From Eqs. (3.3.2.1 and 3.3.2.2) it is easy to see that, when $\delta = 0$, in the detector A the interference is constructive and it is destructive in the detector B. According as δ varies, this condition is modified [19]. The path-length of one of the two arms can be modified by introducing and tilting a glass plate. It can be observed a parallel fringe pattern on a screen at output 2, and the complement of it on the other screen at output 1.

The Mach-Zehnder interferometer, which is shown in Fig. 3.6 can be modified by adding an extra mirror in the upper arm and by putting two half-wave plates with its fast axis in the horizontal direction (parallel to the holographic table), one of them in the lower arm and the other at the output 2 corresponding with the detector A, see figure 3.7. It has been reported that this new experimental configuration works as a transverse mode beam splitter. This means that the *modified Mach-Zehnder interferometer* splits an incident LG beam polarization mode into the two HG beam polarization modes (HG_{10} and HG_{01}). The HG_{10} can be observed at the output 1 and the HG_{01} at the output 2 [1, 20]. If we remember a LG beam polarization mode of first order can be represented as the superposition of two mutually orthogonal HG beam polarization modes (HG_{10} and HG_{01}), which have the same order.

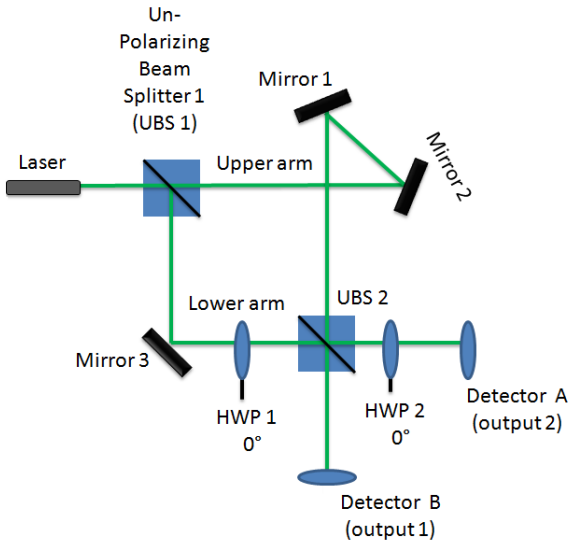

Figure 3.7 Experimental setup of a modified Mach-Zehnder interferometer.

In the experimental setup of Fig. 3.7, two un-polarizer beam splitters (UBS) are used instead of 50%-reflected mirrors of the Mach-Zehnder interferometer (Fig. 3.6); nevertheless, the analysis developed previously can be applied in a similar way. From this analysis, it can be obtained a similar result of the phase shift like the result obtained for the Mach-Zehnder interferometer; that is, there is a phase difference of π between the two beams of light, which arrive to the detectors (A and B, respectively). In this case the phase shift induced by the difference in the path lengths l_1 and l_2, can be modified by varying the distance between the mirrors 1 and 2. The half-wave plate with its fast axis in the horizontal direction modifies the polarization of the incident beam mode, so that, the interference generates the desired HG beam modes.

Chapter 4

Classical entanglement of light

4.1 Introduction

The entanglement is a central concept in quantum mechanics; it refers to correlations between degrees of freedom of different particles. The radial and the azimuthal polarization modes represent a classical analogue of this type of entanglement, where the entanglement is between different degrees of freedom (DoFs), within a single beam of light. It is important to mention that classical entanglement is no longer valid when the non-locality comes into play, in other words, we can differentiate between two types of entanglement: i) entanglement between separate particles called nonlocal entanglement and which represent exclusively quantum mechanical in nature and ii) entanglement between different properties of a single particle or beam of light called classical entanglement [1]. On the one hand, the nonlocal entanglement may yield nonlocal statistical correlations, and on the other hand, the classical entanglement cannot generate nonlocal correlations [1].

In classical optics, radially polarized beams of light are an example of local entanglement, it is demonstrated that they show local entanglement between polarization DoFs and spatial DoFs in a same beam [1].

4.2 Radial polarization mode as a classical entanglement of light

In order to understand the entanglement concept, we are going to write the mathematical representation of a classical entanglement beam of light, where we will see the relation between polarization and spatial DoFs (DoF, degrees of freedom). Considering the paraxial approximation of a polarized (in the xy plane) monochromatic beam of light with angular frequency ω, which propagates along the $+z-axis$:

$$\boldsymbol{E}(\boldsymbol{r},t) = Re\left[E(\boldsymbol{r})e^{i(kz-\omega t)}\right], \qquad (4.2.1)$$

Where

$$\boldsymbol{E}(\boldsymbol{r}) = \left(A_0\boldsymbol{e}_x + A_1\boldsymbol{e}_y\right)\psi(\boldsymbol{r}), \qquad (4.2.2)$$

Where $\psi(\boldsymbol{r})$ denotes the spatial mode of beam, $\boldsymbol{e}_j$ for $j= x, y$, being unit vectors in the correspondent direction, which are related with the polarization state of the beam (electric field components), $\boldsymbol{r} = x\hat{\boldsymbol{e}}_x + y\hat{\boldsymbol{e}}_y + z\hat{\boldsymbol{e}}_z$ stands for the position vector and, $A_1$and A_0 represent the complex amplitudes of the electric field along the $x-$ and $y-$axis, respectively. We can represent the last equation in the Jones notation as [1]:

$$\boldsymbol{E}(\boldsymbol{r}) = \begin{bmatrix} A_0 \\ A_1 \end{bmatrix}\psi(\boldsymbol{r}), \qquad (4.2.3)$$

In this equation, it is possible the identification of the polarization state and the spatial DoFs given by the Jones vector $[A_0, A_1]^T$and the scalar field $\psi(\boldsymbol{r})$, respectively. This electric field is called separable because the expression of $\boldsymbol{E}(\boldsymbol{r})$ is factorizable as the product of a single space independent vector and a single scalar field [21].

Now, if we consider the general case of an electric field of beam spatially non-uniformly polarized in the xy plane given by the following equation [1]:

$$\boldsymbol{E}(\boldsymbol{r}) = A_{00}\boldsymbol{e}_x\psi_{10}(\boldsymbol{r}) + A_{01}\boldsymbol{e}_x\psi_{01}(\boldsymbol{r}) + A_{10}\boldsymbol{e}_y\psi_{10}(\boldsymbol{r}) + A_{11}\boldsymbol{e}_y\psi_{01}(\boldsymbol{r}), \qquad (4.2.4)$$

Where $\psi_{mn}(\boldsymbol{r})$ (for $m, n \in \{0,1\}$) denotes the Hermite-Gaussian (HG) solutions of the paraxial wave equation of order $N = m + n = 1$ and, A_{op} (for $o, p \in \{0,1\}$) represent the complex amplitudes of the field. In the previous Chapter the Hermite-Gaussian beam modes were denoted as: HG_{10} and HG_{01}. Along this work, we use both representations indistinctly, in order to represent the Hermite-Gaussian beam modes (horizontal and vertical respectively). We can write this equation in Jones notation as [1]:

$$\boldsymbol{E}(\boldsymbol{r}) = \begin{bmatrix} A_{00}\psi_{10}(\boldsymbol{r}) + A_{01}\psi_{01}(\boldsymbol{r}) \\ A_{10}\psi_{10}(\boldsymbol{r}) + A_{11}\psi_{01}(\boldsymbol{r}) \end{bmatrix} = \begin{bmatrix} A_{00} \\ A_{10} \end{bmatrix}\psi_{10}(\boldsymbol{r}) + \begin{bmatrix} A_{01} \\ A_{11} \end{bmatrix}\psi_{01}(\boldsymbol{r}), \qquad (4.2.5)$$

From this equation, it is easy to see that one needs two coordinate-independent Jones vectors $[A_{00}, A_{10}]^T$, $[A_{01}, A_{11}]^T$and two independent scalar fields, ψ_{10} and ψ_{01}, in order to represent the electric field completely. It is said that the polarization and the spatial DoFs are non-separable variables or classically entangled states [1]. In the mathematical language, the last equation represents the sum of a tensor product of two (it could be more) vectors which belong to

different vector spaces, indeed this is the central idea of the entanglement. On one hand we have the polarization vector space (which is represented by the Poincarè sphere) and, on the other hand, we have the spatial vector space (which is represented by the first-order spatial modes sphere) [21].

We have that a radially polarized beam presents classical entanglement between the polarization and the spatial DoFs of a single light beam; it is represented by the following expression [1]:

$$\boldsymbol{E} = \frac{1}{\sqrt{2}}\left[\boldsymbol{e}_x\psi_{10}(\boldsymbol{r}) + \boldsymbol{e}_y\psi_{01}(\boldsymbol{r})\right], \qquad (4.2.6)$$

It can be obtained of Eq. (4.2.4) when $A_{00} = A_{11} = \frac{1}{\sqrt{2}}$ and $A_{01} = A_{10} = 0$.

Eq. (4.2.6) shows us that a radially polarized beam can be represented as superposition of HG_{10} and HG_{01} beam modes with $p-$ or $x-$ and $s-$ or $y-$polarizations, respectively. Nevertheless, also we can represent it as a superposition of two diagonal HG beam modes, denoted as $\psi_{\pm} = (\psi_{10} \pm \psi_{01})/\sqrt{2}$ each of them with diagonal polarizations $\boldsymbol{e}_{\pm} = (\boldsymbol{e}_x \pm \boldsymbol{e}_y)/\sqrt{2}$, respectively. Besides, we can represent it as a superposition of two Laguerre-Gauss (LG) spatial beam modes, denoted as $\psi_L = (\psi_{10} + i\psi_{01})/\sqrt{2}$ and $\psi_R = (\psi_{10} - i\psi_{01})/\sqrt{2}$ each of them with circular polarizations $\boldsymbol{e}_L = (\boldsymbol{e}_x + i\boldsymbol{e}_y)/\sqrt{2}$ and $\boldsymbol{e}_R = (\boldsymbol{e}_x - i\boldsymbol{e}_y)/\sqrt{2}$ [7]. See Eqs. (4.2.7 and 4.2.8) [1]:

$$\boldsymbol{E} = \frac{1}{\sqrt{2}}[\boldsymbol{e}_+\psi_+ + \boldsymbol{e}_-\psi_-], \qquad (4.2.7)$$

$$\boldsymbol{E} = \frac{1}{\sqrt{2}}[\boldsymbol{e}_L\psi_R + \boldsymbol{e}_R\psi_L], \qquad (4.2.8)$$

As a general representation we have omitted the $\boldsymbol{r}$ dependency for $\boldsymbol{E}$.

A graphic representation of the spatial distributions of the instantaneous electric field vector of a radially polarized beam as a superposition given by each of above expressions are shown in the following figure:

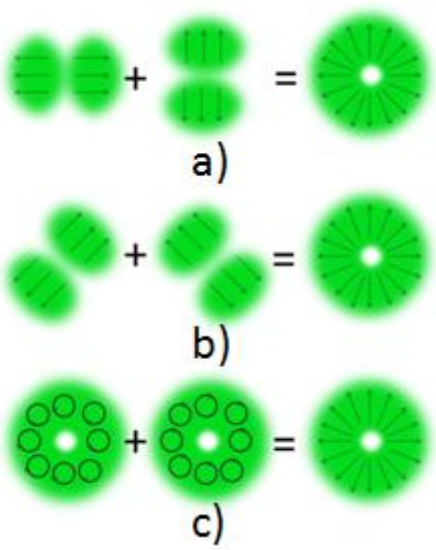

Figure 4.1 Graphical representation of a radially polarized beam as superposition of a) $HG_{10}(\psi_{10})$ and $HG_{01}(\psi_{01})$ modes with p- and s-polarizations respectively, b) HG_{+} and HG_{-} modes with $+45-$ and $-45-$polarizations, respectively, and c) Laguerre-Gauss, LG, modes with $right-hand$ and $left-hand$ polarizations, respectively.

In this sense, a radially polarized beam can be understood as a classically entangled state of light, which carries all the classical polarization states described in Chapter 1 [1].

The mathematical description and the graphical conceptualization (Figure 4.1) of a radially polarized beam show us that it has a well defined local polarization state [1]; experimentally we can observe it, by analyzing a radially polarized beam with a classical PSA. In this sense, we can observe different spatial distributions (non-homogeneous), where each of them has a well defined polarization state (figures 4.1 a), b) and c)), despite the different instantaneous direction of the electric field, which is given by the inhomogeneous phase distribution across the beam. Nevertheless, it is important to note (Figure 3.1) that a radially polarized beam of light, seen as a whole, does not have a well defined polarization state on its transverse spatial profile. Experimentally we can see it by obtaining the Stokes vector of a radially polarized beam, as a whole. In order to do this, we analyze the radially polarized beam with a classical PSA by the six polarization states (s-, p-, +45, -45 and circular right- and left-polarization states) and we employ the classical method in order to calculate the Stokes vector, which is given by Eqs. (2.3.21 through 2.3.24). The algebraic results show us that the Stokes vector of a radially polarized beam provides a spatial average, which does not have a tendency to any polarization state; in other words, the Stokes vector of a radially polarized beam of

light corresponds to a Stokes vector of an un-polarized beam of light $\boldsymbol{S}_{un} = (1\ 0\ 0\ 0)^T$ [1].

The spatial average Stokes vector calculated for a radially polarized beam tests the quality of the experimental arrangement or device, which is used in order to convert a linear polarization state (conventional polarization) of a beam into a radial polarization state (unconventional polarization state). Similarly, it can be used to determine changes in a radially polarized beam, when it interacts with polarizing optical elements or optical elements, which modify the spatial distributions of radially polarized beams, such as mode converters. This parameter is known as *Spatial Average Symmetry* (SAS) Stokes vector, because it is a direct measurement of the symmetry of a radially polarized beam, so that, if the symmetry is perfect then the SAS correspond to an ideal Stokes vector of an un-polarized beam of light [1, 22]. In other case, the SAS corresponds to a Stokes vector with a tendency to a specific polarization state, in the more general case to an elliptically polarized beam of light [22].

It has been reported another set of equations, which allow us to calculate the sixteen Mueller matrix elements. These equations were obtained from a mathematical and physical analysis by taking into account the post-selection technique [1]. This technique consist in the manipulation of the spatial modes by using mode converters and transverse mode beam splitters (modified Mach-Zehnder interferometer) in order to separate each of them knowing that each spatial mode carries a specific polarization state, then it is possible the post-selection of four specific polarization states (spatial modes) in order to analyze each of them by using a classical PSA. We must remember that a radially polarized beam carries all polarization states into a classically entangled state and can be represented as a superposition of two spatial modes with a specific polarization each of them, Eqs.(4.2.6, 4.2.7, 4.2.8). The sixteen Mueller matrix elements are given by the following equations [1]:

$$S_{00} = I_{00} + I_{01} + I_{10} + I_{11} - - - (4.2.9)$$

$$S_{01} = -I_{00} - I_{01} + 2I_{02} - I_{10} - I_{11} + 2I_{12} - - - (4.2.10)$$

$$S_{02} = -I_{00} - I_{01} + 2I_{03} - I_{10} - I_{11} + 2I_{13} - - - (4.2.11)$$

$$S_{03} = I_{00} - I_{01} + I_{10} - I_{11} - - - (4.2.12)$$

$$S_{10} = -I_{00} - I_{01} - I_{10} - I_{11} + 2(I_{20} + I_{21}) - - - (4.2.13)$$

$$S_{11} = I_{00} + I_{01} - 2I_{02} + I_{10} + I_{11} - 2(I_{12} + I_{20} + I_{21} - 2I_{22}) - - - (4.2.14)$$

$$S_{12} = I_{00} + I_{01} - 2I_{03} + I_{10} + I_{11} - 2(I_{13} + I_{20} + I_{21} - 2I_{23}) - - - (4.2.15)$$

$$S_{13} = -I_{00} + I_{01} - I_{10} + I_{11} + 2I_{20} - 2I_{21} - - - (4.2.16)$$

$$S_{20} = -I_{00} - I_{01} - I_{10} - I_{11} + 2(I_{30} + I_{31}) - - - (4.2.17)$$

$$S_{21} = I_{00} + I_{01} - 2I_{02} + I_{10} + I_{11} - 2(I_{12} + I_{30} + I_{31} - 2I_{32}) - - - (4.2.18)$$

$$S_{22} = II_{00} + I_{01} - 2I_{03} + I_{10} + I_{11} - 2(I_{13} + I_{30} + I_{31} - 2I_{33}) - - - (4.2.19)$$

$$S_{23} = -I_{00} + I_{01} - I_{10} + I_{11} + 2I_{30} - 2I_{31} - - - (4.2.20)$$

$$S_{30} = I_{00} + I_{01} - I_{10} - I_{11} - - - (4.2.21)$$

$$S_{31} = -I_{00} - I_{01} + 2I_{02} + I_{10} + I_{11} - 2I_{12} - - - (4.2.22)$$

$$S_{32} = -I_{00} - I_{01} + 2I_{03} + I_{10} + I_{11} - 2I_{13} - - - (4.2.23)$$

$$S_{33} = I_{00} - I_{01} - I_{10} + I_{11} - - - (4.2.24)$$

In this set of equations the elements S_{mn} (where $m, n = 0, 1, 2, 3$) are the sixteen Mueller matrix elements and, the parameter I_{jk} (where $j, k = 0, 1, 2, 3$) represents an intensity value, which can be measured by a photodetector, according to Ref. 1 in this thesis work, we have improved the original idea of Ref. 1, by using a CMOS camera to register the spatial distribution associated to the classical entangled polarization modes. In this case, the subscript j denotes the polarization state and the subscript k denotes the spatial mode. There is a relationship between the subscripts with the spatial modes and the polarization states. For subscript $j(with\ j = 0, 1, 2, 3)$, we have that $\boldsymbol{e}_x$ is denoted by $j = 0$, $\boldsymbol{e}_y$ is denoted by $j = 1$, $\boldsymbol{e}_+$ is denoted by $j = 2$ and $\boldsymbol{e}_r$ is denoted by $j = 3$. For subscript $k(with\ k = 0, 1, 2, 3)$, we have that ψ_{10} is denoted by $k = 0$, ψ_{01} is denoted by $k = 1$, ψ_+ is denoted by $k = 2$ and ψ_L is denoted by $k = 3$.

Here, $\boldsymbol{e}_x, \boldsymbol{e}_y, \boldsymbol{e}_+$ and $\boldsymbol{e}_r$ denote the horizontal, vertical, $+45$ and circular right-handed polarization states, respectively, and $\psi_{10}, \psi_{01}, \psi_+$ and ψ_L denote the horizontal, vertical and diagonal $(+45)$ Hermite-Gauss spatial modes and the left-handed Laguerre-Gauss spatial mode, respectively. So, for example, the parameter I_{00} denotes de intensity measured when we analyze by the horizontal polarization, $\boldsymbol{e}_x$, (using a classical PSA) in the horizontal Hermite-Gauss polarization mode, ψ_{10}. The Mueller matrix can be represented for the following equation.

$$\boldsymbol{M}_T = \begin{pmatrix} S_{00} & S_{01} & S_{02} & S_{03} \\ S_{10} & S_{11} & S_{12} & S_{13} \\ S_{20} & S_{21} & S_{22} & S_{23} \\ S_{30} & S_{31} & S_{32} & S_{33} \end{pmatrix} - - - (4.2.27)$$

Where the T subscript refers to that this Mueller matrix was calculated by using the Professor Töppel and coworkers' method [1].

Chapter 5

Experimental setup

In order to produce a radial polarized beam mode in the laboratory, we employed an optical passive commercially available element, which is known as S-waveplate [10]; that is a super-structure space variant polarization converter. The S-waveplate is an UVFS (UV Fused Silica, SiO2) substrate, which has 1 inch diameter, with and effective 6 mm diameter circular area, and 3mm thickness. It operates with specific wavelengths, in our case at 532 nm $\pm 10\ nm$. The nano-structuring technique used to produce this device was developed by Prof. Peter G. Kazansky's group, from the Optoelectronics Research Centre, at the Southampton University [10]. Some characteristics and benefits are a high damage threshold, high efficiency in polarization conversion (nearly 100% using dedicated wavelengths), a transmission around of 30-90 % depending of the wavelength; it allows us focusing into smaller spot size and so on, according to the manual given by the manufacturer (Altechna, RPC-515-06).

We can get different results depending on the polarization nature of the incident beam; if the incident beam has associated a linear polarization state, we can get radial or azimuthal polarization at the output side. Now, if we employ a circular polarization state as an incident polarization, at the output we get an optical vortex. In figure 5.1 we can see a scheme of an S-waveplate, at the center we can see the super-structured space variant polarization converter, which is the effective zone.

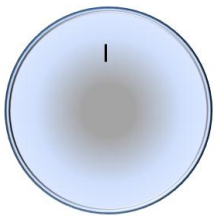

Figure 5.1 Graphical scheme of the S-waveplate employed in order to generate radial polarization.

In our particular problem, we generate radial polarization once an incident horizontally polarized beam travels through the S-waveplate. It is important to take into account the line marked on the S-waveplate, see Fig. 5.1. We need to put the S-waveplate so that the mark is parallel to the incident polarization, in order to guarantee a radially polarized output beam, accordingly to the manufacturer´s manual [10].

The S-waveplate generates a radially polarized beam of light, which carries all classical polarization states according with the theory. Indeed, this beam has three different possible representations, depending on the basis set at which the converter is based; each of them is described as a superposition of two different spatial modes and each mode with a specific polarization. One of them is the superposition of the ψ_{10} (HG_{10}) and ψ_{01} (HG_{01}) beam modes, with $p-$ and $s-$polarization, respectively. Another is the superposition of the diagonal Hermite-Gaussian beam modes, denoted as ψ_{+} and ψ_{-} (with their axes tilted 45° and 135° respect to the horizontal plane, respectively), with $+45-$ and $-45-$polarization, respectively. And finally, we have the superposition of the Laguerre-Gaussian beam modes, denoted as ψ_R and ψ_L (right- and left-handed spatial modes), with right- and left-handed polarization states, respectively.

A radially polarized beam is very useful in polarimetry applications, given that it carries all the polarization states in a classical entangled state [1]. When a transparent and birefringent object is illuminated with a radially polarized beam then the object modifies the polarization states, which this beam carries on. Then, it is necessary to manipulate the beam polarization modes because each of them is related with a specific polarization state. In Chapter 3 was explained that the modified Mach-Zehnder interferometer (MMZI) splits the Laguerre-Gaussian beam mode into the horizontal and vertical Hermite-Gaussian polarization modes (ψ_{10} and ψ_{01}, respectively). Given this, it is easy to see that in order to analyze how were modified the horizontal and vertical polarization states in the radially polarized beam, we must put a classical PSA in each output (outputs 1 and 2, see Fig. 3.7) of the modified Mach-Zehnder interferometer before the detector. Nevertheless, both the diagonal and the circular polarization states are distributed in the beam polarization modes of light, which are different to the ψ_{10} and ψ_{01} beam modes. This is the reason to use the two mode converter configurations after the S-waveplate. The $\pi - mode\ converter$ converts the ψ_{+} and ψ_{-} beam polarization modes into the ψ_{10} and ψ_{01} beam polarization modes, similarly, the $^{\pi}/_{2} - mode\ converter$ converts the ψ_R and ψ_L beam polarization modes into the ψ_{10} and ψ_{01} beam polarization modes; but, in both cases the polarization of

the incident polarization mode is conserved, this means that a mode converter affects the spatial distribution only. With this in mind, we can analyze how both diagonal and circular polarization states were modified by using a classical PSA at each output of the modified Mach-Zehnder interferometer (Fig. 3.7). In this sense, there were necessary to use three different experimental setups, the first uses only the S-waveplate in order to generate a radially polarized beam; the second uses the S-waveplate followed by the $\pi - mode\ converter$ in order to study the modified diagonal Hermite-Gaussian beam modes; and, the last experimental configuration uses a ${}^{\pi}/_{2} - mode\ converter$ after the S-waveplate in order to modify the Laguerre-Gaussian beam modes (if the incident or the modified classical entangled polarized state contain them). The objective of this work is just to implement this technique at the GIPYS laboratory, with the intention to do polarimetry using samples under study. In this sense, it is very important to understand and identify the response of each module that constitutes the complete system. .

The general experimental setups employed in this thesis are shown in the figure 5.2. Basically, it is made up by a laser diode, a spatial filter followed by a collimating lens, after there is a polarizer beam splitter followed by the S-waveplate, which must be illuminated with a linearly polarized beam of light in order to generate a radially polarized beam. After, there is a mode converter or not, depending to the experimental setup (the first setup, see Fig. 5.2 a, does not uses a mode converter; the second setup, see Fig. 5.2 b, uses a $\pi - mode\ converter$; and, the third setup, see Fig. 5.2 c, uses a ${}^{\pi}/_{2} - mode\ converter$), followed by the modified Mach-Zehnder interferometer and finally, a classical PSA followed by a focusing lens and a camera instead of a photodetector. We used the same PSA in order to analyze each output (outputs 1 and 2, see Fig. 3.7) of the modified Mach-Zehnder interferometer (see Fig. 5.2). In Fig. 5.2, we can see at the output 1, the PSA and the camera; while at the output 2 we can see only the half-wave plate (HWP).

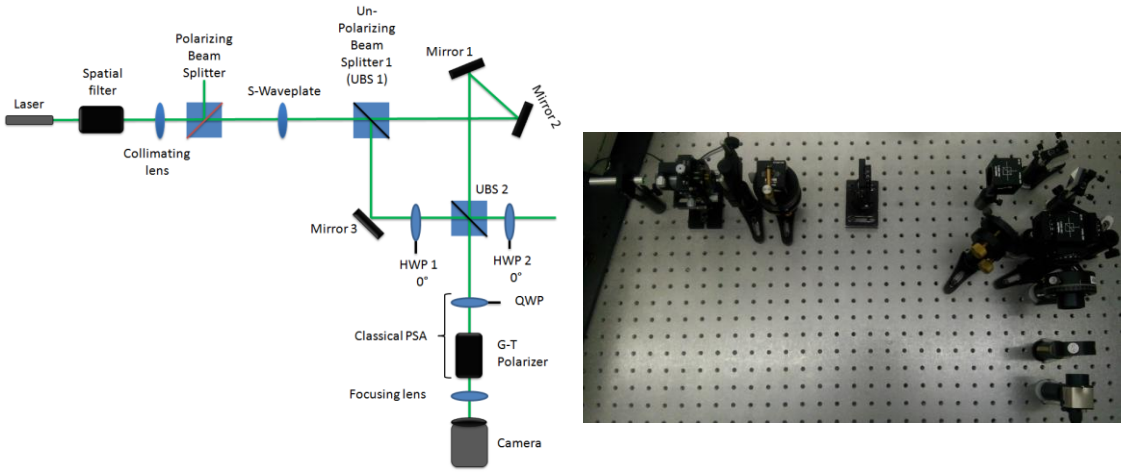
Laser
Spatial filter
Collimating lens
Polarizing Beam Splitter
S-Waveplate
Un-Polarizing Beam Splitter 1 (UBS 1)
Mirror 1
Mirror 2
Mirror 3
UBS 2
HWP 1 0°
HWP 2 0°
QWP
Classical PSA
G-T Polarizer
Focusing lens
Camera

a)

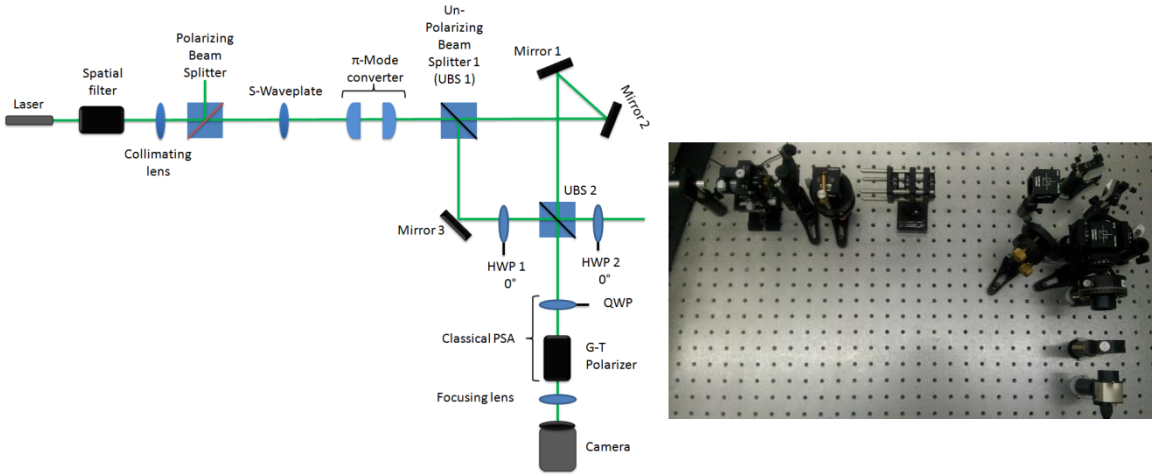
Laser
Spatial filter
Collimating lens
Polarizing Beam Splitter
S-Waveplate
π-Mode converter
Un-Polarizing Beam Splitter 1 (UBS 1)
Mirror 1
Mirror 2
Mirror 3
UBS 2
HWP 1 0°
HWP 2 0°
QWP
Classical PSA
G-T Polarizer
Focusing lens
Camera

b)

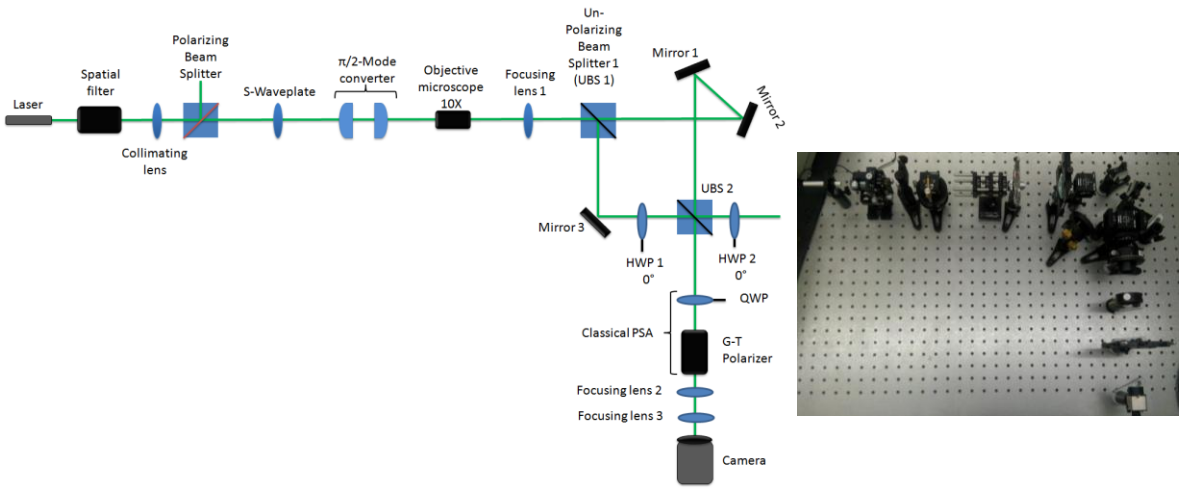

c)

Figure 5.2 General experimental setups: a) we use only the S-waveplate in order to analyze horizontal and vertical polarization states at the outputs of the modified Mach-Zehnder interferometer (MMZI), b) we use the S-waveplate followed by the $\pi - mode\ converter$, with this setup we can analyze by $+45$ and -45 polarization states at the outputs of the (MMZI) and, c) we use the S-waveplate followed by the $\pi/2 - mode\ converter$ in order to analyze circular right- and left-handed polarization states at the outputs of the (MMZI).

Some important details respects to the used elements are mentioned in this paragraph. The source used is a collimated laser diode (Thorlabs, CPS532), which has a wavelength of 532 nm and a power of 4.5 mW. The source is followed by a collimating lens, which has a focal length of 500 mm. It was used a polarizer beam splitter (PBS) in order to polarize the incident beam and, in the modified Mach-Zehnder interferometer there were employed two un-polarizer beam splitters (UBS) (Thorlabs). The spatial filter uses a 10X microscope objective (Newport). The mode converter is formed by a couple of identical cylindrical lenses (Edmund, Lens CYL 25 DIA X 25 FL MGF2 CTD), which have circular shape with a diameter of 25 mm; each of them has an effective focal length of 25 mm and a back focal length of 17.74 mm. Three heat treated coated aluminum plane mirrors in the modified Mach-Zehnder interferometer were used. We used circular achromatic retarders with a diameter of 1 inch (Thorlabs, AHWP05M). It was used a Glan-Thompson linear polarizer in the classical PSA. The focusing lens had a focal length of 1000 mm. Finally, it was used a CMOS color camera (Thorlabs, DCC3240C) as a detector, which is connected to a laptop computer via USB.

When we used the $^{\pi}/_{2} - mode\ converter$, it was necessary to add a second 10X objective of microscope (Edmund Optics) followed by a collimating lens between the mode converter and the modified Mach-Zehnder interferometer input (see Fig. 5.2.c). This was made given that the incident beam of light diverges once that it has traveled through of the $^{\pi}/_{2} - mode\ converter$. In this sense, this setup (10X objective of microscope followed by a collimating lens) focuses the beam, once that it has interacted with the $^{\pi}/_{2} - mode\ converter$. The focal length of the collimating lens was of 500 mm. At each output of the modified Mach-Zehnder interferometer it was used a couple of focusing lenses in order to focus the output beam to the camera, the focal lengths of these lenses were 200 mm and 100 mm, respectively .

If we remember, other important parameter, defined in this thesis and presented in Reference 22, is the Spatial Average Symmetry (SAS). This parameter allows us to test the quality of the device, which generates the radially polarized beam mode. In this sense, it allows us to know the symmetry of the radially polarized beam mode cross-section. On the other hand, we can analyze the radially polarized beam mode once it was modified by a mode converter (MC) in order to determine how it modified the symmetry's beam mode, through the SAS parameter. We can analyze a radially polarized beam mode with a classical PSA by the six polarization states (s-, p-, +45, -45 and circular right- and left-polarization states) and obtain the SAS of that beam (Chapter 4). Figure 5.3 shows the experimental setups to do this. In Fig. 5.3 a, we can see the laser followed by a polarizing beam splitter and the S-waveplate. This setup allows us generates a radially polarized beam. Then, a classical polarization state analyzer (PSA) is putted in order to analyze by the six polarization states in the radially polarized beam generated. Finally, we can see the focusing lens and the camera. This optical system allows us to obtain the experimental measurements. In Fig. 5.3 b, we can see a similar experimental setup like the described one previously. But in that case, there is a mode converter between the S-waveplate and the classical PSA. The mode converter is used on one hand as a $^{\pi}/_{2} - mode\ converter$ (first configuration), and on the other hand as a $\pi - mode\ converter$ (second configuration). The mode converters allow us to convert the polarization beam modes within the radially polarized beam.

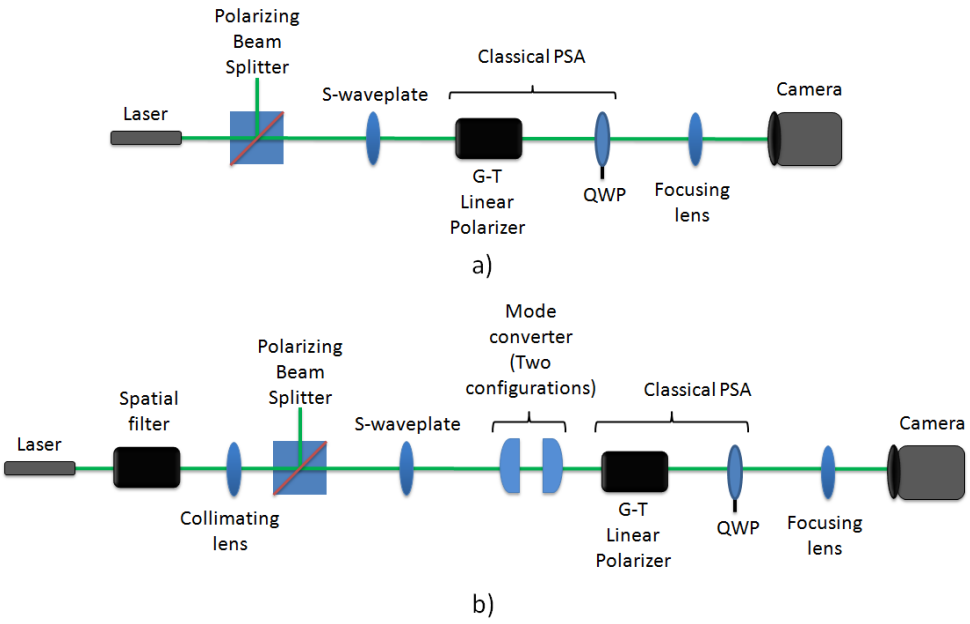

Figure 5.3 Experimental setup used to analyze a radially polarized beam mode (by using a PSA) a) generated by a S-waveplate and b) modified by a mode converter configuration ($\pi - mode\ converter$ and ${}^{\pi}/_{2} - mode\ converter$). With the measurements obtained we can get the SAS for each polarized beam mode (Chapter 4).

Chapter 6

Results

As a first approximation to the experimental setup proposed in this thesis, it is important to understand the principle of functionality of the S-waveplate according to the manufacturer's manual description. We followed the instructions and showed that the S-waveplate does not provide the expected results, at least for the two plates we have purchased from Altechna. Experimentally, we found that the polarization converter generates a radially polarized beam mode, but, this beam is not generated according to the manufacturer´s manual description. In the next paragraphs we describe the experimental method followed in order to probe that. We believe that this inaccuracy must be accepted and corrected by the manufacturer, given that any user who does not take care to probe the correct functionality of the S-waveplate will get unreliable results when uses the S-waveplate following the manufacturer's manual.

Accordingly to the manufacturer´s manual, we need to employ a linearly polarized beam as an incident beam of light on the S-waveplate. The S-waveplate has a mark on one of their parallel faces. It is important that the incident beam fall on the marked face; also, this mark must be parallel with respect to the incident polarization plane. This means that if we employ horizontal polarization then the mark must be aligned also horizontally.

Firstly, it is shown the results obtained by using two different sources, located before the S-waveplate; a) one of them consists of a laser followed by a polarizer beam splitter (we used the p-polarized beam of light, where the laser output profile is considered by the manufacturer as highly Gaussian), and b) the other consists of a laser, which was spatially filtered and collimated to provide an homogeneous illumination, followed by a circular pupil and a polarizer beam splitter (see figure 6.1).

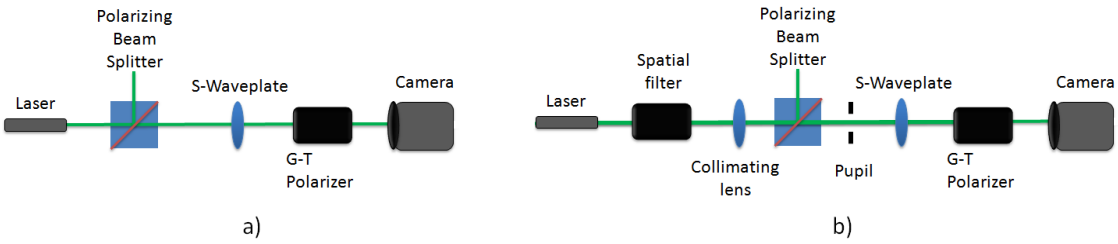

Figure 6.1 Experimental configurations used to generate a radially polarized beam of light.

It was used a Glan-Thompson linear polarizer (G-T linear polarizer) in order to analyze the beam generated, a CCD camera as spatially distributed intensity detector; the transmission axis of the linear polarizer is oriented by an angle of 90° respect to the horizontal plane (holographic table). The experimental results obtained with the previously experimental configurations (Fig. 6.1) are shown in figure 6.2.

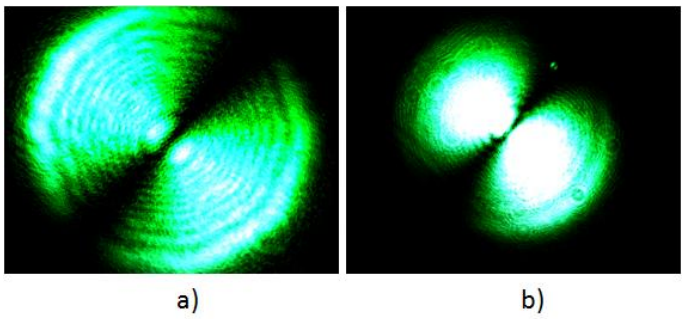

Figure 6.2 Modes observed when we analyze an emergent beam from the S-waveplate. The incident beam has linear polarization (p-polarization), which is parallel to the S-waveplate's mark. These results were obtained by using a) the experimental configuration shown in figure 6.1 a) and b) the experimental setup shown in figure 6.1 b). A Glan-Thompson linear polarizer was used as analyzer. The transmission axis of the linear polarizer is oriented by an angle of 90° with respect to the holographic table.

Given the results, we decide to use a collimated light source as an incident beam, because it generates a uniform intensity distribution, which reduces the intensity noise; in these figures, we do not used a diattenuator (or neutral density filter) in order to modulate the intensity of the output beam because the images are saturated sometimes (like figure 6.2); but, in the next results it was used.

The next step was to probe if the S-waveplate generates a radially polarized beam when we use it according to the manufacturer's manual. The generated beam mode was analyzed with a linear polarizer (LP) by rotating its transmission axis to different angles in order to determine the relation between spatial and polarization DoFs (Fig. 6.1 b). The results show us that the output beam is not like a

radially polarized beam, instead of this, it is like a generalized cylindrical vector (CV) beam, see figure 6.3, where the arrows represent the orientation of the transmission axis.

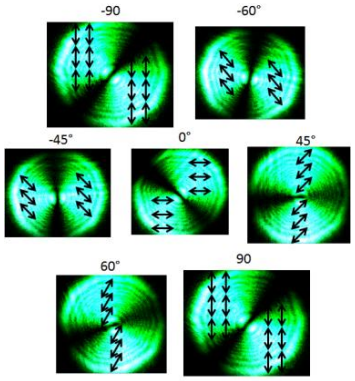

a)

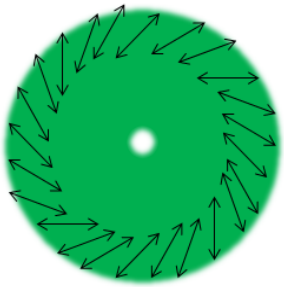

b)

Figure 6.3 In this figure we can observe a) the spatial distribution modes produced by the S-waveplate when it is used according to the manufacturer's manual and, b) a graphical representation of the output beam polarization (which is like a generalized CV beam with spiral symmetry). The beam modes were analyzed with a Glan-Thompson linear polarizer with its transmission axis to different angles respect to the horizontal plane (holographic table). It was used the experimental setup shown in Fig. 6.1 b).

After this analysis, we observed that the polarization of the output beam is not radial; taking into account the inaccuracy present in the actual version of the manufacturer´s manual, we employed the S-waveplate putting its mark to different angles in order to get a radially polarized beam. Experimentally, we found that a radially polarized beam mode is obtained when we orient the S-waveplate's mark to $+45°$ with respect to the incident polarization plane, as can be observed from Fig. 6.4. The experimental setup employed in this case is shown in Fig. 6.1 b).

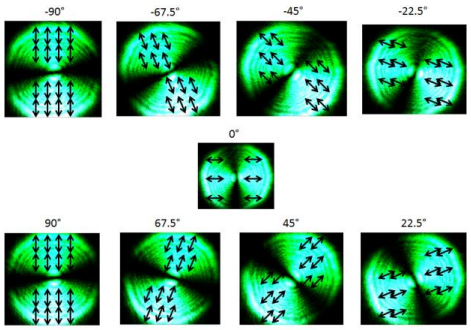

a)

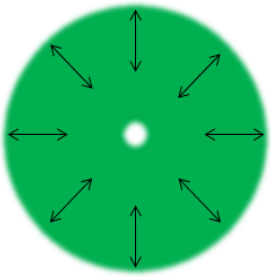

b)

Figure 6.4 In this figure we can observe a) the spatial distribution modes produced by the S-waveplate when its mark is oriented to $+45°$ with respect to the incident polarization plane and, b) a graphical representation of the output beam polarization (which is like a radially polarized beam of light). The beam modes were analyzed with a Glan-Thompson linear polarizer with its transmission axis to different angles respect to the horizontal plane (holographic table). It was used the experimental setup shown in Fig. 6.1 b).

Also, we observed that the azimuthally polarized beam is obtained when the S-waveplate's mark is oriented to $-45°$ respect to incident polarization plane. The figure 6.5 was obtained for different orientations of the linear polarizer transmission axis (analyzer). Also, in this case we used the experimental setup shown in Fig. 6.1 b).

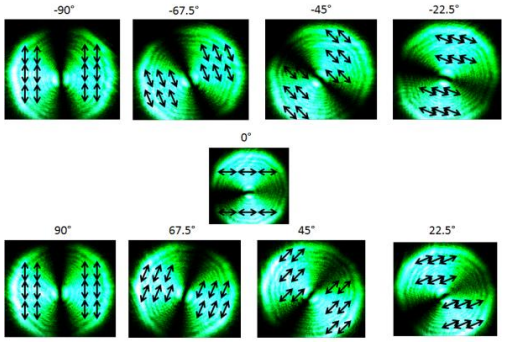

a)

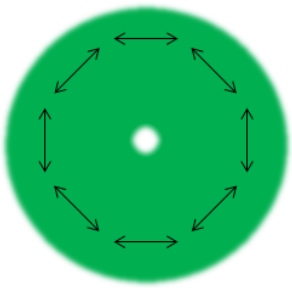

b)

Figure 6.5 In this figure we can observe a) the spatial distribution modes produced by the S-waveplate when its mark is oriented to $-45°$ with respect to the incident polarization plane and, b) a graphical representation of the output beam polarization (which is like an azimuthally polarized beam of light). The beam modes were analyzed with a Glan-Thompson linear polarizer with its transmission axis to different angles with respect to the horizontal plane (holographic table). It was used the experimental setup shown in Fig. 6.1 b).

Once we have determined the right way to operate the S-waveplate in order to generate a radially polarized beam, now, we work with this beam using both the $\pi - mode\ converter$ $(\pi - MC)$ and the $\frac{\pi}{2} - mode\ converter$ $(\frac{\pi}{2} - MC)$, which correspond with two different configurations of a couple of cylindrical lenses: a $\pi - MC$ consists of two identical cylindrical lenses which are separated twice the distance of their focal length, and a $\frac{\pi}{2} - MC$ is similar to $\pi - MC$, but in this case the separation between cylindrical lenses is equal to the focal distance multiplied by the square root of the number two. The objective at this stage, is just to probe it operates correctly. If we remember, when the axis of a $\pi - MC$ is oriented to 22.5° respect to the horizontal plane, then this configuration allows us convert the diagonal HG beam modes, ψ_+ and ψ_-, into the horizontal and vertical HG beam modes, ψ_{10} and ψ_{01}, respectively, without modifying their polarization states. In a similar way, when the axis of a $\pi/2 - MC$ is oriented to $+45°$ respect to the horizontal plane, then this configuration converts the right- and left-handed LG beam modes, ψ_R and ψ_L, into the horizontal and vertical HG beam modes, ψ_{10} and ψ_{01}, respectively, without modifying their polarization states.

Theoretically, the $+45$-diagonal beam mode (the axis of this mode is oriented by an angle of $+45°$ respect to the horizontal plane and looking toward the source, see Fig. 6.4 a) has a $+45$-polarization state given the nature of a radially polarized beam. Similarly, the -45-diagonal beam mode (the axis of this mode is oriented by an angle of -45 respect to the horizontal plane and looking toward the source, see Fig. 6.4 a) has a -45-polarization state. We can observe that in the experimental results shown in Fig. 6.4. Therefore, once they are modified by a $\pi - MC$, we hope

to get the horizontal and the vertical beam modes with $+45$-polarization state and -45-polarization state, respectively. In this sense, the experimental setup used to observe that is shown in figure 6.6.

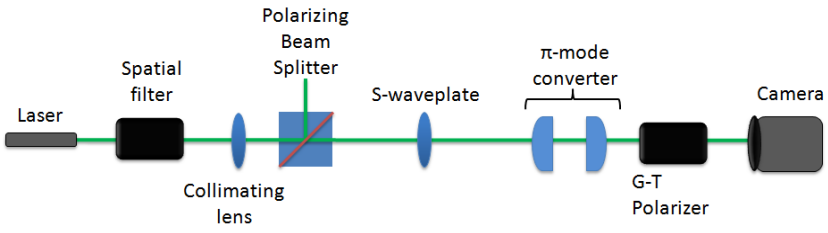

Figure 6.6 Experimental setup used to observe the beam modes when we analyze a radially polarized beam mode once it was modified by a $\pi - MC$. It was used a Glan-Thompson linear polarizer as analyzer.

Experimentally, we got the expected results; that is, a horizontal polarization mode with a $+45 - polarization$ state and, a vertical polarization mode with a $-45 - polarization$ state. These results are shown in figure 6.7.

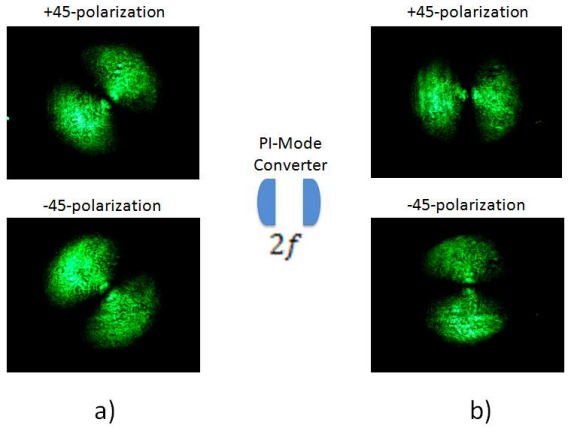

Figure 6.7 These experimental results were obtained by analyzing the $+45$- and -45-polarization states (using a Glan-Thompson linear polarizer) a) before and, b) after that a radially polarized beam is modified by a $\pi - MC$. The axis of the $\pi - MC$ is oriented by an angle of +22.5° with respect to the horizontal plane (holographic table). The experimental setup shown in figure 6.6 was used to this end.

We can see that the spatial modes were modified by a $\pi - MC$, but it conserves its polarization state, that is, we have generated a ψ_{10} beam mode with a $+45$-polarization state and a ψ_{01} beam mode with a-45-polarization state. We must remember that given the symmetry of a radially polarized beam, when we analyze it by the p- and s- polarization states without any MC (mode converter), then the

result shows us the ψ_{10} and ψ_{01} beam modes, respectively. We used the following experimental setup (Fig. 6.8) to obtain the results shown in figure 6.9.

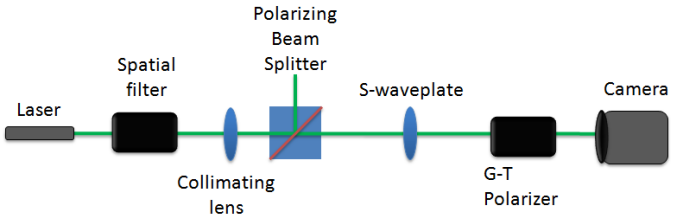

Figure 6.8 Experimental setup used to observe the beam modes when we analyze a radially polarized beam mode by using a Glan-Thompson linear polarizer as analyzer.

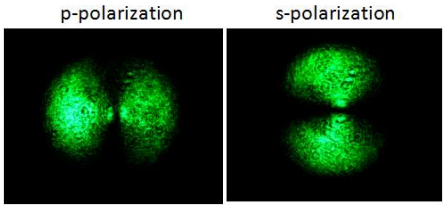

Figure 6.9 These experimental results were obtained by analyzing the p −and s −polarization states (by using a Glan-Thompson linear polarizer) to a radially polarized beam, without the presence of any MC. Fig. 6.8 shows the experimental setup used to this end.

Finally, we can remember that the right- and left-handed polarization states are spatially distributed as Laguerre-Gaussian (LG) beam modes within the radially polarized beam, which was generated by the S-waveplate (this must occur only if the S-waveplate has a basis set constituted by Laguerre-Gauss right- and left-handed polarized modes). The right-handed LG beam mode has circular right-handed polarization state and, the left-handed LG beam mode has circular left-handed polarization state. In this sense, we use a $\pi/2 - MC$ (the axis of the $\pi/2 - MC$ oriented by an angle of $+45°$ respect to the horizontal plane) in order to convert the left-handed LG beam mode with circular left-handed polarization state, into the horizontal HG beam mode, ψ_{10}, with the same polarization state. In the same way, the right-handed LG beam mode with circular right-handed polarization state is converted into a vertical HG beam mode, ψ_{01}, with the same polarization state. It was used a classical PSA (QWP with its fast axis set at $45°$ and $-45°$ respect to the holographic table followed by a LP with its transmission axis parallel to it) in order to analyze by circular right- and left-handed polarization states in both cases: after and before the radially polarized beam has been modified by the $\pi/2 - MC$. See figure 6.10.

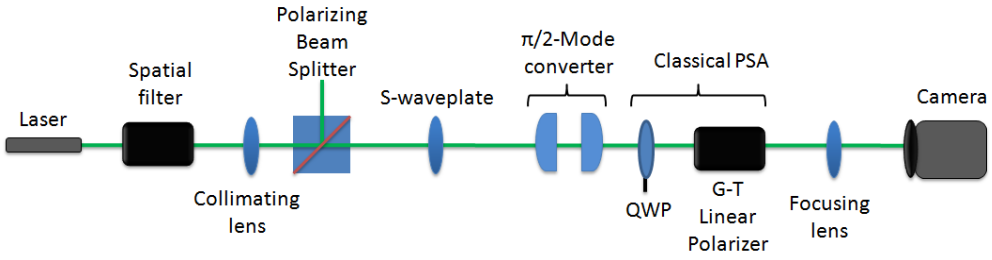

Figure 6.10 Experimental setup used to observe the beam modes when we analyze a radially polarized beam mode once it was modified by a $\pi/2 - MC$. It was used a classical PSA in order to analyze circular right- and left-handed polarization states (QWP with its fast axis set at $-45°$ and $45°$ respect to the holographic table followed by a LP with its transmission axis parallel to it, respectively).

The experimental results obtained in this case are shown in the following figure (Fig. 6.11):

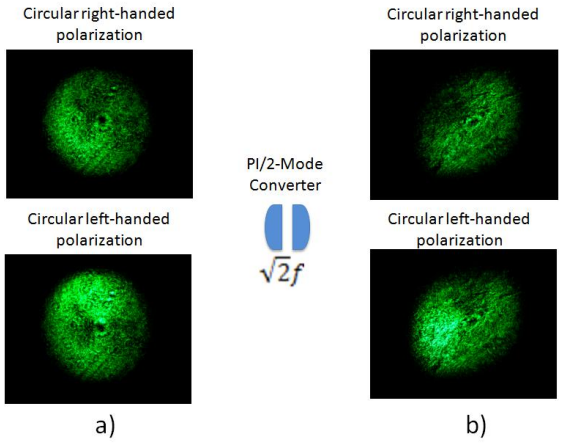

Figure 6.11 These experimental results were obtained by analyzing circular right- and left-handed polarization states (using a classical PSA) in both cases: a) before and, b) after that the radially polarized beam was modified by the $\pi/2 - MC$. The experimental setup used to obtain these results is shown in Fig. 6.7.

In Fig. 6.11, it is not clear the conversion between LG and HG polarization beam modes. Theoretically, we expect observe a vertical HG polarization mode with circular left-handed polarization and, a horizontal HG polarization mode with right-handed polarization. We know that the most difficult polarization state that can be generated is the circular polarization state. In a similar way, we have that the most difficult transformation is from LG to HG beam modes. Three possible error sources about it are the following: the correct parallel alignment between the axes of the cylindrical lenses, the required separation between the lenses, and tilting the mode converter by the angle necessary in order it works as expected. Besides,

we know that the cylindrical lenses are not ideal optical elements and the focal distance is not the exact value, which is provided by the manufacturer technical chart. In this case, it is important to mention that we found an experimental value of the focal distance of 24.26 mm, approximately (the focal distance provided by the manufacturer is 25 mm).

We analyzed the radially polarized beam generated by the S-waveplate by using a classical PSA in order to obtain its SAS (Spatially Average Symmetry [22]). By using the PSA we can obtain the measurements, which correspond with the six polarization states analyzed ($p-$, $s-$, $+45$, -45, circular right-handed and left-handed polarization states) and then, we used the equations 2.3.21 to 2.3.24, in order to obtain the SAS of the beam mode. If we remember, the SAS allows us to know the quality of the beam produced by the S-waveplate. In a similar way, we analyzed and obtained the SAS, which corresponds to the beams' cross-section symmetry, once they were modified by the two mode converter configurations, which were described previously. The experimental setups used to obtain the measurements are shown in Fig. 5.3. The experimental results obtained by applying the polarimetric analysis for the radially polarized beam mode generated by the S-waveplate, the radially polarized beam mode modified by the $\pi - mode\ converter$ ($\pi - MC$) and, the radially polarized beam mode modified by the $\pi/2 - mode\ converter$ ($\pi/2 - MC$), are shown in the following figure.

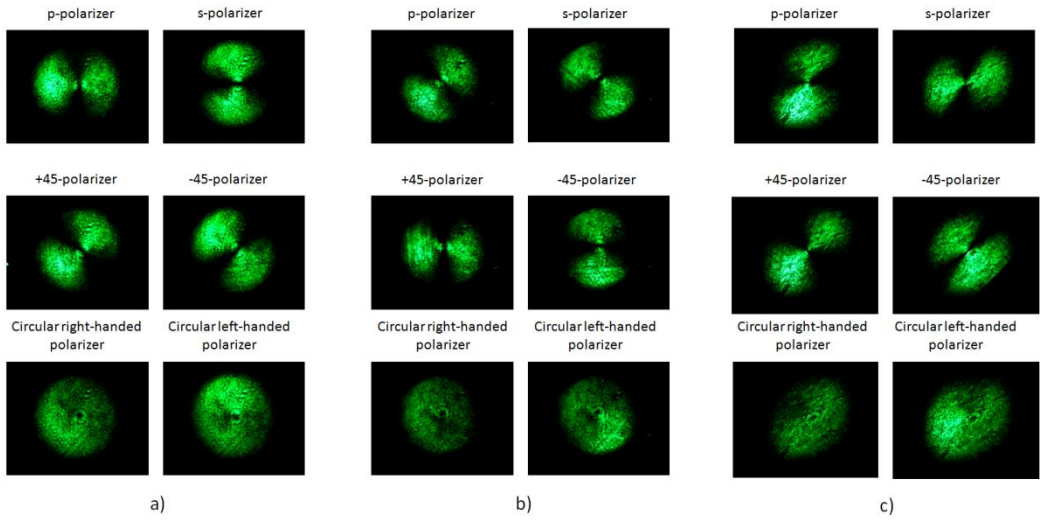

Figure 6.12 Experimental results obtained by applying the polarimetric analysis to a) the radially polarized beam mode generated by the S-waveplate, b) the radially polarized beam mode modified by the $\pi - MC$ and, c) the radially polarized beam mode modified by the $\pi/2 - MC$.

In Fig. 6.12 we can see the polarization modes for the three cases mentioned previously. We can determine how the polarization modes were modified once they interact with the mode converters by analyzing them with a classical PSA. The experimental SAS obtained by using the results of the Fig. 6.12 are shown in the figure 6.13. It is clear that each SAS have four elements denoted as s_0, s_1, s_2 and s_3 (from upper to lower). The first,s_0, has information about the total intensity of beam. The second, s_1 describes the predominance of horizontal polarization state. The third, s_2, describes the tendency of linear $+45$ polarization state. The four, s_3, describes the predominance of circular right-handed polarization state.

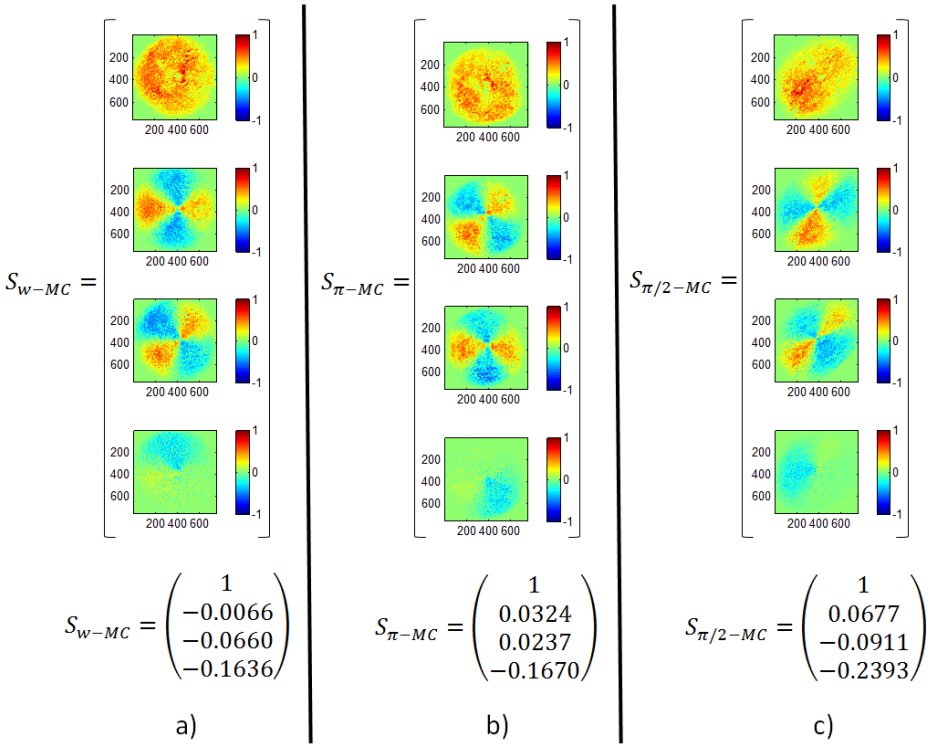

Figure 6.13 Experimental results for the SAS obtained by using the setups of Fig. 5.3: a) the analysis for the radially polarized beam produced by the S-waveplate or without mode converter (wMC), b) the analysis for the beam produced by the S-waveplate and modified by the $\pi - mode\ converter$ ($\pi - MC$) and, c) the analysis for the beam produced by the S-waveplate and modified by the $\pi/2 - mode\ converter$ ($\pi/2 - M$).

Fig. 6.13 shows the SAS of images and their numerical values associated, which were obtained for the three cases, see Fig. 6.12. The SAS of images was obtained by acquiring the experimental images (Fig. 6.12) and by applying the arithmetic operations, which are given by Eqs. 2.3.21 to 2.3.24. In this case, we used the images shown in Fig. 6.12 as experimental data directly. The numerical SAS was obtained by applying the arithmetic mean of each experimental image and by

applying the same equation set (Eqs. 2.3.21 to 2.3.24). In this case, we calculated the mean of each image shown in fig. 6.12 and then we used those numerical values as experimental data. It is clear that, the SAS (of images and numerical) shown in Fig. 6.13 a, was obtained by using the experimental data shown in Fig. 6.12 a. In a similar way, we obtained the SAS (of images and numerical) shown in Figs. 6.13 b, and 6.13 c, by using the experimental data shown in Figs. 6.12 b, and 6.12 c. This method was programmed in Matlab and the Matlab code is showed in the Appendix C. These results show us a tendency to elliptical polarization state, which are the expected results, given that the beams analyzed have a non-perfect symmetry respect to its polarization distribution on the transversal section. Also, it is possible to distinguish how the incident beam modes are modified by each mode converter configuration. We can observe the element s_1 of the Stokes vector of images (Fig. 6.13 a), which corresponds to the difference between the HG_{10} and HG_{01} modes, which have horizontal and vertical polarization states, respectively. Similarly, the element s_2 of the Stokes vector of images (Fig. 6.13 b) shows us the difference between the HG_{10} and HG_{01} modes, but in this case they have +45 and -45- polarization sates, respectively. Finally, if we observe the element s_3 of the Stokes vector of images (Fig. 6.13 c), it is not clear the difference between the HG_{10} and HG_{01} modes, which have circular left- and right-handed polarization states, respectively. In this case (Fig. 6.13 c, element s_3), we cannot observe a symmetric image (as it is shown in Fig. 6.13 a, and Fig. 6.13 b); indeed, the numeric value, associated to the element s_3 of Fig. 6.13 c, is not very close to zero (-0.2393). This means that perhaps the S-waveplate basis set is not constituted by Laguerre-Gaussian beam modes (which have circular left- and right-handed polarization states) and therefore the $\pi/2 - mode\ converter$ does not generate the Hermite-Gaussian beam modes, HG_{10} and HG_{01} (which have circular left- and right-handed polarization states, respectively). Perhaps, the intensity pattern observed in the element S_3 (Fig. 6.13 c) is only an effect due to the cylindrical lenses, when the beam travels through them. Therefore, when we obtain the difference between the HG_{10} and HG_{01} modes, the result is not axially symmetric.

In a similar way, we analyzed the beam polarization modes of each output of the modified Mach-Zehnder interferometer and we obtained the SAS of each of them. The analysis was made for three experimental setups, which are shown in figure 5.2. The main idea is determine how was modified the SAS of the mode beams, once they have traveled through the experimental setup. Similar to the previous case, we analyzed by using a PSA the polarization modes by the six polarization

sates ($p-$, $s-$, $+45$, -45, circular right-handed and left-handed polarization states). We analyzed each output polarization mode (at the two outputs of the MMZI) for the three experimental setups shown in Fig. 5.2. If we remember, a modified Mach-Zehnder interferometer has two outputs, see Fig. 5.2. We analyzed each output by using a classical PSA for each experimental setup (Fig. 5.2 a, Fig.5.2 and Fig. 5.2 c). The experimental results are shown in the following figures (Fig. 6.14, Fig. 6.15 and, Fig. 6.16).

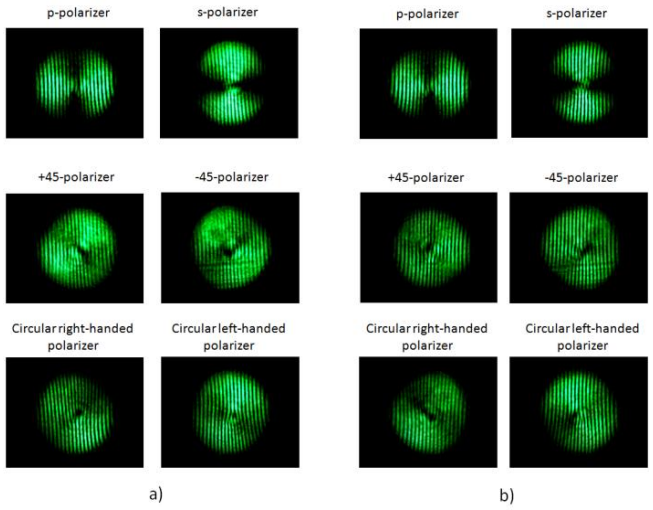

Fig. 6.14 Experimental results obtained by analyzing the polarization modes of a radially polarized beam mode produced by a S-waveplate. We analyzed them, by using a PSA a) at output 1 and b) at output 2 of the MMZI. The experimental setup used in this case is shown in Fig. 5.2 a.

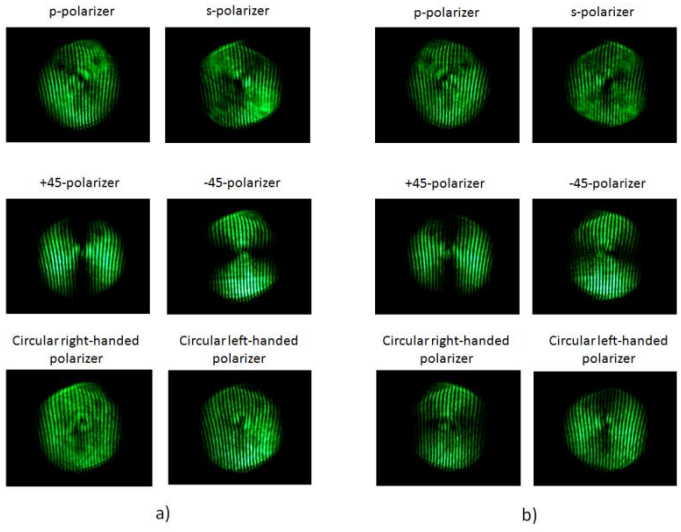

Fig. 6.15 Experimental results obtained by analyzing the polarization modes of a radially polarized beam mode modified by a $\pi - MC$. We analyzed them, by using a PSA a) at output 1 and b) at output 2 of the MMZI. The experimental setup used in this case is shown in Fig. 5.2 b.

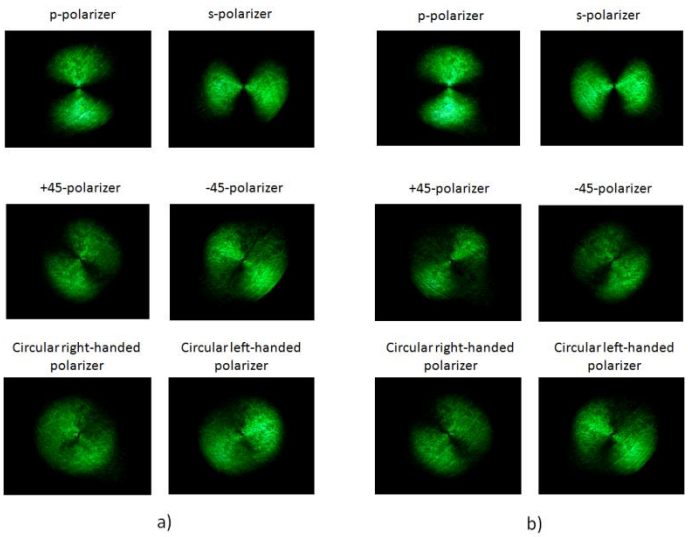

Fig. 6.16 Experimental results obtained by analyzing the polarization modes of a radially polarized beam mode modified by a $\pi/2 - MC$. We analyzed them, by using a PSA a) at output 1 and b) at output 2 of the MMZI. The experimental setup used in this case is shown in Fig. 5.2 c.

The experimental SAS obtained by using the results of the Fig. 6.14, Fig. 6.15 and Fig. 6.16 are shown in the following figures (Fig. 6.17, Fig. 6.18 and, Fig. 6.19).

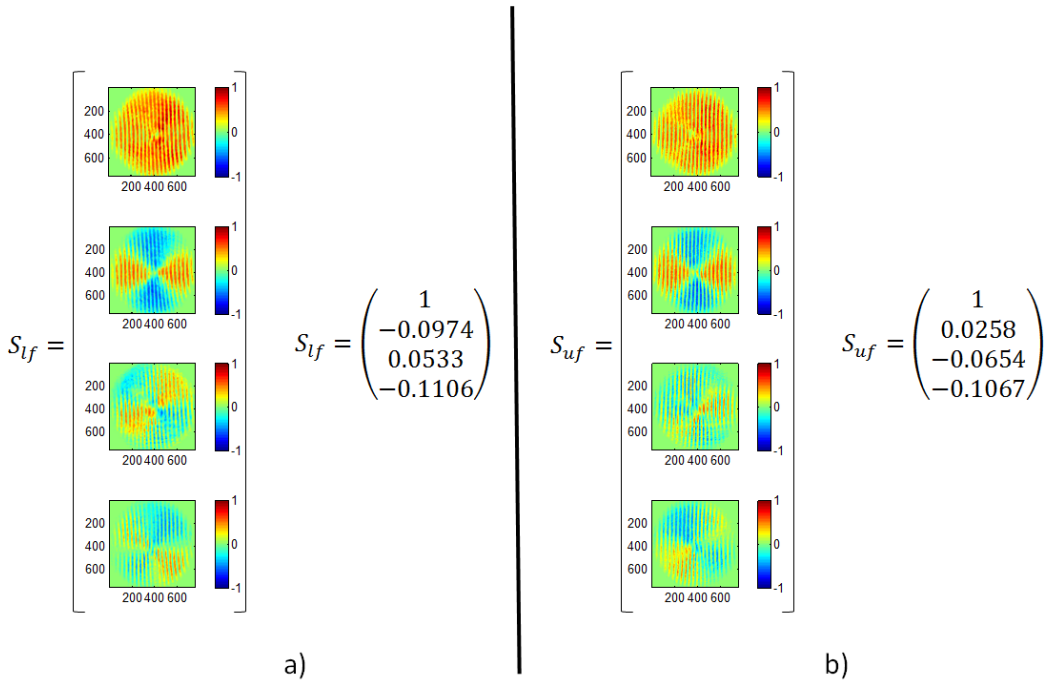

Figure 6.17 Experimental results for the SAS obtained when we analyze the a) output 1, S_{lf}, and the b) output 2, S_{uf}, of the modified Mach-Zehnder interferometer (first experimental setup), which is shown in figure 5.2 a.

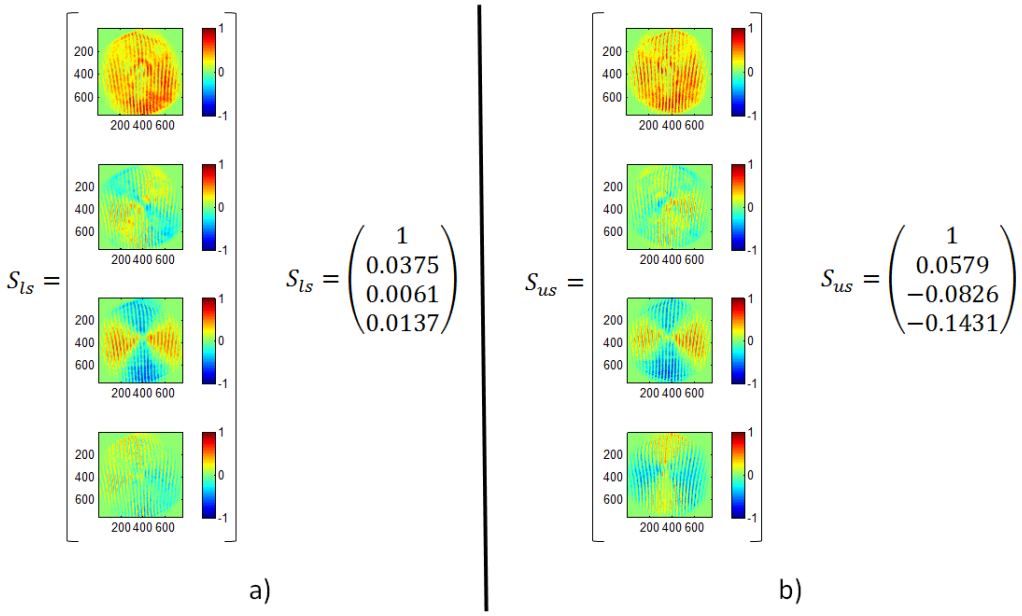

Figure 6.18 Experimental results for the SAS obtained when we analyze the a) output 1, S_{ls}, and the b) output 2, S_{us}, of the modified Mach-Zehnder interferometer (second experimental setup), which is shown in figure 5.2 b.

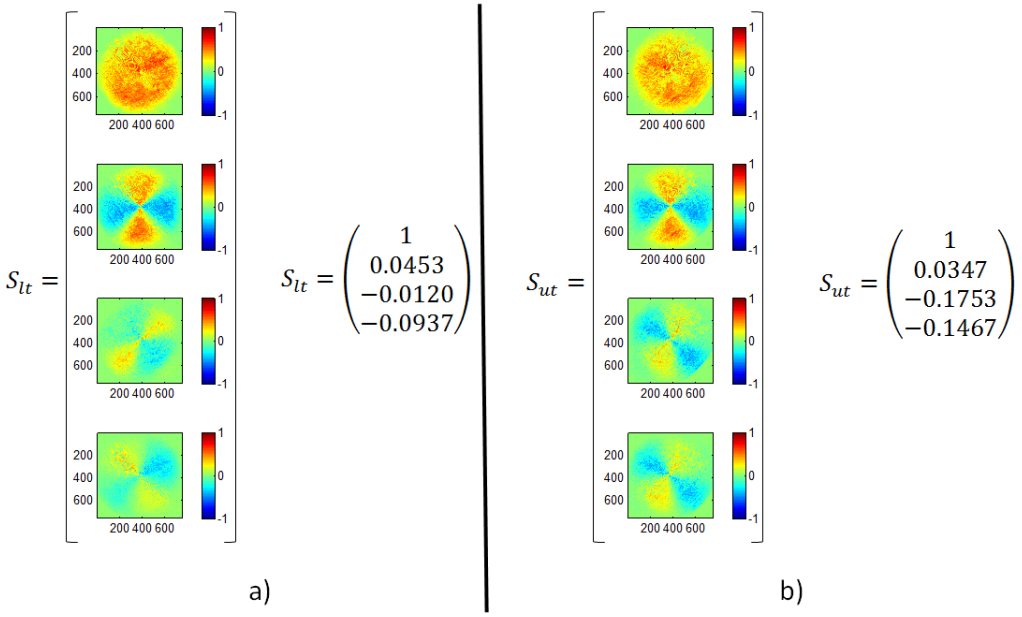

Figure 6.19 Experimental results for the SAS obtained when we analyze the a) output 1, S_{lt}, and the b) output 2, S_{ut}, of the modified Mach-Zehnder interferometer (third experimental setup), which is shown in figure 5.2 c.

In general, we can see in figures 6.17 through 6. 19 that the SAS, obtained for each case, has a tendency to an elliptical polarization state. That means that the beam polarization modes analyzed have not a perfect axial symmetry. We know that the beam polarization modes are modified as the beam travels through the polarizing elements of the optical system (polarizers and retarders, for example) and, therefore the polarization modes change their distribution over the transversal beam section. In Fig. 6.17, we can see the element s_1 (in both 6.17 a, and 6.17 b images). We can remember that the element s_1 of the SAS is related with the difference between the polarization modes, which have horizontal and vertical polarization (HG_{10} and HG_{01}, respectively). The numerical values for s_1 shown in Fig. 6.17 a, and Fig. 6.17 b, are very close to zero but, they are not exactly zero. Therefore, we can say that the horizontal HG_{10} and vertical HG_{01} polarized beam modes are not perfect symmetric over the transversal beam section. Similarly, we can analyze the element S_2 of the SAS shown in Fig. 6.18 a, and Fig. 6.18 b. We can remember that this element is the difference between the polarization modes with +45- and -45-polarization states (HG_{10} and HG_{01}, respectively). The numeric values of each of them are very close to zero, but are not exactly zero. We can say that the HG_{10} and HG_{01} beam modes are not perfect symmetric over the transversal beam section. Finally, if we observe the element S_3 (Fig. 6.19 a, and Fig. 6.19 b), the numeric value is not very close to zero, with respect to the above cases (Fig. 13 and Fig. 14). If we remember this element is related with the difference between the polarization modes, which have circular left- and right-handed polarization states (HG_{10} and HG_{01}, respectively). It is clear that in Fig. 6.15, the element S_3 is not the difference between the HG_{10} and HG_{01} beam polarization modes.

The mode converters, which were described previously, are very important for this work, since they allow us to convert the spatial distribution of both diagonal and circular polarizations states. In principle these polarization states are distributed in diagonal HG and right- and left-handed LG beam modes within the radially polarized beam, respectively. As it was mentioned previously, the $p-$ and $s-$polarization states are distributed in the ψ_{10} and ψ_{01} beam modes (horizontal and vertical Hermite-Gaussian beam modes), respectively; the previous statement is a consequence of the nature of the radial polarization. When the mode converters ($\pi - MC$ and $\pi/2 - MC$) work over the spatial distribution of both diagonal and circular polarization states; we obtain the $+45$- and -45-polarization states and circular left- and right-handed polarization states distributed in the ψ_{10} and ψ_{01} beam modes (horizontal and vertical Hermite-Gaussian beam modes), respectively for each case. At this point, we do not forget

that in each case the ψ_{10} and ψ_{01} beam modes are superposed as a LG beam mode of first order (Laguerre-Gaussian beam mode). Therefore, we need to use the transverse mode beam splitter (or modified Mach-Zehnder interferometer), which allows us to split the LG beam mode into the ψ_{10} and ψ_{01} beam polarization modes. With this, we can analyze each of the six polarization states (p-, s-, +45, -45, right- and left-polarization states) in order to quantify the change induced by a sample in each of them, simply by using a classical PSA at each output of the Modified Mach-Zehnder interferometer.

Experimentally, we have analyzed the behavior of the radially polarized beam through the modified Mach-Zehnder interferometer in order to understand how it works. The analysis was made by using a linear polarizer (Glan-Thompson linear polarizer). We have analyzed only the case when we used a radially polarized beam as an incident beam, by simplicity. Nevertheless, the configurations where we have used mode converters can be analyzed in a similar way. The graphical result is shown in figure 6.20:

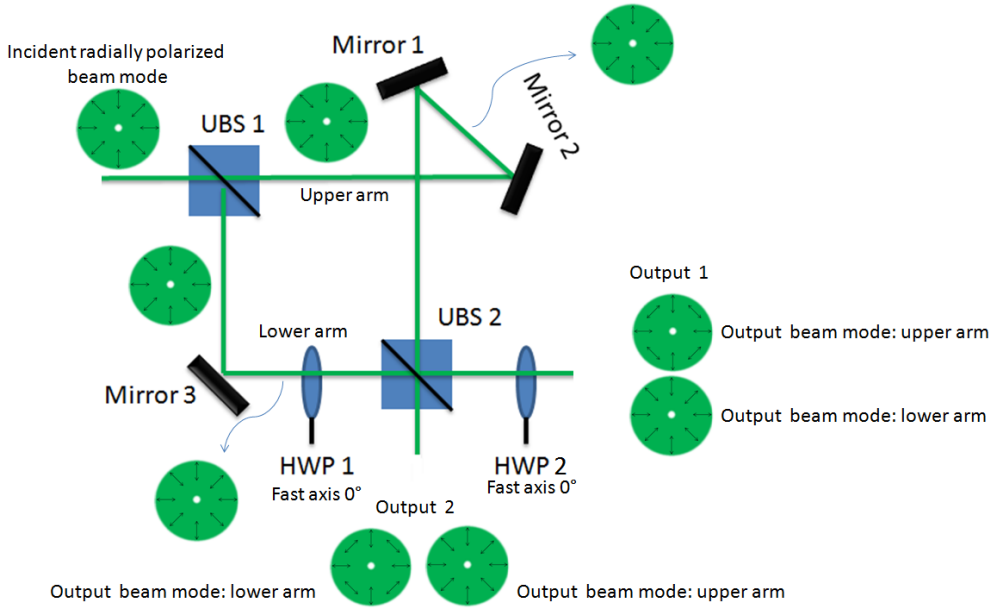

Figure 6.20 Graphical representation of the behavior of a radially polarized mode beam through a modified Mach-Zehnder interferometer. Here, we have used a couple of un-polarizing beam splitter (UBS) and two half-wave plates (or retarders, HWP) with their fast axes parallel respect to the horizontal plane (holographic table).

We can see that a reflection on a plane mirror modifies both the spatial and the polarization degrees of freedom (DoFs), while a half-wave plate (HWP) modifies only the polarization DoF.

In this work we have used a CMOS camera as a detector and therefore we have obtained the image of each measurement (a two-dimensional matrix), and the arithmetic mean of this spatially distributed image (a scalar). We must remember that the main idea is to do the measurements of the six polarization states ($p-$, $s-$, $+45$, -45, circular right-handed and left-handed polarization states) by using a PSA at each output of the transverse-mode beam splitter (or modified Mach-Zehnder interferometer). This procedure is realized for each experimental setup, see Fig. 5.2. In this sense, we are reporting a Mueller matrix of images (this is, images of the elements of the Mueller matrix). Each element of the Mueller matrix is calculated by employing the images of the intensity measurements. Also a spatially averaged numerical Mueller matrix is reported. The numerical Mueller matrix is calculated by employing the scalar values (which are obtained by calculating the arithmetic mean of the two dimensional matrix or images of the intensity measurements). The Mueller matrix elements are calculated by applying on the one hand, the IPA method, Eqs. (2.4.2.1 through 2.4.2.16), which were coded by the Matlab code presented in the Appendix A; and, on the other hand, the method described in Reference 1 (RM, Professor Töppel and coworkers' method), Eqs.(4.2.9 through 4.2.24), which were coded by the Matlab code of Appendix B. As a first approximation we have calculated the characteristic Mueller matrix of the system. In the figures 6.21 and 6.22, we show both the numerical Mueller matrix and the Mueller matrix of images obtained through Professor Töppel and coworkers' method and also the IPA method.

$$M_{IPA} =$$

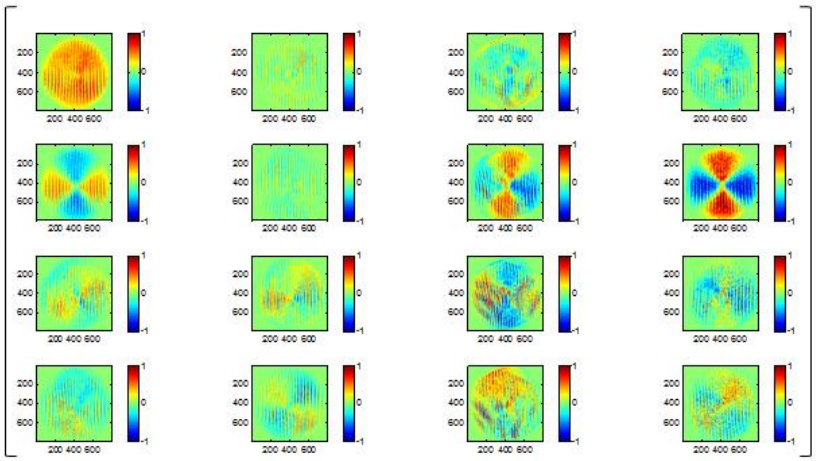

$$M_{IPA} = \begin{bmatrix} 1 & 0.0938 & -0.0745 & -0.2545 \\ -0.0423 & -0.0642 & 0.0797 & 0.0675 \\ 0.0949 & 0.1351 & -0.1315 & -0.2587 \\ -0.1845 & -0.0835 & 0.3277 & 0.0337 \end{bmatrix}$$

Figure 6.21 Experimental Mueller matrix calculated by using the IPA method.

$M_{RM} =$

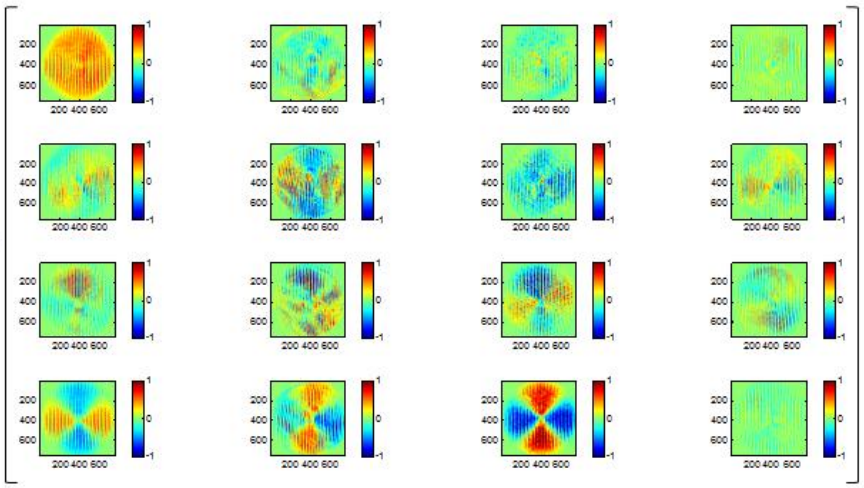

$$M_{RM} = \begin{bmatrix} 1 & -0.0780 & -0.0990 & 0.0934 \\ 0.0965 & -0.1324 & -0.4668 & 0.1355 \\ 0.0347 & 0.0954 & -0.0687 & -0.0585 \\ -0.0405 & 0.0760 & 0.0835 & -0.0640 \end{bmatrix}$$

Figure 6.22 Experimental Mueller matrix calculated by using the method described in the Reference 1 (Professor Töppel and coworkers' method).

Since we have obtained the previous experimental results (Fig. 6.21 and Fig. 6.22) without analyzing any sample, then, we expect to obtain the air Mueller matrix. If we remember, the Mueller matrix associated to air is an identity matrix given that, theoretically, the polarization state of an incident beam of light is not modified when it interacts with air. Therefore, we can conclude that the Mueller matrices of the figures 6.21 and 6.22 and theirs associated averaged numerical Mueller matrices are not the expected results.

In this sense, it was necessary to carry out an analysis of the principal components of the experimental setup. Experimentally, we found that the S-waveplate generates a radially polarized beam, we analyzed this beam with a linear polarizer; the results were shown previously (Fig. 6.4). Similarly, we found that the $\pi - Mode\ converter$ works rightly, we can see the experimental results obtained in the laboratory (see Fig. 6.7). Fig. 6.11 shows the experimental results obtained when a radially polarized beam mode is modified by a $\pi/2 - Mode\ converter$. In this case we cannot see a clear mode conversion (LG to HG, beam polarization modes), with respect to the $\pi - Mode\ converter$ (diagonal to horizontal, HG beam polarization modes). Also, experimentally we saw that the modified Mach-Zehnder interferometer does not work rightly, because, it does not split the mutually orthogonal transversal beam modes (horizontal and vertical HG beam

modes, with orthogonal polarization states each of them), see Fig. 6.14, Fig. 6.15 and Fig. 6.16. Professor Töpple and his coworkers have showed that a modified Mach-Zehnder (MMZI) interferometer splits a radially polarized beam, which is described mathematically as a superposition of two mutually orthogonal Hermite-Gaussian beam modes (horizontal HG beam mode with horizontal polarization and vertical HG beam mode with vertical polarization). They showed a mathematically description of the MMZI by using the Jones formalism [1], our contribution is a simulation of this optical system (MMZI). We generated a radially polarized beam as a superposition of two linearly polarized HG beam modes (mutually orthogonal, HG_{10} and HG_{01}). After that, we used the Jones transformations described by professor Töppel (which describe the Mueller matrix of each polarizing optical element used in the MMZI) [1], in order to simulate the radially polarized beam through the modified Mach-Zehnder interferometer. The simulation allowed proving the right functionality of the modified Mach-Zehnder interferometer. We observed that, when an incident radially polarized Laguerre-Gaussian beam mode, which is generated as a superposition of two mutually orthogonal HG beam modes, which have orthogonal polarization states (horizontal and vertical HG beam modes with horizontal and vertical polarization states, respectively), then, we can use a modified Mach-Zehnder interferometer in order to split the transversal HG beam modes of the incident radially polarized Laguerre-Gaussian beam mode. In the following figure it is shown the radially polarized beam generated by the simulation and the Matlab code developed is shown in Appendix E.

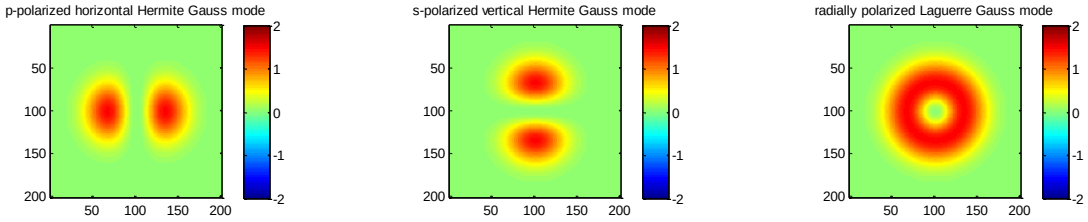

Figure 6.23 Graphical representation of a numerically simulated radially polarized Laguerre-Gaussian beam mode, which is generated as a superposition of two transversal Hermite-Gaussian beam modes with orthogonal polarization states.

Similarly to the experimental case, we can obtain the SAS for the radially polarized beam numerically simulated. In order to do this, it was necessary analyzing the incident beam by the six polarization states (p-, s-, +45, -45 and circular right- and left-handed polarization states). The Matlab code used in order to obtain the polarimetric analysis is shown in Appendix E and we have used the Matlab code of

Appendix C in order to obtain the SAS. The results are shown in figure 6.24 and 6.25, respectively (we show the Stokes vector of images and the numerical Stokes vector).

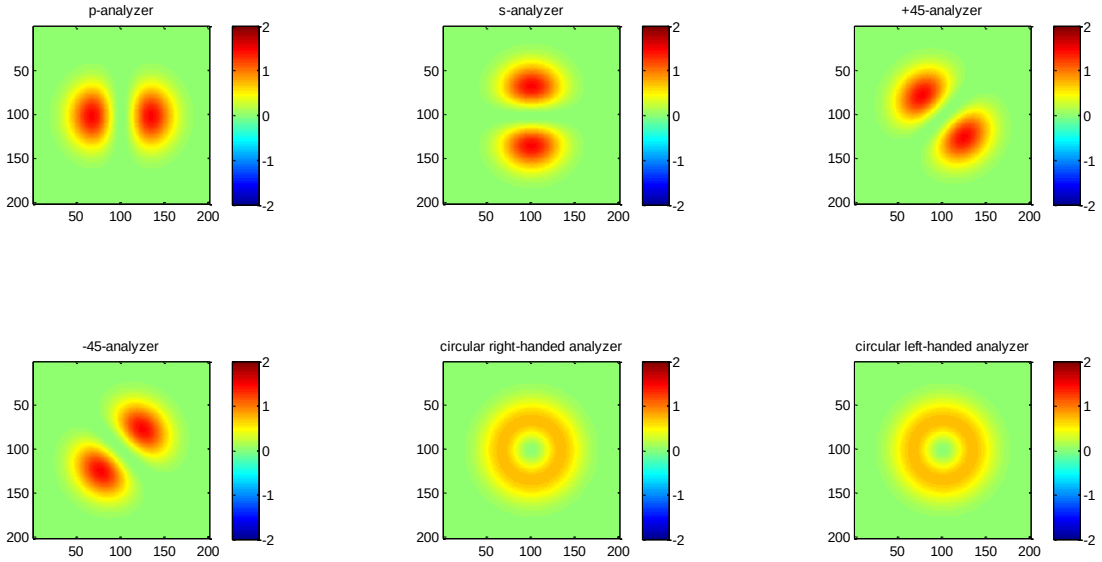

Figure 6.24 Polarimetric analysis of the radially polarized beam shown in Figure 6.23.

$$S_{sim} = \begin{bmatrix} \\ \\ \\ \\ \end{bmatrix} \qquad S_{sim} = \begin{pmatrix} 1 \\ 0 \\ 0 \\ 0 \end{pmatrix}$$

Figure 6.25 SAS corresponding to the radially polarized Laguerre-Gaussian beam mode shown in Fig. 6.23 (S_{sim}).

We can see in figure 6.24 that, the results obtained when we analyze by $+45$ − and -45 −polarization states do not coincide with the experimental results obtained in the same polarimetric analysis (see Figure 6.7); in fact, the results are opposite. That is, the result of the simulation when we analyze by $+45$ −polarization state corresponds to the result obtained experimentally, when we analyze by -45 −polarization state. Similarly, it occurs with the result of the simulation when we analyze by -45 −polarization state. In this case the simulated result when we analyze by -45 −polarization state corresponds to the experimental result, when we analyze by $+45$ −polarization state. This observation is important because the modes shown in Fig. 6.24 generate a radially polarized beam. Nevertheless, we need to take into account that the Matlab software works by using a coordinate system, which is different respect to the coordinate system used in this thesis (see Fig. 6.26). We must remember that the coordinate system used in this thesis is respect to an observer who looks toward the source (see Fig. 2.1).

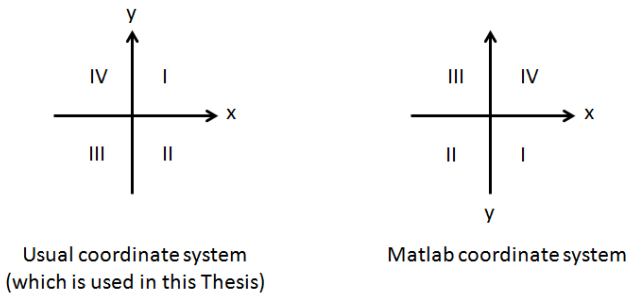

Figure 6.26 Coordinate system used in this Thesis and the Matlab coordinate system.

It is important to say that we have obtained the SAS simulated of the radially polarized beam (Fig. 6.25) by using the results of the polarimetric analysis simulated (Fig. 6.24); that is, we obtained it by taking into account the Matlab Coordinate system and therefore the simulated SAS will be different with respect to the experimental SAS. Specifically, the element s_2 is different (opposite graphically in the Mueller matrix of images), in the experimental SAS with respect to the simulated SAS. Nevertheless, the arithmetic mean is not changed for this fact. It is important to emphasize the above observations in order to analyze the experimental and simulated results. If we compare the Fig. 6.12 a, with the Fig. 6.25, we can see similarities between them, except the element s_2.

Now, we used the Jones transformations described in Reference 1 in order to simulate the modified Mach-Zehnder interferometer (MMZI). The radially polarized beam simulated previously (Fig. 6.24) is modified by each polarizing

optical element of the MMZI. By using the Jones transformations [1] for each polarizing element, we can simulate the modified beam mode. In this sense, it is possible to simulate the output beam mode, which has traveled through each arm of the MMZI (upper and lower arms, see Fig. 6.20). Finally, we can simulate the beam mode for each output of the MMZI (1 and 2 outputs, see Fig. 6.20) by superposing the resultant beam modes of the two arms. The Matlab code of this simulation is shown in Appendix E. In the following figure (Fig. 27), we can see the simulated beam modes for each arm of the MMZI. Also, it is shown the beam mode generated once we superpose the beam modes of each arm. Fig. 27 a, shows the beam mode generated at the output 1, and Fig. 27 b, shows the beam mode at the output 2 of the MMZI.

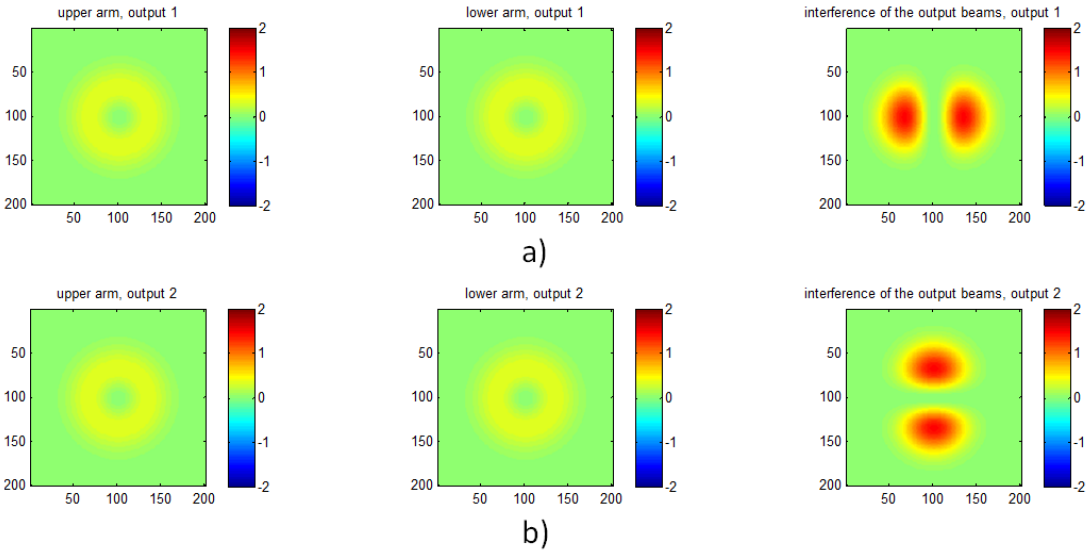

Figure 6.27 Simulation of the modified Mach-Zehnder interferometer. We can see the superposition of the lower and upper output beam modes at a) output 1 and, b) output 2 of the MMZI.

The simulation results show (Fig. 6.23) a right functionality of the MMZI, when a radially polarized beam mode of light travels through it. In this case, the radially polarized LG beam mode was simulated as a superposition of two mutually orthogonal polarization modes, HG_{10} and HG_{10}, which have orthogonal polarization states (horizontal and vertical polarization states, respectively, see Fig. 6.19). At the output 1 of the MMZI we got the HG_{10} polarization mode and, at the output 2 of the MMZI we got the HG_{01} polarization mode.

We can obtain the SAS for each output beam mode of the modified Mach-Zehnder interferometer (MMZI) shown in Fig. 6.27. In this sense, we can observe the similarities between the simulated results (Fig. 6.27) and the experimental results

(Fig. 6.13) obtained for each output of the MMZI. It is necessary to do a polarimetric analysis to each output beam mode of the MMZI. The Matlab code used to do this is shown in Appendix E. We have employed the Matlab code shown in Appendix C in order to obtain the SAS. In the following figures, we show the results.

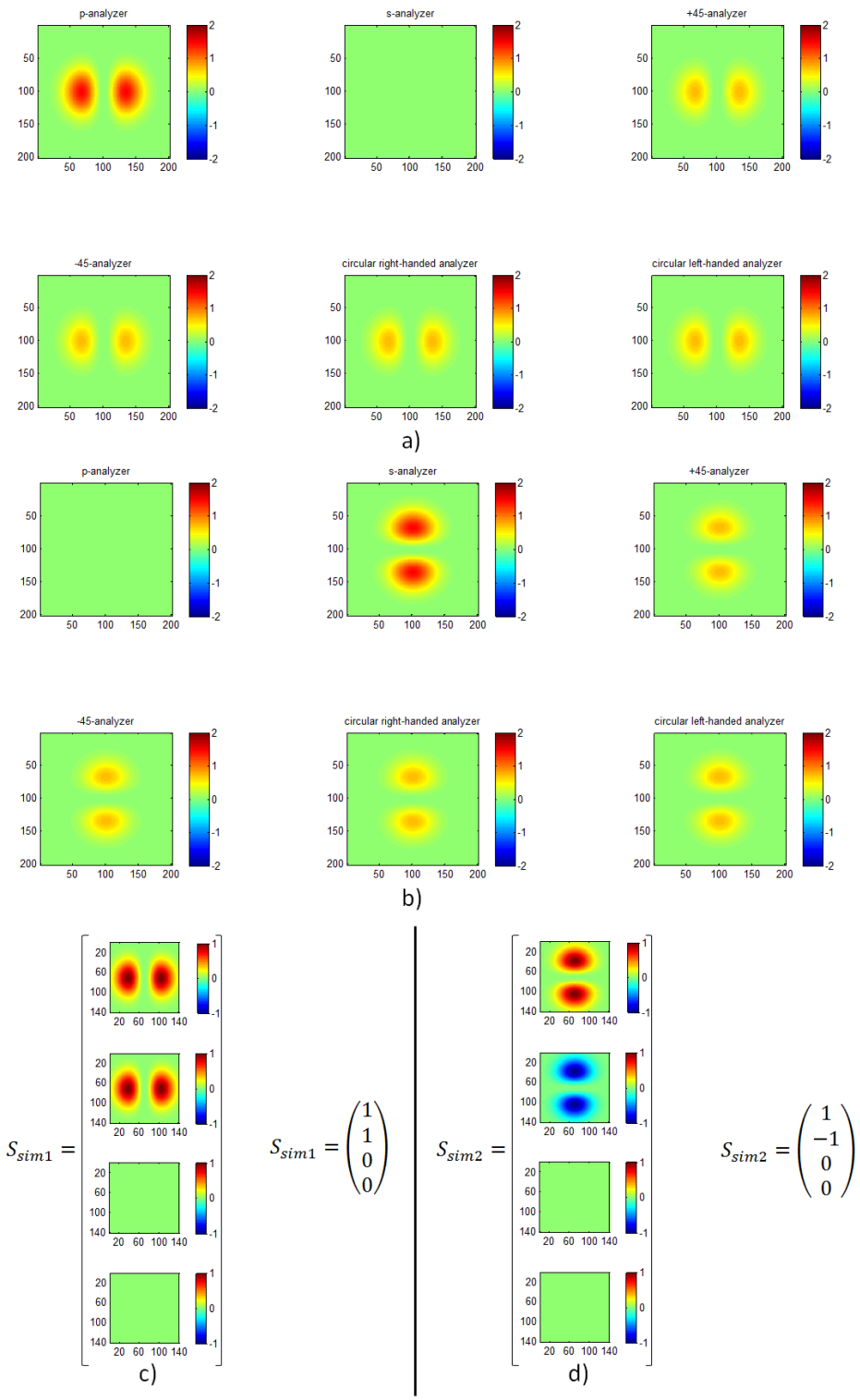

Fig. 6.28 Simulation of the a) polarimetric analysis to the beam mode at output 1 of the MMZI, b) polarimetric analysis to the beam mode at output 2 of the MMZI, c) SAS corresponding to the beam mode at output 1 of the MMZI, S_{sim1}, and, d) SAS corresponding to the beam mode at output 2 of the MMZI, S_{sim2}.

If we compare Fig. 6.13 a, and Fig. 6.13 b, with the corresponding simulated results, Fig. 6.28 c, and Fig. 6.28 d, respectively; we can observe that they are different. Both, the SAS of images like so numerical SAS are not similar between experimental and simulated results. This is a consequence of incorrect functionality of the MMZI. Also, this simulation generates the expected results. That means, the simulation generates the mutually orthogonal polarization modes, HG_{10} and HG_{01}, which have horizontal and vertical polarization states, respectively. It is clear from the SAS obtained on the simulation.

Finally, it is possible to obtain at least four of the sixteen Mueller matrix elements by using the polarimetric analysis results shown in Fig. 6.28 a, and Fig. 6.28 b. Depending of the method used to do that we can obtain different Mueller matrix elements. If we use the IPA method, it is possible to obtain the following Mueller matrix elements: m_{00}, m_{01}, m_{10} and m_{11} (see Eq. 2.4.2.17). On the other hand, when we use a Professor Töppel and coworkers' method, we can obtain the following Mueller matrix elements: S_{00}, S_{03}, S_{30} and S_{33} (see Eq. 4.2.27). The results obtained in this case are shown in the following figure and, the Matlab code used to obtain the results are shown in Appendix A (IPA method) and Appendix B (Professor Töppel and coworkers' method).

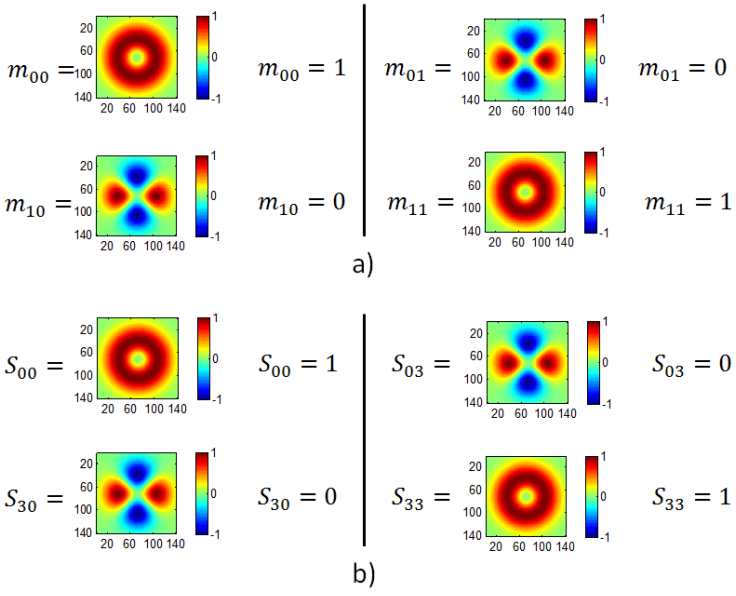

Fig. 6.29 Simulated results for the Mueller matrix elements obtained when we use the a) IPA method and the d) Professor Töppel and coworkers' method. It is shown the image element and the numerical element.

Fig. 6.29 shows both the image element and the numerical element for the Mueller matrix. Similarly to the experimental case, we obtain the images of the Mueller matrix elements by applying the corresponding equation set (2.4.2.1 through 2.4.2.16, IPA method and, 4.2.9 through 4.2.24, Professor Töppel method), in this case we use the images of the polarimetric analysis as intensity measurements (Fig. 6.28 a, and Fig. 6.28 b), directly. On the other hand, the numerical Mueller matrix elements were obtained by calculating the arithmetic mean of each image corresponding to the polarimetric analysis (Fig. 6.28 a, and Fig. 6.28 b) and then, we apply the equation set corresponding (IPA or Professor Töppel methods), in this case we use the values obtained in the previous step.

By comparing the simulated Mueller matrix elements simulated (Fig. 6.29) with the corresponding experimental ones (Fig. 6. 21 and Fig. 6.22), we can see that they are different between them. We have simulated only four elements of the Mueller matrix by using the IPA method and the Professor Töppel method. For the IPA method we simulated the elements m_{00}, m_{01}, m_{10} and m_{11}. In this sense, we can observe the similarities between m_{00}, m_{01}, m_{10} and m_{11} Mueller matrix elements simulated and the m_{00}, m_{01}, m_{10} and m_{11}experimental Mueller matrix elements, which are shown in Fig. 6.21 within the experimental Mueller matrix. For the Professor Töppel method, we have simulated the S_{00}, S_{03}, S_{30} and S_{33} Mueller matrix elements, so, we can observe the similarities between them and the S_{00}, S_{03}, S_{30} and S_{33} experimental Mueller matrix elements, which are shown in Fig. 6.22 within the experimental Mueller matrix. Only the elements m_{00} and m_{10} for the IPA method, and the elements S_{00} and S_{30} for the Professor Töppel method, are similar between experimental and simulated results. But, in general it is a coincidence for us, given that experimentally we observed that the MMZI does not work rightly. That means, the MMZI does not split the mutually orthogonal polarization modes and therefore the polarimetric analysis results are not the expected results. By contrast, the simulated Mueller matrix elements (6.25) show us the expected results. In this sense, we can say that the experimental Mueller matrix obtained is wrong. This is a consequence of the wrong functionality of the MMZI. If we remember, we are not analyzing a specific sample for now (retarder or polarizer for example). The sample is the air in this simulation and therefore the Mueller matrix expected is an identity matrix. From the simulated results, we can see that they correspond to elements of an identity Mueller matrix. At this time, we have not simulated the mode converters and therefore we cannot obtain the complete simulated Mueller matrix.

Chapter 7

Conclusions

In this work we have reviewed about an interesting classification of the polarization of light; on the one hand we have talked about the conventional polarization and, on the other hand, the unconventional polarization. We said that the conventional polarization refers to polarization states of light, which are spatially uniform within the beam cross-section. In other words, a conventional polarized beam has the same polarization state at any point over the beam cross-section. By contrast, the unconventional polarization (or non-conventional polarization) is related with non-spatially homogeneous polarization states of light within the beam cross-section; this means, that an unconventional polarized beam of light has a well defined local polarization state, but globally these beams do not have a well defined polarization state. In other words, the polarization state of an unconventional polarized beam depends of the point within the beam cross-section. Radial and azimuthal axial symmetries represent the two most known unconventional polarization states. In fact, we can remember that (ideally speaking) a radially polarized beam mode is associated with a Stokes vector of a non-polarized beam of light (Fig. 6.25). Generally, the unconventional polarization states arise as a solution of the vector wave equation in terms of the electric field and they are named cylindrical vector beams or CV beams. One important characteristic of these beams is the azimuthal dependence term, which is related with an orbital angular momentum in addition to the spin angular momentum (related with its polarization state). Generally, these beams are distributed on a characteristic annular spatial distribution, which can be described by Bessel-Gauss or Laguerre-Gauss polynomials. Specifically, we have that a radially polarized Laguerre-Gaussian beam mode of light can be represented as a superposition of two Hermite-Gaussian beam modes linearly polarized (horizontal HG beam mode with horizontal polarization state and vertical HG beam mode with vertical polarization state).

Along this thesis we have analyzed a polarimetric optical system, which allows us to obtain the Mueller matrix of a transparent sample, the air. One important characteristic of this polarimetric system is that, it uses a radially polarized beam as an incident beam over the sample. We saw that a radially polarized beam represents a classically entangled state of light, which in principle carries all polarization states at once [1]. In this sense, this is an important advantage of the unconventional polarization respect to the conventional polarization of light, because we can obtain the Mueller matrix of a sample by using only one radially polarized beam as an incident beam over the sample. We can select the polarization states (polarization degrees of freedom) by manipulating the spatial distributions (spatial degrees of freedom) of the radially polarized beam in order to perform the polarimetric analysis (by using a polarization state analyzer, PSA) of a specific spatial distribution. We must remember that each spatial distribution within the radially polarized beam of light is related with a specific polarization state. By contrast, for the Ideal Polarimetric Arrangement method, which is used to obtain the Mueller matrix of a sample, we need generate at least four conventional polarized beams of light ($p-$, $s-$, $+45$ and circular right-handed polarized beams) by using a PSG. These polarized beams of light are used as incident beams over the sample. Once the first polarized beam of light ($p-$polarized beam of light, for example) interacts with the sample, we must analyze it with a PSA in order to determine how it was modified by the sample. We need repeat this procedure at least with the 3 remaining conventional polarized beams ($s-$, $+45$ and circular right-handed polarized beams). The experimental setup used in this work is different respect to the experimental setup proposed in the Reference 1. The experimental setup is constituted by only one mode converter (a couple of cylindrical lenses, which allows us two configurations: $\pi/2-mode\ converter$ and $\pi-mode\ converter$) and only one transverse mode beam splitter or modified Mach-Zehnder interferometer (MMZI). The number of optical elements used in our experimental setup is less respect to the experimental setup, which is shown in Reference 1. One important advantage of this is that we have a better control respect to each optical device (mode converter, MMZI, PSA, for example) in the experimental setup.

To generate a radially polarized beam mode we used a commercial device (passive method) called S-waveplate, which is a polarization converter. Basically, this device allows us to generate a radially polarized beam mode by converting the incident linear polarization state through a spatially variant birefringence transformation. At the output of the S-waveplate we can observe the polarization modes or

Hermite-Gaussian beam modes linearly polarized, when we analyze this beam by using a linear polarizer. Experimentally, we found that the modified Mach-Zehnder interferometer, MMZI, does not split the radially polarized beam generated by the S-waveplate into the horizontal and vertical Hermite-Gaussian beam modes, which are horizontally and vertically polarized, respectively. These experimental results induce us to think that, perhaps, the S-waveplate does not generate a radially polarized beam based in a couple of two mutually-orthogonal Hermite-Gaussian or Laguerre-Gaussian polarized beam modes. On the other hand, it is possible that the MMZI does not induce the necessary phase difference between the beams of the two arms, and therefore, when these beams interfere each other, the destructive interference is not observed and finally, it does not split the incident radially polarized beam. In this sense, it is important to analyze the optical elements in the MMZI in order to determine the phase difference induced on an incident beam. In other words, we need to characterize each element of the MMZI in order to know the difference phase induced on an incident beam of light (specifically the phase difference induced by the beam splitters). Also, we need to take into account that although we used un-polarizing beam splitters, in practice these optical devices affect the polarization state of an incident beam of light. We need consider carefully this change in the polarization state of the incident beam, in order to interpret the results. Finally, it is important say that we did not found specific characteristics about the optical devices, which were used to assemble the modified Mach-Zehnder interferometer in the literature. So, we used optical devices available in the GIPyS (Grupo Interinstitucional de Polarización y Scattering) laboratory.

We simulated a radially polarized Laguerre-Gaussian beam mode as a superposition of the horizontally polarized HG_{10} and vertically polarized HG_{01} beam modes (two mutually-orthogonal Hermite-Gaussian beam modes). Similarly, it was numerically simulated the propagation of this beam through the modified Mach-Zehnder interferometer. The simulated results show the separation of the mutually orthogonal HG beam modes (which generate the radially polarized Laguerre-Gaussian beam mode) at the outputs of this optical system (Fig. 6.23). We based our simulation in the mathematical description of the professor Falk Töppel and his coworkers [1]. The simulation was an important tool in order to probe the right functionality of the MMZI. In this sense, we can say that there are other bases to generate a radially polarized beam of light and therefore the modified Mach-Zehnder interferometer does not split it into the mutually orthogonal Hermite-Gauss beam modes (HG_{10} and HG_{01}). Perhaps the S-

waveplate generates a radially polarized beam mode based in another polarization modes base, which is different to the mutually-orthogonal Hermite-Gaussian or Laguerre-Gaussian polarized beam modes. Thus, the Mueller matrix obtained with the experimental system does not correspond to the expected matrix. We can think in that Mueller matrix as a matrix, which characterizes the system.

It is necessary the generation of a radially polarized Laguerre-Gaussian beam mode as a superposition of the horizontally polarized HG_{10} and vertically polarized HG_{01} beam modes in order to split it by using a transverse-mode beam splitter (modified Mach-Zehnder interferometer). One way to do this is by using a $\pi/2 - mode\ converter$ and a Hermite-Gaussian beam mode as an incident beam in order to generate a radially polarized Laguerre-Gaussian beam mode. Nevertheless, one of the difficulties found when we used a $\pi/2 - mode\ converter$ is the divergence of the output beam, given that it is not an easy work to collimate it. Perhaps, other way to generate a radially polarized Laguerre-Gaussian beam mode is by using interferometric methods, nevertheless, we think that this would be useful just for research purposes because this method is not very competitive in comparison with passive methods, the S-waveplate for example.

Finally, we can conclude that the Spatial Average Symmetry (SAS) [22] is an important parameter, since it provides us the information about the quality of the polarization axial symmetry. In this sense, we can know about the quality of the device, which generates the radially polarized beam, as well as, how a radially polarized beam was modified by optical elements, like mode converters.

Chapter 8

Appendix

Appendix A

In this appendix is described the Matlab code, which was used in order to obtain the experimental Mueller matrix of the used sample. This Matlab code was developed by using the IPA method. The Matlab code of the cropp function employed in this method is shown in the Appendix D.

```
% This Matlab code allows us to obtain a numerical Mueller matrix
and a
% Mueller matrix of images by applying the IPA method

% Obtaining experimental data. The crop function allows us to cut
the experimental images
% in order to get only the illuminated zone of each of them. The
mask function allows us
% to get the mean value only on the circle shape, which is
illuminated by the incident beam
% on the camera. Using these images, it was calculated the Mueller
matrix of images.
% Once the experimental image was cropped then it is obtained the
arithmetic mean. In
% this sense, it was obtained a scalar value, which was used in
order to calculate the
% numerical Mueller matrix

IMpp=imread('Ipp.tif');
[Ipp]=cropp(IMpp);
ipp=mean(mean(Ipp));

IMps=imread('Ips.tif');
[Ips]=cropp(IMps);
ips=mean(mean(Ips));

IMsp=imread('Isp.tif');
[Isp]=cropp(IMsp);
isp=mean(mean(Isp));

IMss=imread('Iss.tif');
[Iss]=cropp(IMss);
iss=mean(mean(Iss));

IMplusp=imread('I+p.tif');[Iplusp]=cropp(IMplusp);
```

```
iplusp=mean(mean(Iplusp));

IMpluss=imread('I+s.tif');
[Ipluss]=cropp(IMpluss);
ipluss=mean(mean(Ipluss));

IMrp=imread('Irp.tif');
[Irp]=cropp(IMrp);
irp=mean(mean(Irp));

IMrs=imread('Irs.tif');
[Irs]=cropp(IMrs);
irs=mean(mean(Irs));

IMpplus=imread('Ip+.tif');
[Ipplus]=cropp(IMpplus);
ipplus=mean(mean(Ipplus));

IMsplus=imread('Is+.tif');
[Isplus]=cropp(IMsplus);
isplus=mean(mean(Isplus));

IMplusplus=imread('I++.tif');
[Iplusplus]=cropp(IMplusplus);
iplusplus=mean(mean(Iplusplus));

IMrplus=imread('Ir+.tif');
[Irplus]=cropp(IMrplus);
irplus=mean(mean(Irplus));

IMpr=imread('Ipr.tif');
[Ipr]=cropp(IMpr);
ipr=mean(mean(Ipr));

IMsr=imread('Isr.tif');
[Isr]=cropp(IMsr);
isr=mean(mean(Isr));

IMplusr=imread('I+r.tif');
[Iplusr]=cropp(IMplusr);
iplusr=mean(mean(Iplusr));

IMrr=imread('Irr.tif');
[Irr]=cropp(IMrr);
irr=mean(mean(Irr));

% Obtaining elements of the numerical Mueller matriz

m00s=(0.5*(ipp+ips+isp+iss))/(0.5*(ipp+ips+isp+iss));
m01s=(0.5*(ipp+ips-isp-iss))/(0.5*(ipp+ips+isp+iss));
m02s=(iplusp+ipluss-0.5*(ipp+ips+isp+iss))/(0.5*(ipp+ips+isp+iss));
m03s=(irp+irs-0.5*(ipp+ips+isp+iss))/(0.5*(ipp+ips+isp+iss));
m10s=(0.5*(ipp-ips+isp-iss))/(0.5*(ipp+ips+isp+iss));
m11s=(0.5*(ipp-ips-isp+iss))/(0.5*(ipp+ips+isp+iss));
```

```
m12s=(iplusp-ipluss-0.5*(ipp-ips+isp-iss))/(0.5*(ipp+ips+isp+iss));
m13s=(irp-irs-0.5*(ipp-ips+isp-iss))/(0.5*(ipp+ips+isp+iss));
m20s=(ipplus+isplus-0.5*(ipp+ips+isp+iss))/(0.5*(ipp+ips+isp+iss));
m21s=(ipplus-isplus-0.5*(ipp+ips-isp-iss))/(0.5*(ipp+ips+isp+iss));
m22s=(2*iplusplus-iplusp-ipluss-ipplus-
isplus+0.5*(ipp+ips+isp+iss))/(0.5*(ipp+ips+isp+iss));
m23s=(2*irplus-irp-irs-ipplus-
isplus+0.5*(ipp+ips+isp+iss))/(0.5*(ipp+ips+isp+iss));
m30s=(ipr+isr-0.5*(ipp+ips+isp+iss))/(0.5*(ipp+ips+isp+iss));
m31s=(ipr-isr-0.5*(ipp+ips-isp-iss))/(0.5*(ipp+ips+isp+iss));
m32s=(2*iplusr-iplusp-ipluss-ipr-
isr+0.5*(ipp+ips+isp+iss))/(0.5*(ipp+ips+isp+iss));
m33s=(2*irr-irp-irs-ipr-
isr+0.5*(ipp+ips+isp+iss))/(0.5*(ipp+ips+isp+iss));

% Numeric Mueller matrix

M=[m00s m01s m02s m03s;m10s m11s m12s m13s;m20s m21s m22s m23s;m30s
m31s m32s m33s];

% Obtaining the images of each element of the Mueller matrix

m00=(0.5*(Ipp+Ips+Isp+Iss))./max(max(0.5*(Ipp+Ips+Isp+Iss)));
subplot(4,4,1)
imagesc(m00)
axis 'square'
caxis([-1 1])
colorbar

m01=(0.5*(Ipp+Ips-Isp-Iss))./max(max(0.5*(Ipp+Ips+Isp+Iss)));
subplot(4,4,2)
imagesc(m01)
axis 'square'
caxis([-1 1])
colorbar

m02=(Iplusp+Ipluss-
0.5*(Ipp+Ips+Isp+Iss))./max(max(0.5*(Ipp+Ips+Isp+Iss)));
subplot(4,4,3)
imagesc(m02)
axis 'square'
caxis([-1 1])
colorbar

m03=(Irp+Irs-
0.5*(Ipp+Ips+Isp+Iss))./max(max(0.5*(Ipp+Ips+Isp+Iss)));
subplot(4,4,4)
imagesc(m03)
axis 'square'
caxis([-1 1])
colorbar

m10=(0.5*(Ipp-Ips+Isp-Iss))./max(max(0.5*(Ipp+Ips+Isp+Iss)));
subplot(4,4,5)
imagesc(m10)
```

```
axis 'square'
caxis([-1 1])
colorbar

m11=(0.5*(Ipp-Ips-Isp+Iss))./max(max(0.5*(Ipp+Ips+Isp+Iss)));
subplot(4,4,6)
imagesc(m11)
axis 'square'
caxis([-1 1])
colorbar

m12=(Iplusp-Ipluss-0.5*(Ipp-Ips+Isp-
Iss))./max(max(0.5*(Ipp+Ips+Isp+Iss)));
subplot(4,4,7)
imagesc(m12)
axis 'square'
caxis([-1 1])
colorbar

m13=(Irp-Irs-0.5*(Ipp-Ips+Isp-
Iss))./max(max(0.5*(Ipp+Ips+Isp+Iss)));
subplot(4,4,8)
imagesc(m13)
axis 'square'
caxis([-1 1])
colorbar

m20=(Ipplus+Isplus-
0.5*(Ipp+Ips+Isp+Iss))./max(max(0.5*(Ipp+Ips+Isp+Iss)));
subplot(4,4,9)
imagesc(m20)
axis 'square'
caxis([-1 1])
colorbar

m21=(Ipplus-Isplus-0.5*(Ipp+Ips-Isp-
Iss))./max(max(0.5*(Ipp+Ips+Isp+Iss)));
subplot(4,4,10)
imagesc(m21)
axis 'square'
caxis([-1 1])
colorbar

m22=(2*Iplusplus-Iplusp-Ipluss-Ipplus-
Isplus+0.5*(Ipp+Ips+Isp+Iss))./max(max(0.5*(Ipp+Ips+Isp+Iss)));
subplot(4,4,11)
imagesc(m22)
axis 'square'
caxis([-1 1])
colorbar

m23=(2*Irplus-Irp-Irs-Ipplus-
Isplus+0.5*(Ipp+Ips+Isp+Iss))./max(max(0.5*(Ipp+Ips+Isp+Iss)));
subplot(4,4,12)
imagesc(m23)
```

```
axis 'square'
caxis([-1 1])
colorbar

m30=(Ipr+Isr-
0.5*(Ipp+Ips+Isp+Iss))./max(max(0.5*(Ipp+Ips+Isp+Iss)));
subplot(4,4,13)
imagesc(m30)
axis 'square'
caxis([-1 1])
colorbar

m31=(Ipr-Isr-0.5*(Ipp+Ips-Isp-
Iss))./max(max(0.5*(Ipp+Ips+Isp+Iss)));
subplot(4,4,14)
imagesc(m31)
axis 'square'
caxis([-1 1])
colorbar

m32=(2*Iplusr-Iplusp-Ipluss-Ipr-
Isr+0.5*(Ipp+Ips+Isp+Iss))./max(max(0.5*(Ipp+Ips+Isp+Iss)));
subplot(4,4,15)
imagesc(m32)
axis 'square'
caxis([-1 1])
colorbar

m33=(2*Irr-Irp-Irs-Ipr-
Isr+0.5*(Ipp+Ips+Isp+Iss))./max(max(0.5*(Ipp+Ips+Isp+Iss)));
subplot(4,4,16)
imagesc(m33)
axis 'square'
caxis([-1 1])
colorbar
```

Appendix B

Another method, which can be used in order to obtain the experimental Mueller matrix of a sample, is described in the Reference 1 of this work. It was developed a Matlab code by using this method, which is shown in this appendix. The Matlab code of the 'cropp function' employed in this method is shown in the Appendix D.

```
% This Matlab code allows us to obtain a numerical Mueller matrix
and a
% Mueller matrix of images by applying the method described in the
following
% paper: Falk Töppel, Andrea Aiello, Christoph Marquardt, Elisabeth
Giacobino,
% Gerd Leuchs, Classical entanglement in polarization metrology,
Institute
% of Physics 16, 1-21 (2014)
```

```
% Obtaining experimental data. The crop function allows us to cut
the experimental images
% in order to get only the illuminated zone of each of them. Using
these images, it was
% calculated the Mueller matrix of images.
% Once the experimental image was cropped then it is obtained the
arithmetic mean. In
% this sense, it was obtained a scalar value, which was used in
order to calculate the
% numerical Mueller matrix

IM00=imread('I00.tif');
[I00]=cropp(IM00);
I00s=mean(mean(I00));

IM10=imread('I10.tif');
[I10]=cropp(IM10);
I10s=mean(mean(I10));

IM20=imread('I20.tif');
[I20]=cropp(IM20);
I20s=mean(mean(I20));

IM30=imread('I30.tif');
[I30]=cropp(IM30);
I30s=mean(mean(I30));

IM01=imread('I01.tif');
[I01]=cropp(IM01);
I01s=mean(mean(I01));

IM11=imread('I11.tif');
[I11]=cropp(IM11);
I11s=mean(mean(I11));

IM21=imread('I21.tif');
[I21]=cropp(IM21);
I21s=mean(mean(I21));

IM31=imread('I31.tif');
[I31]=cropp(IM31);
I31s=mean(mean(I31));

IM02=imread('I02.tif');
[I02]=cropp(IM02);
I02s=mean(mean(I02));

IM12=imread('I12.tif');
[I12]=cropp(IM12);
I12s=mean(mean(I12));

IM22=imread('I22.tif');
[I22]=cropp(IM22);
I22s=mean(mean(I22));
```

```
IM32=imread('I32.tif');
[I32]=cropp(IM32);
I32s=mean(mean(I32));

IM03=imread('I03.tif');
[I03]=cropp(IM03);
I03s=mean(mean(I03));

IM13=imread('I13.tif');
[I13]=cropp(IM13);
I13s=mean(mean(I13));

IM23=imread('I23.tif');
[I23]=cropp(IM23);
I23s=mean(mean(I23));

IM33=imread('I33.tif');
[I33]=cropp(IM33);
I33s=mean(mean(I33));

% Obtaining elements of the numerical Mueller matriz

S00s=(I00s+I01s+I10s+I11s)/(I00s+I01s+I10s+I11s);
S01s=(-I00s-I01s+2*I02s-I10s-I11s+2*I12s)/(I00s+I01s+I10s+I11s);
S02s=(-I00s-I01s+2*I03s-I10s-I11s+2*I13s)/(I00s+I01s+I10s+I11s);
S03s=(I00s-I01s+I10s-I11s)/(I00s+I01s+I10s+I11s);
S10s=(-I00s-I01s-I10s-I11s+2*(I20s+I21s))/(I00s+I01s+I10s+I11s);
S11s=(I00s+I01s-2*I02s+I10s+I11s-2*(I12s+I20s+I21s-
2*I22s))/(I00s+I01s+I10s+I11s);
S12s=(I00s+I01s-2*I03s+I10s+I11s-2*(I13s+I20s+I21s-
2*I23s))/(I00s+I01s+I10s+I11s);
S13s=(-I00s+I01s-I10s+I11s+2*I20s-2*I21s)/(I00s+I01s+I10s+I11s);
S20s=(-I00s-I01s-I10s-I11s+2*(I30s+I31s))/(I00s+I01s+I10s+I11s);
S21s=(I00s+I01s-2*I02s+I10s+I11s-2*(I12s+I30s+I31s-
2*I32s))/(I00s+I01s+I10s+I11s);
S22s=(I00s+I01s-2*I03s+I10s+I11s-2*(I13s+I30s+I31s-
2*I33s))/(I00s+I01s+I10s+I11s);
S23s=(-I00s+I01s-I10s+I11s+2*I30s-2*I31s)/(I00s+I01s+I10s+I11s);
S30s=(I00s+I01s-I10s-I11s)/(I00s+I01s+I10s+I11s);
S31s=(-I00s-I01s+2*I02s+I10s+I11s-2*I12s)/(I00s+I01s+I10s+I11s);
S32s=(-I00s-I01s+2*I03s+I10s+I11s-2*I13s)/(I00s+I01s+I10s+I11s);
S33s=(I00s-I01s-I10s+I11s)/(I00s+I01s+I10s+I11s);

% Numeric Mueller matrix

M=[S00s S01s S02s S03s;S10s S11s S12s S13s;S20s S21s S22s S23s;S30s
S31s S32s S33s];

% Obtaining the images of each elemnt of the Mueller matriz

S00=(I00+I01+I10+I11)./max(max(I00+I01+I10+I11));
subplot(4,4,1)
imagesc(S00)
```

```
axis 'square'
caxis([-1 1])
colorbar

S01=(-I00-I01+2*I02-I10-I11+2*I12)./max(max(I00+I01+I10+I11));
subplot(4,4,2)
imagesc(S01)
axis 'square'
caxis([-1 1])
colorbar

S02=(-I00-I01+2*I03-I10-I11+2*I13)./max(max(I00+I01+I10+I11));
subplot(4,4,3)
imagesc(S02)
axis 'square'
caxis([-1 1])
colorbar

S03=(I00-I01+I10-I11)./max(max(I00+I01+I10+I11));
subplot(4,4,4)
imagesc(S03)
axis 'square'
caxis([-1 1])
colorbar

S10=(-I00-I01-I10-I11+2*(I20+I21))./max(max(I00+I01+I10+I11));
subplot(4,4,5)
imagesc(S10)
axis 'square'
caxis([-1 1])
colorbar

S11=(I00+I01-2*I02+I10+I11-2*(I12+I20+I21-
2*I22))./max(max(I00+I01+I10+I11));
subplot(4,4,6)
imagesc(S11)
axis 'square'
caxis([-1 1])
colorbar

S12=(I00+I01-2*I03+I10+I11-2*(I13+I20+I21-
2*I23))./max(max(I00+I01+I10+I11));
subplot(4,4,7)
imagesc(S12)
axis 'square'
caxis([-1 1])
colorbar

S13=(-I00+I01-I10+I11+2*I20-2*I21)./max(max(I00+I01+I10+I11));
subplot(4,4,8)
imagesc(S13)
axis 'square'
caxis([-1 1])
colorbar
```

```
S20=(-I00-I01-I10-I11+2*(I30+I31))./max(max(I00+I01+I10+I11));
subplot(4,4,9)
imagesc(S20)
axis 'square'
caxis([-1 1])
colorbar

S21=(I00+I01-2*I02+I10+I11-2*(I12+I30+I31-
2*I32))./max(max(I00+I01+I10+I11));
subplot(4,4,10)
imagesc(S21)
axis 'square'
caxis([-1 1])
colorbar

S22=(I00+I01-2*I03+I10+I11-2*(I13+I30+I31-
2*I33))./max(max(I00+I01+I10+I11));
subplot(4,4,11)
imagesc(S22)
axis 'square'
caxis([-1 1])
colorbar

S23=(-I00+I01-I10+I11+2*I30-2*I31)./max(max(I00+I01+I10+I11));
subplot(4,4,12)
imagesc(S23)
axis 'square'
caxis([-1 1])
colorbar

S30=(I00+I01-I10-I11)./max(max(I00+I01+I10+I11));
subplot(4,4,13)
imagesc(S30)
axis 'square'
caxis([-1 1])
colorbar

S31=(-I00-I01+2*I02+I10+I11-2*I12)./max(max(I00+I01+I10+I11));
subplot(4,4,14)
imagesc(S31)
axis 'square'
caxis([-1 1])
colorbar

S32=(-I00-I01+2*I03+I10+I11-2*I13)./max(max(I00+I01+I10+I11));
subplot(4,4,15)
imagesc(S32)
axis 'square'
caxis([-1 1])
colorbar

S33=(I00-I01-I10+I11)./max(max(I00+I01+I10+I11));
subplot(4,4,16)
imagesc(S33)
axis 'square'
```

```
caxis([-1 1])
colorbar
```

Appendix C

In this appendix we show the Matlab code, which allows us to obtain the SAS (Spatial Average Symmetry) of a beam. The analyzed beam was produced by a polarization converter or was previously modified by an optical device (mode converter or transverse mode beam splitter). We must remember that the SAS allows us to know the quality of the beam, which was produced or modified by an optical device.

```
% This Matlab code allows us to obtain the SAS (Spatial Average
Symmetry)of
% a beam. We must remember that the SAS allows us to know the
quality of
% the beam, which was produced or modified by an optical device.

% Obtaining experimental data: in this step we get the experimental
data
% and we crop it in order to get only the zone, which was
illuminated by
% the incident beam. We obtain the six images, which correspond
with the
% six polarization states (p-, s-, +45, -45 and, circular right-
and
% left-handed polarization states) analyzed by the PSA.

IMI0=imread('hp.tif');
[I0]=cropp(IMI0);
i0=mean(mean(I0));

IMI90=imread('vp.tif');
[I90]=cropp(IMI90);
i90=mean(mean(I90));

IMIp45=imread('+45.tif');
[Ip45]=cropp(IMIp45);
ip45=mean(mean(Ip45));

IMIm45=imread('-45.tif');
[Im45]=cropp(IMIm45);
im45=mean(mean(Im45));

IMIr=imread('rhp.tif');
[Ir]=cropp(IMIr);
ir=mean(mean(Ir));

IMIl=imread('lhp.tif');
[Il]=cropp(IMIl);
il=mean(mean(Il));
```

```
% Obtaining the SAS image elements: in this part we get the
elements of the
% SAS of images by using the equations 2.3.20 to 2.3.23. The SAS of
images
% is calculated by using the images of the six measurements, which
were
% taken with the PSA. If we remember, we used a camera as a
detector. The
% SAS of images was normalized respect to the maximum value of the
element
% s0.

S0=(I0+I90)./max(max(I0+I90));
subplot(4,1,1)
imagesc(S0)
axis 'square'
caxis([-1 1])
colorbar

S1=(I0-I90)./max(max(I0+I90));
subplot(4,1,2)
imagesc(S1)
axis 'square'
caxis([-1 1])
colorbar

S2=(Ip45-Im45)./max(max(I0+I90));
subplot(4,1,3)
imagesc(S2)
axis 'square'
caxis([-1 1])
colorbar

S3=(Ir-Il)./max(max(I0+I90));
subplot(4,1,4)
imagesc(S3)
axis 'square'
caxis([-1 1])
colorbar

% Obtaining the numerical SAS: in this part is calculated the
numerical
% SAS, this is made by using the arithmetic mean of each image (six
% measurements, which corresponds with the six polarization
states). The
% numerical SAS was normalized respect to the value s0.

s0=(i0+i90)/(i0+i90);
s1=(i0-i90)/(i0+i90);
s2=(ip45-im45)/(i0+i90);
s3=(ir-il)/(i0+i90);

S=[s0;s1;s2;s3];
```

Appendix D

In this appendix, it is shown the Matlab code of the 'cropp function', which is used in the IPA and the MR (method described in reference 1) methods. Also it was used in the Matlab code, which allows us to calculate the SAS.

```
function [P_cropped]=cropp(P1)

% This function allows us to crop an experimental image. This
function
% converts a input RGB image to graycale before crop it.

P=rgb2gray(im2double(P1(:,:,1:3)));
imagesc(P)
[x,y]=ginput;
P_cropped=imcrop(P,[x-390,y-390,780,780]);
imagesc(P_cropped)
axis 'square'
colorbar
saveas(figure(1),'1_P_cropped','tif');
close all
```

Appendix E

Here, we show the Matlab code used to generate the radially polarized mode beam, the polarimetric analysis of the radially polarized beam and the modified Mach-Zehnder interferometer simulation.

```
% This Matlab code allows us to generate a radially polarized
% Laguerre-Guassian beam mode as a superposition of a horizontal
% Hermite-Gaussian beam mode with horizontal polarization and a
vertical
% Hermite-Gaussian beam mode with vertical polarization. Also, it
allows us
% to do an polarimetric analysis to this beam (taking into account
that the
% coordinate system of Matlab is different respect to the
coordinate system
% used in the thesis work). This Matlab code also allows us to
simulate the
% modified Mach-Zehnder interferomer, which splits the radially
polarized
% beam generated into its transversal Hermite-Gauss beam modes in
order to
% analyze the polarization of each HG beam mode at each output of
this
% optical system.

% Radially polarized beam generation

[Ey,Ex]=radial_polarization(632E-9,1,0,6);
```

```
% Intensity profile of the linearly polarized HG beam modes
% and the radially polarized LG beam mode as asuperposition of HG
beam
% modes.

I_Ex=real(Ex.*conj(Ex));
I_Ey=real(Ey.*conj(Ey));
I_E=real(Ex.*conj(Ex)+Ey.*conj(Ey));

figure (1)
subplot(1,3,1)
imagesc(I_Ex)
title('p-polarized horizontal Hermite Gauss mode')
caxis([-2 2])
axis 'square'
colorbar
subplot(1,3,2)
imagesc(I_Ey)
title('s-polarized vertical Hermite Gauss mode')
caxis([-2 2])
axis 'square'
colorbar
subplot(1,3,3)
imagesc(I_E)
title('radially polarized Laguerre Gauss mode')
caxis([-2 2])
axis 'square'
colorbar

% Transformation of the linearly polarized HG beam modes ( and
which
% generate the radially polarized LG beam mode), when they travel
through
% the modified Mach-Zehnder interferometer.

% Upper arm, output 1

[Ey_1u,Ex_1u]=transmission(Ey,Ex); % transmission
[Ey_2u,Ex_2u]=reflection_mirror(Ey_1u,Ex_1u); % reflection_mirror
[Ey_3u,Ex_3u]=reflection_mirror(Ey_2u,Ex_2u); % reflection_mirror
[Ey_4u,Ex_4u]=transmission(Ey_3u,Ex_3u); % transmission_BS

% Intensity profile of the output beam mode from the upper arm at
output 1

figure (2)
I_E_u1=real(Ex_4u.*conj(Ex_4u)+Ey_4u.*conj(Ey_4u));
subplot(1,3,1)
imagesc(I_E_u1)
title('upper arm, output 1')
caxis([-2 2])
axis 'square'
colorbar

% Lower arm, output 1
```

```
[Ey_1l,Ex_1l]=reflection_BS(Ey,Ex); % reflection_BS
[Ey_2l,Ex_2l]=reflection_mirror(Ey_1l,Ex_1l); % reflection_mirror
[Ey_3l,Ex_3l]=HWP(Ey_2l,Ex_2l); % transmission_HWP
[Ey_4l,Ex_4l]=reflection_BS(Ey_3l,Ex_3l); % reflection_BS

% Intensity profile of the output beam mode from the lower arm at
output 1

I_E_l1=real(Ex_4l.*conj(Ex_4l)+Ey_4l.*conj(Ey_4l));
subplot(1,3,2)
imagesc(I_E_l1)
title('lower arm, output 1')
caxis([-2 2])
axis 'square'
colorbar

% Intensity profile of the beam mode at output 1 (interference of
the
% output beams from the upper and lower arms)

Ey_o1=Ey_4u+Ey_4l;
Ex_o1=Ex_4u+Ex_4l; % interference

I_E_o1=real(Ex_o1.*conj(Ex_o1)+Ey_o1.*conj(Ey_o1));
subplot(1,3,3)
imagesc(I_E_o1)
title('interference of the output beams from the upper and lower
arms')
caxis([-2 2])
axis 'square'
colorbar

% Upper arm, output 2

[Ey_5u,Ex_5u]=transmission(Ey,Ex); % transmission
[Ey_6u,Ex_6u]=reflection_mirror(Ey_5u,Ex_5u); % reflection_mirror
[Ey_7u,Ex_7u]=reflection_mirror(Ey_6u,Ex_6u); % reflection_mirror
[Ey_8u,Ex_8u]=reflection_BS(Ey_7u,Ex_7u); % reflection_BS
[Ey_9u,Ex_9u]=HWP(Ey_8u,Ex_8u); % transmission_HWP

% Intensity profile of the output beam mode from the upper arm at
output 2

figure (3)
I_E_u2=real(Ex_9u.*conj(Ex_9u)+Ey_9u.*conj(Ey_9u));
subplot(1,3,1)
imagesc(I_E_u2)
title('upper arm, output 2')
caxis([-2 2])
axis 'square'
colorbar

% Lower arm, output 2
```

```
[Ey_5l,Ex_5l]=reflection_BS(Ey,Ex); % reflection_BS
[Ey_6l,Ex_6l]=reflection_mirror(Ey_5l,Ex_5l); % reflection_mirror
[Ey_7l,Ex_7l]=HWP(Ey_6l,Ex_6l); % transmission_HWP
[Ey_8l,Ex_8l]=transmission(Ey_7l,Ex_7l); % transmission_BS
[Ey_9l,Ex_9l]=HWP(Ey_8l,Ex_8l); % transmission_HWP

% Intensity profile of the output beam mode from the lower arm at
output 2

I_E_l2=real(Ex_9l.*conj(Ex_9l)+Ey_9l.*conj(Ey_9l));
subplot(1,3,2)
imagesc(I_E_l2)
title('lower arm, output 2')
caxis([-2 2])
axis 'square'
colorbar

% Intensity profile of the beam mode at output 2 (interference of
the
% output beams from the upper and lower arms)

Ey_o2=Ey_9u+Ey_9l;
Ex_o2=Ex_9u+Ex_9l; % interference

I_E_o2=real(Ex_o2.*conj(Ex_o2)+Ey_o2.*conj(Ey_o2));
subplot(1,3,3)
imagesc(I_E_o2)
title('interference of the output beams from the upper and lower
arms')
caxis([-2 2])
axis 'square'
colorbar

% Polarimetric analysis of the radially polarized beam

% p-polarization state analysis
[Ey_p,Ex_p]=hor_analyzer(Ey,Ex);
I_p=real(Ex_p.*conj(Ex_p)+Ey_p.*conj(Ey_p));

figure (4)
subplot (2,3,1)
imagesc(I_p)
title('p-analyzer')
caxis([-2 2])
axis 'square'
colorbar

% s-polarization state analysis
[Ey_s,Ex_s]=ver_analyzer(Ey,Ex);
I_s=real(Ex_s.*conj(Ex_s)+Ey_s.*conj(Ey_s));

subplot (2,3,2)
imagesc(I_s)
```

```
title('s-analyzer')
caxis([-2 2])
axis 'square'
colorbar

% +45-polarization state analysis
[Ey_p45,Ex_p45]=plus45_analyzer(Ey,Ex);
I_p45=real(Ex_p45.*conj(Ex_p45)+Ey_p45.*conj(Ey_p45));

subplot (2,3,3)
imagesc(I_p45)
title('+45-analyzer')
caxis([-2 2])
axis 'square'
colorbar

% -45-polarization state analysis
[Ey_m45,Ex_m45]=minus45_analyzer(Ey,Ex);
I_m45=real(Ex_m45.*conj(Ex_m45)+Ey_m45.*conj(Ey_m45));

subplot (2,3,4)
imagesc(I_m45)
title('-45-analyzer')
caxis([-2 2])
axis 'square'
colorbar

% circular right-handed polarization state analysis
[Ey_rh,Ex_rh]=rha_analyzer(Ey,Ex);
I_rh=real(Ex_rh.*conj(Ex_rh)+Ey_rh.*conj(Ey_rh));

subplot (2,3,5)
imagesc(I_rh)
title('circular right-handed analyzer')
caxis([-2 2])
axis 'square'
colorbar

% circular left-handed polarization state analysis
[Ey_lh,Ex_lh]=lha_analyzer(Ey,Ex);
I_lh=real(Ex_lh.*conj(Ex_lh)+Ey_lh.*conj(Ey_lh));

subplot (2,3,6)
imagesc(I_lh)
title('circular left-handed analyzer')
caxis([-2 2])
axis 'square'
colorbar
```

The ‘radial_polarization function’, which is used in this Matlab code, allows us to generate the radially polarized Laguerre-Gaussian beam mode as a superposition of two mutually orthogonal Hermite-Gaussian beam modes. The following code corresponds to this function.

```
function [E01,E10]=radial_polarization(lambda,E0,z,w0)

% Radially polarized beam generation
[x,y]=meshgrid((-1:0.01:1)*2E7*lambda);
k=2*pi/lambda;
z0=(k*w0^2)/2;
wz=w0*sqrt(1+(z/z0)^2);
h1_y=2*sqrt(2).*y/wz;
h1_x=2*sqrt(2).*x/wz;
m=0;
n=1;
phy=(1+m+n)*atan(z/z0);
E01=E0*w0/wz*h1_y.*exp(-1i*phy).*exp(-(x.^2+y.^2)/(wz^2));
E10=E0*w0/wz*h1_x.*exp(-1i*phy).*exp(-(x.^2+y.^2)/(wz^2));
```

Similar functions are used in order to simulate the transformation of the incident beam components once they interact with the optical elements of the modified Mach-Zehnder interferometer. We describe those functions by using the Jones formalism.

References

[1] Falk Töppel, Andrea Aiello, Christoph Marquardt, Elisabeth Giacobino, Gerd Leuchs, Classical entanglement in polarization metrology, New Journal of Physics **16**, 0730019 (2014).

[2] David J. Griffiths, Introduction to Electrodynamics, Prentice Hall (1999).

[3] Qiwen Zhan, Cylindrical vector beams: from mathematical concepts to applications, Advances in Optics and Photonics **1**, 1-57 (2009).

[4] Rafael Espinosa-Luna, Qiwen Zhan, Polarization and Polarizing Optical Devices, Ch. 9, Handbook of Optical Engineering, edited by Daniel Malacara and Brian Thompson, Taylor and Francis (to be published in 2016).

[5] Dennis H. Goldstein, Polarized light, Taylor and Francis (2003).

[6] Russell A. Chipman, Polarimetry, Ch. 22, pp 22.1-22.37, in Handbook in Optics II (Michael Bass, Editor in Chief), McGraw-Hill, NY, 1995.

[7] W. S. Bickel and W. M. Bailey, Stokes vectors, Mueller matrices, and polarized scattered light, Am. J. Phys. **53**, 468-478 (1985).

[8] Gelacio Atondo-Rubio, Rafael Espinosa-Luna, Alberto Mendoza-Suárez, Mueller matrix determination for one-dimensional rough surfaces with a reduced number of measurements, Optics Communications **244**, 7-13 (2005).

[9] Dennis G. Hall, Vector-beam solutions of Maxwell's wave equation, Optics Letters **21**, 9-11 (1996).

[10] http://www.altechna.com/download/wop/Operation-Manual-_130701.pdf

[11] Martynas Beresna, Mindaugas Gecevičius, Peter G. Kazansky, Titas Gertus, Radially polarized optical vortex converter created by femtosecond laser nanostructuring of glass, Applied Physics Letters, **98**, 1-3 (2011)

[12] Alison M. Yao, Miles J. Padgett, Orbital angular momentum: origins, behavior and applications, Advances in Optics and Photonics **3**, 161-204 (2011).

[13] Miles J. Padgett, Johannes Courtial, Poincarè-sphere equivalent for light beams containing orbital angular momentum, Optics Letters **24**, 430-432 (1999).

[14] Marco W. Beijersbergen, Les Allen, H.E.L.O. van der Veen, J.P. Woerdman, Astigmatic laser mode converters and transfer of orbital angular momentum, Optics Communications **96**, 123-132 (1993).

[15] Ram Oron, Nir Davison, Asher A. Friesem, Erez Hasman, *Transverse mode shaping and selection in laser resonators* (Optical Engineering Laboratory, Faculty of Mechanical Engineering, Technion, Israel Institute of Technology, Haifa 32000, Israel, 2001), p. 327.

[16] Miles Padgett, Johannes Courtial, Les Allen, Light's Orbital Angular Momentum, Physics Today **57**, 35-40 (May 2004).

[17] Les Allen, Miles Padgett, The Orbital Angular Momentum of Light: An Introduction, Edited by Juan P. Torres and Lluis Torner, Willey-VCH Verlag GmbH & Co. KGaA, Weinheim (2011).

[18] Johannes Courtial, Miles J. Padjett, Performance of the cylindrical lens mode converter for producing Laguerre-Gaussian laser modes, Optics Communications **159,** 13-18 (1999).

[19] K. P. Zetie, S. F. Adams, R. M. Tocknell, How does a Mach-Zehnder interferometer work?, Physics Education **35,** 46-48 (2000).

[20] Sasada Hiroyuki, Okamoto Megumi, Transverse-mode beam splitter of a light beam and its application to quantum cryptography, Physical Review **68**, 1-7 (2003).

[21] Robert J. C. Spreeuw, A Classical Analogy of Entanglement, Foundations of Physics **28**, 361-374 (1998).

[22] R. Espinosa-Luna, G. López-Morales, V. M. Rico-Botero, E. Aguilar-Fernández, *Spatial Average Symmetry Associated to Unconventional Polarization. (Submitted to Rev. Mex. Fís., Sept. 2016)*